AD-A170 708 DURABILITY OF STRUCTURAL ADHESIVELY BONDED SYSTEMS(U) 1/2
TECHNION RESEARCH AND DEVELOPMENT FOUNDATION LTD HAIFA
(ISRAEL) O ISHAI ET AL. JAN 86 DAJA45-84-C-0050

UNCLASSIFIED F/G 20/11 NL

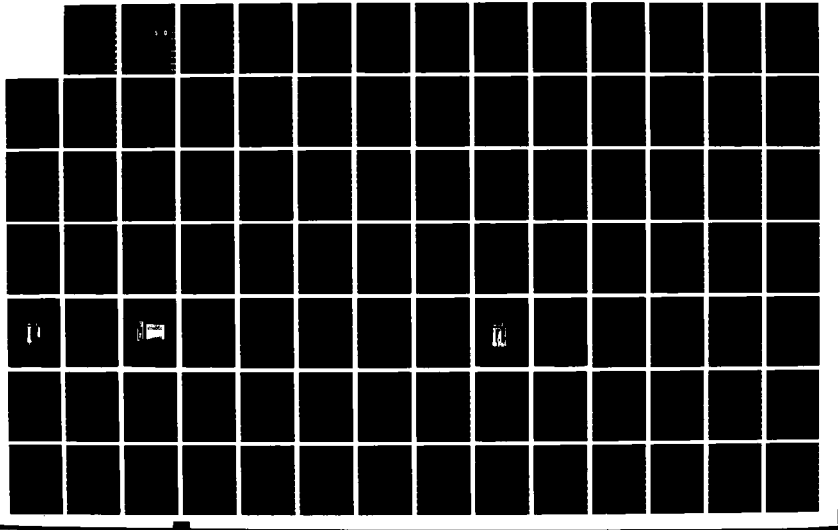

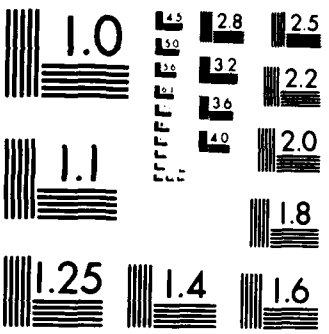

(10)

DURABILITY OF STRUCTURAL ADHESIVELY BONDED SYSTEMS

by

O. Ishai, G. Yaniv and P. Bar Yoseph

December 1985

United States Army

European Research Office of the U.S. Army

London, England

Contract Number DAJA 45-84-C-0050

Technion Research & Development Foundation Ltd.

Technion — Israel Institute of Technology

Haifa, Israel

Approved for Public Release: Distribution Unlimited

DURABILITY OF STRUCTURAL ADHESIVELY-BONDED SYSTEMS

by

O. Ishai, G. Yaniv and P. Bar-Yoseph

December 1985

United States Army

European Research Office of the U.S. Army

London, England

Contract Number DAJA 45-84-C-0050

Technion Research & Development Foundation Ltd.

Technion - Israel Institute of Technology

Haifa, Israel

(When Data Entered)

SECURITY CLASSIFICATION OF THIS PAGE (When Data Entered)

DOCUMENTATION PAGE

READ INSTRUCTIONS BEFORE COMPLETING FORM

20. (continued)

well with ...
Experimental ... Adhesively-Bonded Systems
diff...
diff...
correla...

2. GOVT ACCESSION NO. ADA170708	3. RECIPIENT'S CATALOG NUMBER
	5. TYPE OF REPORT & PERIOD COVERED: Final Nov. '84 - Jan. '86
	6. PERFORMING ORG. REPORT NUMBER
...ar-Yoseph	8. CONTRACT OR GRANT NUMBER(S): DAJA45-84-C-0050
...AND ADDRESS: ...ment Foundation Ltd. ... Haifa, Israel.	10. PROGRAM ELEMENT, PROJECT, TASK AREA & WORK UNIT NUMBERS: 61102A 1L161102BH57-04
...DRESS	12. REPORT DATE: January 1986
	13. NUMBER OF PAGES: 109
...different from Controlling Office)	15. SECURITY CLASS. (of this report): Unclassified
	15a. DECLASSIFICATION/DOWNGRADING SCHEDULE

...report

...ase; distribution unlimited.

...Abstract entered in Block 20, if different from Report)

...ssary and identify by block number)

...y, Diffusion, Interlaminar, Hygrothermal, ...ability, Time-Dependent, Viscoelastic, ... Deformation, Stress Analysis, Stress- ... Element Method, Swelling, Heat

...ary and identify by block number)

...rical study was conducted for quantita- ...dependence of stress, strain, moisture ... in a polymeric adhesive-bonded layer ... experimental evaluation of the ... nonlinear coupled differential ... the finite strip method.

... correlates

(When Data Entered)

SECURITY CLASSIFICATION OF THIS PAGE (When Data Entered)

DURABILITY OF STRUCTURAL ADHESIVELY-BONDED SYSTEMS

O. Ishai*), G. Yaniv*) and P. Bar-Yoseph*)

ABSTRACT

An experimental and analytical study was conducted for quantitative evaluation of the interdependence of stress, strain, moisture diffusion and heat conduction in a polymeric adhesive-bonded layer as a function of time. Following experimental evaluation of the necessary coefficients, a set of nonlinear coupled differential equations is solved numerically by the finite strip method.

It was shown that moisture diffusion coefficient correlates well with the volumetric changes in the stressed materials. Experimental data of the deformation behavior vs. moisture diffusion in an assymmetrical epoxy-aluminum model exposed to different hygrothermomechanical histories have shown a good correlation with analytical prediction.

---

*) Professor, Research Assistant and Senior Lecturer respectively - Faculty of Mechanical Engineering, Technion, Israel Institute of Technology.

List of Keywords

Adhesive, Adherend, Bonding, Diffusion, Interlaminar, Hygrothermal, Hygroelastic, Moisture, Durability, Time-Dependent, Viscoelastic, Viscoplastic, Relaxation, Deformation, Stress Analysis, Stress-Diffusion-Coupling, Finite Element Method, Swelling, Heat Conduction, Polymer

Acknowledgement

The authors would like to express their gratitude to Mr. P. Shechter for his assistance in the experimental work and preparation of the report.
The contribution of Mr. Ofer Weiss to the numerical solution of the NSD model is highly appreciated.

TABLE OF CONTENTS

List of Figures

List of Tables

PREFACE

The research on: "Durability of adhesively-bonded systems of has been extended over three years and comprises of three main parts as follows:

Part A: Hygrothermal effect on the deformational behavior of the adhesive material as a bulk and as an in-situ bonded layers.

Part B: The hygrothermal effect on the viscoelastic and time-dependent response of the bonded system.

Part C: The third part which is presented in the present report, covers the stress-strain-time relationship of the bonded adhesive as affected by the coupling between the hygrothermal processes and the mechanical stress-strain field.

The final goal of this study is the prediction of time-dependant deformational behavior and ultimate-strength limit, of the bonded system under hygrothermal service conditions. Such prediction can be based on the available analytical formulation and experimental findings which were accomplished during the three years research effort.

The personel involved in the research consisted of three academic faculty members working part time and two Ph.D. candidates, as well as a full-time qualified high-level technician. Technical assistance was provided by the Laboratory of Mechanics of Material at the Department of Mechanical Engineering of the Technion.

1. Introduction

The effect of moisture and temperature on the mechanical properties of bulk polymeric material has been widely studied. It can be stated generally that following a raise in temperature and moisture content, the mechanical properties usually undergo accelerated degradation.

When a material system is subjected to extra humidity and thermal changes, an internal redistribution of the moisture content or temperature develops across it. Since the distribution is nonuniform, hygroelastic (thermoelastic) stresses develop and may persist even after steady state is attained.

It is a well-known phenomenon that most polymeric materials swell due to moisture absorption. However, when this hygroelastic expansion is mechanically restrained, the absorption process is likely to proceed differently compared with unrestrained material.

The effect of stress on moisture diffusion can be observed, for example, when imposing a tensile stress on an angleply composite laminate in a humid environment. It was found by Broutman et al [1, 2] that as the angle between the direction of load application and fiber orientation is increased (thereby increasing the tensile stress on the matrix) the rate of moisture diffusion into the matrix is enhanced. One of the first attempts to evaluate qualitatively the effect of stress on the moisture diffusion rate was made by Fahmy and Hurt [3]; they developed an expression for the coefficient of moisture diffusion as a function of the average

hydrostatic pressure (AHP), which was found to be linear for low values of AHP.

The constraints affecting hygroelastic swelling and the diffusion process fall into the following four main categories:

(a) Free swelling - when the specimen is very thin there is practically no dependence of moisture concentration on thickness.

(b) Homogeneous constraint - when the specimen is thick, a distribution of moisture will develop depending on the distance from the outer surface; each element of the material will tend to expand according to its own moisture content, with the attendant effect on the adjacent elements.

(c) Heterogeneous constraint - in specimens composed of two or more different materials, (i.e. bonded systems, composites etc.) the restrained hygroelastic swelling has two main causes:

1. Moisture differentials due to different diffusivities, and 2. Difference in hygroelastic coefficients of expansion.

(d) External application of mechanical and/or thermal loading.

The experimental part of the present research deals with the effects of the above constraints on the diffusion process. The analytical study is mainly concerned with the interactions between the three different processes and mechanisms which are active simultaneously, namely: heat conduction, mechanical response and moisture diffusion. Several studies evaluated the extent to which these processes affect each other.

Sih and Shih [3,4,5] take account of the combined effects

of moisture and temperature by expressing the moisture diffusion coefficient, D, as an exponential function of the absolute temperature, and by inserting coefficients linking moisture and temperature into the diffusion equations. The effect of temperature on the hygroelastic expansion coefficient, $\underset{\sim}{\beta}$, (HEC) and the effect of moisture on the thermoelastic expansion coefficient, $\underset{\sim}{\alpha}$, (TEC) has been evaluated experimentally by Ishai, Gali and Yaniv [6].

The combined influence of stress and temperature is expressed through considering the rate of plastic work as a distributed heat generation source. In case of slow rates of heat transfer from the stressed body to the environment, the temperature is likely to rise. This in turn may affect the mechanical properties and therefore the state of stress [7,8].

Chung and Bradshaw [9] have developed a set of interdependent equations governing moisture diffusion, heat conduction, and mechanical behavior. In order to describe the mechanical behavior of polymers, a kernal function of a viscoelastic nature was adopted. Further experimental data and analytical studies on this subject have been reported by Springer et al [10,11].

When a polymeric material is stressed as a phase in a bonded system or a composite material, it may exhibit a pronounced time-dependent elasto-viscoplastic behavior. Such behavior is usually sensitive to hygrothermal effects. Due to the complexity of the processes involved, there seems to be no solution available to date which rigorously considers the interdependence of and the links between, the time-

dependent mechanical behavior and the hygrothermal processes. The present work is an attempt to fill this gap by tackling the subject both theoretically and experimentally.

2. Experimental Investigation

2.1 - Effect of external load on moisture diffusion

The effect of stress on moisture diffusion can be determined by measuring and calculating the amount of water gain per unit weight of the material in its dry state, as a function of the loading level (see Appendix A).

2.1.1: compressive loading

Two kinds of polymers were examined - Epoxy resin (Epon 828 and Varsamid), and FM-73®, which usually serves as structural adhesive film. Two types of specimens were machined from cured bulks - thin-walled tubes for low and moderate loads (up to 8.0 MPa) and thick-walled ones for high load (up to 25.0 MPa), as shown in Fig.1.

The level of the externally applied compressive load was determined by presetting the length of the spring (1) in the

device shown in Fig.2. By releasing the nut (4), the force exerted by the spring is transferred through the arm (5) and disk (2) to the specimens (3). The spring coefficent was designed to maintain the applied load within less than 5% change due to swelling and creeping of the specimens during the test. The device can accommodate three to four specimens in series, a fact that ensures an identical force on all of them. In order to minimize interruptions of the test due to readings, rapid removal of the specimens is effected by closing nut (4) and opening nut (6).

Six devices under different loads, comprising specimens preliminarily dried in a vacuum oven at 80°C were assembled in a distilled water container, which was kept in an oven at 40° ±5°C (Fig.3) for different durations. Weight and dimensional change readings were taken at regular intervals, and compared to a reference set of specimens kept dry at 40°C. An additional set was kept undisturbed in the water container throughout the test in order to examine the effect of removal of the specimens on moisture uptake. Test conditions for all variants are summarized in Tables 1 through 3.

Figs. 4 to 6 show the relative moisture absorption vs. exposure time at the different load levels. It is clearly seen that the higher the compressive load level, the lower the moisture absorption. Because of the relative shortness of the test the long-term effect of compressive load on the maximum amount of water gain cannot be conclusively established, but a general picture can be derived, as outlined in Section 3.

2.1.2: tensile loading

The tensile specimens were machined to a dog-bone shape from a cured FM-73 plate. Four different lengths of the inner zone (I) were used (Fig.7) in order to isolate the deformation in it from the nonuniform stress field at the end zones (E), which were identical in all specimens. Each device accommodated four specimens. The tensile test procedure was similar to its compressive counterpart using the device shown in Fig.8. Test conditions are summarized in Table 4. Moisture content vs. exposure time at different load levels is shown in Fig.9. The procedure for determination of moisture content in specimens under tension is described in Appendix A.

2.2 - The effect of homogeneous material constraint on diffusion of moisture

For this series five sets of specimens were prepared from cured FM-73® plate of different thickness. The specimens, also preliminarily dried in a vacuum oven at 80°C for seven days, were tested with periodical examination as under (2.1). Test duration was 14 days.

Fig.10 shows the relative moisture content vs. exposure time. A significantly higher moisture absorption rate was found for the thinnest specimen, which will serve later as constraint-free reference.

2.3 - The effect of heterogeneous restraint on moisture diffusion

The second objective of the experimental phase was to obtain experimental data in which the effect of the reciprocal

influences between moisture, temperature, and mechanical behavior, will be represented. These data were used to verify the analytical results.

Three types of asymmetrical doubler (NSD) specimens were manufactured (Fig.11), the material composition and dimensions of which are listed in Table 5. In specimens of series C-1 and C-2, the FM-73 polymeric layer was cured at 123°C during specimen manufacture, while in series T-1, the polymeric layer was first cured separately and was later cemented to the aluminum layer and cured at 75°C. After curing, the specimens had become warped (Fig.11) due to the difference in the TECs of the material constituents. Because of the higher thermal loading the central deflection, and thus the compressive stresses in the outer strata of the polymeric layer of C-1 and C-2 specimens were greater than those in the T-1 series.

All specimens were immersed in a water container, which was placed in an oven. At certain time intervals the central deflection (Fig.11) and water uptake was measured. Due to the diffusion of moisture the polymeric layer swelled, a fact that was reflected as a decrease in the central deflection. The experimental results shown in Figs. 12 to 15, clearly show that the rate of diffusion in the specimens with the less compressed outer layer, i.e. series T-1, is higher than in series C-1 and C-2. Furthermore, between the 11th and the 13th day of exposure, a deviation from the initial slope of the T-1 curve in Fig.13 is evident, caused by an increase in the value of the moisture diffusion coefficient. Examination

of the deflection vs. time curve (Fig.14) reveals that at the stage referred to the curvature of T-1 specimens changes direction. As a result of the bending, the stresses on the outer side become tensile instead of compressive, but no such reversal occurs in series C-1 and C-2. This explains the increased rate of moisture diffusion in T-1 specimens shown in Figs. 13 to 15.

3. Analytical Formulation For the Moisture Process

Isothermal moisture diffusion in polymers can be described by Fick's law [12], as follows:

$$D_x \frac{\partial^2 C}{\partial x^2} = \frac{\partial C}{\partial t} \qquad (3.1)$$

with boundary and initial conditions:

$$C = C_i \qquad 0 < x < h \qquad t \leq 0$$

$$C = C_m \qquad x = 0,h \qquad t > 0 \qquad (3.2)$$

where D_x - diffusion coefficient in-x direction,

C - moisture concentration

C_i - initial concentration

C_m - final concentration (saturation)

h - plate thickness

Eq.(3.1), solved subject to condition (3.2), yields the

well-known expression:

$$\frac{C-C_i}{C_m-C_i} = 1 - \frac{4}{\pi} \sum_{j=0}^{\infty} (2j+1)^{-1} \sin \frac{(2j+1)\pi x}{h} \exp\left[- \frac{(2j+1)^2 \pi^2 D_x t}{h^2} \right] . \quad (3.3)$$

For a given moisture distribution, the water uptake (in weight) is given by:

$$m = n\ell \int_0^h C \, dx \quad . \quad (3.4)$$

Taking into account the finite dimensions of the plate (n - width, ℓ - length), integration eq.(3.3) yields:

$$\frac{m-m_i}{m_m-m_i} = 1 - \frac{8}{\pi^2} \sum_{j=0}^{\infty} (2j+1)^{-2} \exp\left[-(2j+1)^2 \pi^2 \frac{Dt}{h^2} \right] , \quad (3.5)$$

where

$$D = D_x \left(1 + \frac{h}{n} + \frac{h}{\ell}\right)^2 \quad . \quad (3.6)$$

The total weight of the specimen will be then:

$$W = W_d + m \quad (3.7)$$

and the relative water gain, M, is given by:

$$M = \frac{W-W_d}{W_d} = \frac{m}{W_d} \quad (3.8)$$

where W_d is the dry-state weight.

For short exposure periods*, where $\frac{Dt}{h^2} < 1$, using eq.(3.8) equation (3.5) can be approximated by:

---

* A typical short period, for h ≅ 2mm plate, is about 10 days.

Figures 16 to 18 show the RMC vs $\sqrt{t}$ at different compressive loads, bearing out the predictions of eq.(3.9). The higher the compressive load, the lower the diffusion rate, i.e. the CMD.

The plots in figs.16-18 permit determination of the ratio $M(\sigma)/M(0)$ and the nondimensional diffusivity $D(\sigma)/D_0$ can be calculated eq.(3.11) and plotted vs stress. Fig.19 indicates that at low compressive stresses* there is a linear relation between CMD and stress which can be expressed as:

$$D(\sigma) = D_0(1+kJ_1) \quad . \tag{3.12}$$

J_1 being the first invariant of the general stress tensor and k a constant. The present values for eq.(3.12) are:

$$D(\sigma) = D_0[1+(9.12 \pm ,32)10^{-2} J_1] \quad . \tag{3.13}$$

The effect of tensile load on the increase in diffusion rates is shown in fig.20. Plotting the relative diffusivity vs stress show that the linear relation again exists only at low stress levels (fig.21). The nonlinearity at higher stresses is attributable to the visco plastic mechanical behavior rather than to stress-diffusion coupling as will be discussed later.

If the "Relative Reduced Volume" (RRV) is defined as the difference between the relative total volume change and the free hygroelastic swelling per unit volume, the following may be stated: The greater the RRV, the greater the rate of moisture diffusion, and vice versa; in other words, if the

---

* But not at high ones - see [3] and [15].

$$\frac{M}{M_m} = \frac{4}{\sqrt{\pi}} \left(\frac{Dt}{h^2}\right)^{\frac{1}{2}}$$

or

$$M = \left(\frac{4M_m}{\sqrt{\pi}} \frac{\sqrt{t}}{h}\right) \sqrt{D} \quad . \tag{3.9}$$

Based on the above assumptions, a linear relation between the relative moisture content, M, and the square root of the coefficient of moisture diffusion (CMD), is obtained. The plot of M vs $\frac{\sqrt{t}}{h}$ for short periods should be a straight line the slope of which is directly proportional to $\sqrt{D}$.

The ratio of the relative moisture content (RMC) of a stressed and an unstressed specimens (of equal thickness) at a given time is as follows:

$$\frac{M(\sigma)}{M(0)} = \frac{M_m(\sigma)}{M_m(o)} \left[\frac{D(\sigma)}{D_0}\right]^{\frac{1}{2}} \quad , \tag{3.10}$$

where (σ) and (0) refer to the stressed and unstressed conditions, respectively.

In earlier studies, [13] and [14], it was found that external loading usually does not affect the saturation content, but the diffusion rates only. Since loads, in the present experiments are relatively low, this assumption can be employed here to give:

$$\frac{M(\sigma)}{M(0)} = \left[\frac{D(\sigma)}{D_0}\right]^{\frac{1}{2}} \quad . \tag{3.11}$$

total state of stress causes a decrease in the RRV, the rate of diffusion may be expected to decrease. The experimental results (Fig.21) and the fact that in a state of yielding or plastic flow the change in the relative volume usually approaches zero, confirm the above assumption about the dependence of the diffusivity on RRV. This justifies the expression of the diffusivity in terms of strains rather than by relating it directly to stresses. Such an approach permits a simple formulation of the link between stresses and moisture diffusion, as will be shown later on .

The effect of homogeneous constraint on moisture diffusion is shown in fig.22. In spite of the large differences in specimen thickness, diffusion rates are almost the same. It can be assumed, then, that the developed low hygroelastic stresses have a negligible effect on moisture diffusivity. An equivalent hygroelastic stress was computed (see Appendix B), and the results are shown in Fig.23. The two figures indicate that, for most practical purposes, the effect of homogeneous material constraint on the CMD is negligible.

Better insight into the nature of the mutual influence of stress and of moisture diffusion may be achieved by examining some of the results in the micro level. After the empty spaces of the specimen have been filled with water, further intake is conditional on its expansion, which in turn entails overcoming the intermolecular forces. Resistance of the material to swelling which increases with the amount of

additional moisture diffusion is effected by application of a compressive load. By contrast, tensile load tends to release the resistance to swelling and the diffusion rate increases.

The difference between the total relative volume change and the free hygroelastic swelling per unit volume was defined as the Relative Reduced Volume (RRV). As the net result of mechanical and hygrothermal loading is reduction or increase of the RRV of a certain unit volume, so the rate of moisture diffusion is also reduced or increased respectively. This postulation is in agreement with the nonlinear stress-diffusion relation mentioned earlier. It is well known that the volumetric changes in a material under yielding or flow usually tend to zero and so do the changes in the RRV. Thus the diffusivity approaches a constant value at high stress levels.

4. Mathematical Formulation For the Hygrothermal-Elasto-Viscoplastic Coupling Effect

The differential equations from which moisture and temperature distributions are determined can be obtained from the basic laws of mass conservation and energy conservation (first law of thermodynamics) and from the inequality of the second law of thermodynamics [16]. The equations necessary for describing the mechanical response can be obtained from the law of momentum conservation, and by assuming a certain model of viscoplastic behavior. These basic laws lead to the well known heat conduction, moisture diffusion and equilibrium equations.

4.1 - Diffusion equations

The linked form of the heat conduction and moisture diffusion equations in a 2-D rectangular domain (Fig.24) is expressed as:

$$\frac{\partial}{\partial x}\left({}_{C}D_{x}\frac{\partial C}{\partial x}\right) + \frac{\partial}{\partial y}\left({}_{C}D_{y}\frac{\partial C}{\partial y}\right) - \frac{\partial}{\partial t}(C-\lambda_{T}T) = 0$$

$$\frac{\partial}{\partial x}\left({}_{T}D_{x}\frac{\partial T}{\partial x}\right) + \frac{\partial}{\partial y}\left({}_{T}D_{y}\frac{\partial T}{\partial y}\right) - \frac{\partial}{\partial t}(T-\lambda_{C}C-\frac{1}{\rho c}W) = 0 \qquad (4.1)$$

where ${}_{T}D_{i}$ is the thermal diffusivity and ${}_{C}D_{i}$ is the coefficient of moisture diffusion in the i-th direction (i = x,y); λ_{C} and λ_{T} are coefficients linking moisture and temperature; ρ and c are respectively the density and the specific heat, and W is the heat generated within the domain.

The initial conditions are:

$$U(x,y,0) = \bar{U}(x,y) \qquad (4.2)$$

where U represents either T or C.

The boundary conditions can be, for example:

$$U(x,a,t) = U_{02} \qquad \text{on } \Gamma_2 \qquad (4.3)$$

and due to symmetry

$$\frac{\partial U}{\partial y} = 0 \qquad \text{on } \Gamma_1 \qquad (4.4)$$

where U_{02} is a given value on Γ_2 .

The dimensionaless variables are defined as:

$$\xi \equiv \frac{x}{h} \; ; \quad \eta \equiv \frac{y}{a} \; ; \quad \tau \equiv \frac{{}_{R}D}{h^2}\, t \qquad (4.5)$$

where τ is dimensionaless time and ${}_{R}D$ is a certain reference value of diffusivity. The physical variables C and T are shifted and scaled as follows:

$$U \equiv \frac{U - U_{02}}{\bar{U}_R - U_{02}} \tag{4.6}$$

where

$$\bar{U}_R \equiv \max_{\underline{x} \in \Omega} [\bar{U}(\underline{x})] \quad . \tag{4.7}$$

No special symbols are used to distinguish dimensional variables from dimensionless ones. The context affords sufficient means to avoid confusion. Thus, the dimensionless form of the diffusion equations is given by:

$$\frac{\partial}{\partial \xi}\left({}_C D_x \frac{\partial C}{\partial \xi}\right) + \psi^2 \frac{\partial}{\partial \eta}\left({}_C D_Y \frac{\partial C}{\partial \eta}\right) - \frac{\partial}{\partial \tau}(C - \lambda_T T) = 0$$

$$\frac{\partial}{\partial \xi}\left({}_T D_x \frac{\partial T}{\partial \xi}\right) + \psi^2 \frac{\partial}{\partial \eta}\left({}_T D_y \frac{\partial T}{\partial \eta}\right) - \frac{\partial}{\partial \tau}(T - \lambda_C C - \lambda_W W) = 0 \tag{4.8}$$

where

$$\psi \equiv \frac{h}{a}$$

$$U^{D_i} \equiv \frac{u^{D_i}}{R^D}$$

$$\lambda_T \equiv \frac{\bar{C}_R - C_{02}}{\bar{T}_R - T_{02}} \lambda_T$$

$$\lambda_C \equiv \frac{\bar{T}_R - T_{02}}{\bar{C}_R - C_{02}} \lambda_C$$

$$\lambda_W \equiv \frac{\bar{T}_R - T_{02}}{\rho c} \tag{4.9}$$

The uniform initial conditions are:

$$U(\xi, \eta, 0) = 1 \tag{4.10}$$

and boundary conditions:

$$U(0, \eta, \tau) = U(1, \eta, \tau) = U(\xi, 1, \tau) = 0$$

$$\text{on } \Gamma_2, \Gamma_3, \Gamma_4 \tag{4.11}$$

and

$$\frac{\partial U}{\partial \eta} = 0 \qquad \text{on } \Gamma_1 \tag{4.12}$$

When moisture and temperature fields are approximately described by $\tilde{C}$ and $\tilde{T}$ respectively, the coupled nonlinear diffusion equations can be transformed into the weak form by Galerkin's formulation, as follows:

$$\int_{\Omega}\left[\frac{\partial (G_c)_i}{\partial \xi}\, {}_cD_x \frac{\partial \tilde{C}}{\partial \xi} + \psi^2 \frac{\partial (G_c)_i}{\partial \eta}\, {}_cD_y \frac{\partial \tilde{C}}{\partial \eta} + \frac{\partial}{\partial \tau}(\tilde{C}-\lambda_T \tilde{T})(G_c)_i\right] d\Omega = 0$$

$$\int_{\Omega}\left[\frac{\partial (G_T)_i}{\partial \xi}\, {}_TD_x \frac{\partial \tilde{T}}{\partial \eta} + \psi^2 \frac{\partial (G_T)_i}{\partial \eta}\, {}_TD_y \frac{\partial \tilde{T}}{\partial \tau} + \frac{\partial}{\partial \tau}(\tilde{T}-\lambda_c \tilde{C}-\lambda_w W)(G_T)_i\right] d\Omega = 0 \qquad (4.13)$$

where $(G_c)_i$ and $(G_T)_i$ are the i-th test function of $\tilde{C}$ and $\tilde{T}$ respectively.

4.2 - The plasto-viscoplastic model

4.2.1: basic equations

The general strain tensor, $\underset{\sim}{\varepsilon}$, can be expressed as:

$$\underset{\sim}{\varepsilon} = \underset{\sim}{\varepsilon}_e + \underset{\sim}{\varepsilon}_{vp} + \underset{\sim}{\varepsilon}_T + \underset{\sim}{\varepsilon}_H \qquad (4.14)$$

where the constituents are the elastic, viscoplastic, free thermoelastic, and free hygroelastic, strain tensors respectively. The elastic strain tensor is related to the general stress tensor $\underset{\sim}{\sigma}$, by:

$$\underset{\sim}{\sigma} = \underset{\sim\sim}{D}\underset{\sim}{\varepsilon}_e \qquad (4.15)$$

where $\underset{\sim}{D}$ is the matrix of elasticity which, in the general case, is moisture and temperature dependent. Assuming that $\underset{\sim}{\beta}$ and $\underset{\sim}{\alpha}$ are independent of moisture and temperature respectively, in the specific ranges, the hygrothermal strain tensors can be written as:

$$\underset{\sim}{\varepsilon}_H = \underset{\sim}{\beta}\Delta C$$

$$\underset{\sim}{\varepsilon}_T = \underset{\sim}{\alpha}\Delta T \qquad (4.16)$$

Viscoplastic flow occurs when a scalar yield function, $\bar{F}$, is positive (Owen and Hinton [18]):

$$\bar{F} = F(\underset{\sim}{\sigma}, \underset{\sim}{\varepsilon}_{vp}, T, C) - F_o > 0 \qquad (4.17)$$

where F is the equivalent stress in accordance with the accepted yield criterion, and F_o is the yield stress which, in the case of linear strain-hardening, has the form:

$$F_o = \sigma_Y + \kappa \bar{\varepsilon}_{vp} \quad . \qquad (4.18)$$

Here κ is the strain-hardening parameter, σ_Y is the initial yield stress, and $\bar{\varepsilon}_{vp}$ is the effective viscoplastic strain - defined by:

$$\bar{\varepsilon}_{vp} \equiv [\tfrac{2}{3}(\varepsilon_{vp})_{ij}(\varepsilon_{vp})_{ij}]^{\frac{1}{2}} \quad (i,j = 1,2,3) \qquad (4.19)$$

Here and in the following the summation convention is used.

As in plasticity, the flow law of viscoplasticity can be defined as:

$$\dot{\underset{\sim}{\varepsilon}}_{vp} = \lambda \frac{\partial \bar{Q}}{\partial \underset{\sim}{\sigma}} \qquad (4.20)$$

The dot ($\dot{}$) indicates time differentiation; $\bar{Q}$ is the plastic potential, which has the value of the equivalent stress, F. This approach is similar to that used in the associated theory of plasticity. The viscoelastic multiplyer, λ, is given by:

$$\lambda = \gamma \phi(\bar{F}) \qquad (4.21)$$

where

$$\phi(\bar{F}) \equiv \begin{cases} \phi & \bar{F} > 0 \\ 0 & \bar{F} \leq 0 \end{cases} \qquad (4.22)$$

and γ is the fluidity parameter. The following viscoplastic flow function is used:

$$\phi = (\bar{F}/F_o)^N \quad . \tag{4.23}$$

The model parameters, γ and N, are determined experimentally. With the above assumptions, the viscoplastic strain-rate tensor becomes:

$$\dot{\underset{\sim}{\varepsilon}}_{vp} = \gamma \ \phi(\bar{F}) \ \frac{\partial F}{\partial \underset{\sim}{\sigma}} \tag{4.24}$$

It depends on the equivalent stress F, whose value is determined depending on what yield criteria are employed. Most of the commonly used criteria can be expressed thus:

$$F = c_1 J_1 + c_2 (J_2')^{\frac{1}{2}} \tag{4.25}$$

where J_1 is the first invariant of the general stress tensor, J'_2 is the second invariant of the deviatoric stress tensor, and c_1 and c_2 are constants which define the specific yield criterion.

Rather than the classical Von-Mises and Drucker-Prager criteria, a modified yield criterion is used in this work [6]. This criterion is suitable for specially ductile materials such as the FM-73 employed here. The constants in this case are:

$$c_1 = \frac{\lambda_m - 1}{2\lambda_m}$$

$$c_2 = \frac{\sqrt{3}(\lambda_m + 1)}{2\lambda_m} \tag{4.26}$$

λ_m being the ratio between the tensile and the compressive strengths.

4.2.2: the weak form of equilibrium equations

The principle of virtual work in the absence of body forces is written as:

$$\int_{\Omega} \delta \underset{\sim}{\varepsilon}^T \underset{\sim}{\sigma} d\Omega - \int_{\Gamma_f} \delta \underset{\sim}{u}^T \underset{\sim}{f} d\Gamma = 0 \qquad (4.27)$$

where $\underset{\sim}{u} = \{u,v\}$ is the displacement vector, $\underset{\sim}{f}$ is an external traction vector, and Γ_f is the boundary portion of the domain, Ω, the tractions on which are given. Using the strain displacement relation $\underset{\sim}{\varepsilon} = \underset{\sim}{B}\underset{\sim}{u}$ produces the equilibrium equations:

$$\int_{\Omega} \underset{\sim}{B}^T \underset{\sim}{\sigma} d\Omega - \underset{\sim}{F} = \underset{\sim}{0} \qquad (4.28)$$

in which the external force vector is given by:

$$\underset{\sim}{F} = \int_{\Gamma_f} \underset{\sim}{f} d\Gamma \quad . \qquad (4.29)$$

In the general case the matrix operator $\underset{\sim}{B}$ is composed of a linear and a nonlinear part, but since the role of the nonlinear part is negligible when small displacements are considered, it has been omitted in this work.

The incremental form of equilibrium equations, for the n-th time interval, $\Delta\tau_n$, is written as:

$$\int_{\Omega} \underset{\sim}{B}^T \Delta \underset{\sim}{\sigma}^n d\Omega - \Delta \underset{\sim}{F}^n = \underset{\sim}{0} \qquad (4.30)$$

where $\Delta\underset{\sim}{\sigma}^n$ and $\Delta\underset{\sim}{F}^n$ are the changes in, respectively, the stress tensor and in the external load vector, during the time interval $\Delta\tau_n$, which is defined by:

$$\Delta\tau_n = \tau_{n+1} - \tau_n \quad . \qquad (4.31)$$

The relation between stress and elastic strain increment is:

$$\Delta\underset{\sim}{\sigma}^n = \underset{\sim}{D}^n \Delta\underset{\sim}{\varepsilon}_e^n \tag{4.32}$$

or, using equation 4.14:

$$\Delta\underset{\sim}{\sigma}^n = \underset{\sim}{D}^n [\Delta\underset{\sim}{\varepsilon}^n - \Delta\underset{\sim}{\varepsilon}_{vp}^n - \Delta\underset{\sim}{\varepsilon}_T^n - \Delta\underset{\sim}{\varepsilon}_H^n] \quad . \tag{4.33}$$

Substitution of equation 4.33 into equation 4.30 and applying the strain displacement relation, yields the following equilibrium equations:

$$\int_\Omega \underset{\sim}{B}^T \underset{\sim}{D}^n \underset{\sim}{B} \Delta\underset{\sim}{u}^n d\Omega - [\Delta\underset{\sim}{F}^n + \int_\Omega \underset{\sim}{B}^T \underset{\sim}{D}^n (\Delta\underset{\sim}{\varepsilon}_{vp}^n + \Delta\underset{\sim}{\varepsilon}_{HT}^n) d\Omega] = \underset{\sim}{0} \tag{4.34}$$

where

$$\Delta\underset{\sim}{\varepsilon}_{HT}^n = \Delta\underset{\sim}{\varepsilon}_H^n + \Delta\underset{\sim}{\varepsilon}_T^n \quad . \tag{4.35}$$

4.2.3: the mutual influence of moisture diffusion heat conduction, and mechanical behavior

Moisture and temperature affect both the state of stress and deformation, directly through hygrothermal strains and indirectly by affecting mechanical properties. However, the mechanical behavior may also affect the moisture and temperature distributions within the system.

During the viscoplastic process, heat is generated through dissipation and is assumed to be proportional to the rate of the specific viscoplastic work, $\dot{W}_{vp}$ [7]. While the effect of this heat generation source can be neglected in metals due to their high thermal conductivity, in polymers, in which thermal conductivity is relatively low,

temperature profiles may be noticeably affected by this source.

In section 3 it was stated that the tensor of the moisture diffusion coefficients $\underset{\sim}{D}_c$ is affected by the changes in the Relative Reduced Volume (RRV). Let, then, the reduced strain tensor be defined as:

$$\hat{\underset{\sim}{\varepsilon}} \equiv \underset{\sim}{\varepsilon} - \underset{\sim}{\varepsilon}_H = \underset{\sim}{\varepsilon}_e + \underset{\sim}{\varepsilon}_{vp} + \underset{\sim}{\varepsilon}_T \tag{4.36}$$

hence, the RRV can be expressed as:

$$\hat{V}_R \equiv \hat{\varepsilon}_{ii} \tag{4.37}$$

In the present work the discussion has been restricted to isotropic materials, and the only nonzero terms of $\underset{\sim}{D}_c$ are therefore the diagonal terms, which are described by:

$$c^D_{ii} = (_cD_o)_{ii}[1 + \lambda_D(\hat{S}_R)_i] \quad \text{(no sum)} \tag{4.38}$$

where $(_cD_o)_{ii}$ is the i-th diagonal term of $\underset{\sim}{D}_c$ in the stress-free reference state, λ_D is a constant, and $(\hat{S}_R)_i$ is defined by:

$$(\hat{S}_R)_i \equiv \hat{V}_R - \hat{\varepsilon}_{ii} \quad \text{(no sum)} \tag{4.39}$$

The physical meaning of $(\hat{S}_R)_i$ is the relative change in the area, the normal of which is colinear with the direction of the i-th diffusion component. In a like manner as RRV, $(\hat{S}_R)_i$ can be called the Relative Reduced Surface - RRS.

To sum up, the governing equations to be solved simultaneously are the diffusion equations:

$$\int_\Omega [\frac{\partial (G_c)_i}{\partial \xi} {}_cD_x \frac{\partial \tilde{C}}{\partial \xi} + \psi^2 \frac{\partial (G_c)_i}{\partial \eta} {}_cD_y \frac{\partial \tilde{C}}{\partial \eta} + \frac{\partial}{\partial \tau}(\tilde{C} - \lambda_T \tilde{T})(G_c)_i] d\Omega = 0$$

$$\int_\Omega [\frac{\partial (G_T)_i}{\partial \xi} {}_TD_x \frac{\partial \tilde{T}}{\partial \xi} + \psi^2 \frac{\partial (G_T)_i}{\partial \eta} {}_TD_y \frac{\partial \tilde{T}}{\partial \eta} + \frac{\partial}{\partial \tau}(\tilde{T} - \lambda_c \tilde{C} - \lambda_p W_{vp})(G_T)_i] d\Omega = 0 \tag{4.40}$$

and the equilibrium equations:

$$\int_{\Omega} \underset{\sim}{B}^T \underset{\sim}{D}^n \underset{\sim}{B} \Delta \underset{\sim}{u}^n d\Omega - [\Delta \underset{\sim}{F}^n + \int_{\Omega} \underset{\sim}{B}^T \underset{\sim}{D}^n (\Delta \underset{\sim}{\varepsilon}^n_{vp} + \Delta \underset{\sim}{\varepsilon}^n_{HT}) d\Omega] = \underset{\sim}{0} \quad . \qquad (4.41)$$

The above set of equations is coupled and nonlinear as regards both time and space. The numerical solution of these equations will be described in the next section.

5. Computational Model

The physical problem of the present model is composed of three different but simultaneous processes, viz. heat conduction, mechanical response, and moisture diffusion. Each process has a typical time scale - the temperature time scale is of $O(10^{-2}$ min), viscoplastic response is of O(1 min) and diffusion time scale is of $O(10^{3}$ min). Hence, time step size is automatically changed in accordance with the respective time scales. For the convenience of the numerical solution, the diffusion equations were solved first at each time step, followed by the equilibrium equations. The flow charts describing the computational procedure are given in Appendix C.

5.1 - Diffusion equations

According to the Finite Strip Method (FSM), the representations of moisture and temperature distributions within the given domain (Fig.25) are approximated by:

$$\underset{\sim}{U} = \begin{Bmatrix} C \\ T \end{Bmatrix} \sim \begin{Bmatrix} \tilde{C} \\ \tilde{T} \end{Bmatrix} = \begin{Bmatrix} C(\tau) \\ T(\tau) \end{Bmatrix}_i^m N_i(\xi) Y^m(\eta) \qquad (5.1)$$

where N_i and Y^m are, respectively, the local and the global trial functions; C_i^m and T_i^m are the approximated values of C

and T at the i-th nodal point, corresponding to the m-th global trial function. The summation in equation 5.1 is over all I nodal points and M global trial functions. Substitution of the above approximation into the Bubnov-Galerkin formulation of eqs.4.41 yields the following equations for the i-th nodal point:

$$\int_{\eta=0}^{1}\int_{\xi}\frac{\partial(G_c)_i}{\partial\xi}\,{}_{c}D_{x}\frac{\partial\tilde{C}}{\partial\xi}+\psi^2\frac{\partial(G_c)_i}{\partial\eta}\,{}_{c}D_{y}\frac{\partial\tilde{C}}{\partial\eta}+\frac{\partial}{\partial\tau}\,(\tilde{C}-\lambda_T\tilde{T})(G_c)_i\,d\xi d\eta=0$$

$$\int_{\eta=0}^{1}\int_{\xi}\frac{\partial(G_T)_i}{\partial\xi}\,{}_{T}D_{x}\frac{\partial\tilde{T}}{\partial\xi}+\psi^2\frac{\partial(G_T)_i}{\partial\eta}\,{}_{T}D_{y}\frac{\partial\tilde{T}}{\partial\eta}+\frac{\partial}{\partial\tau}(\tilde{T}-\lambda_c\tilde{C}-\lambda_p W_{vp})(C_T)_i\,d\xi d\eta=0 \qquad (5.2)$$

Essential boundary conditions are:

$$\tilde{\underset{\sim}{U}}(\xi,1,\tau)=\underset{\sim}{0}\qquad\text{on }\Gamma_2\ . \qquad (5.3)$$

Since this condition must be satisfied for every ξ, it is required that:

$$Y^m(1)=0\qquad(m=1,2,\ldots,M) \qquad (5.4)$$

The following set of complete functions satisfies this requirement:

$$Y^m(\eta)=\cos(\mu_m\eta) \qquad (5.5)$$

where

$$\mu_m=\frac{2m-1}{2}\pi\qquad(m=1,2,\ldots,M) \qquad (5.6)$$

Boundary conditions of symmetry are also fully satisfied exactly by this approximation, although this is not strictly necessary,

i.e.

$$\frac{\partial Y^m(o)}{\partial\eta}=0\qquad(m=1,2,\ldots,M) \qquad (5.7)$$

Substituting approximation (5.1) into (5.2) gives the following semidiscrete equation:

$$\underset{\sim}{K}\underset{\sim}{U} + \underset{\sim}{C}\dot{\underset{\sim}{U}} = \underset{\sim}{F} \tag{5.8}$$

where

$$\underset{\sim}{U}^T = [(\underset{\sim}{U}^1)^T, (\underset{\sim}{U}^2)^T, \ldots, (\underset{\sim}{U}^i)^T, \ldots, (\underset{\sim}{U}^M)^T]$$

$$(\underset{\sim}{U}^i)^T = [C_1, T_1, C_2, T_2, \ldots, C_I, T_I]^i \tag{5.9}$$

and

$$\underset{\sim}{A} = \begin{bmatrix} \underset{\sim}{A}^{11}, \underset{\sim}{A}^{12}, \ldots, \underset{\sim}{A}^{1j}, \ldots, \underset{\sim}{A}^{1M} \\ \underset{\sim}{A}^{21}, \underset{\sim}{A}^{22}, \ldots, \underset{\sim}{A}^{2j}, \ldots, \underset{\sim}{A}^{2M} \\ \vdots \\ \underset{\sim}{A}^{i1}, \underset{\sim}{A}^{i2}, \ldots, \underset{\sim}{A}^{ij}, \ldots, \underset{\sim}{A}^{iM} \\ \vdots \\ \underset{\sim}{A}^{M1}, \underset{\sim}{A}^{M2}, \ldots, \underset{\sim}{A}^{Mj}, \ldots, \underset{\sim}{A}^{MM} \end{bmatrix}$$

Here $\underset{\sim}{A}$ represents the structure of both the $\underset{\sim}{K}$ and the $\underset{\sim}{C}$ coefficient matrices.

According to Hughes' implicit time marching scheme [17], equation 4.8 can be written at time $\tau_{n+\theta} = (n+\theta)\Delta\tau$ as:

$$\underset{\sim}{K}_{n+\theta}\underset{\sim}{U}_{n+\theta} + \underset{\sim}{C}_{n+\theta}\dot{\underset{\sim}{U}}_{n+\theta} = \underset{\sim}{F}_{n+\theta} \tag{5.10}$$

where:

$$0 \leq \theta \leq 1$$

$$\dot{\underset{\sim}{U}}_{n+\theta} = \frac{1}{\Delta\tau}(\underset{\sim}{U}_{n+1} - \underset{\sim}{U}_n)$$

$$\underset{\sim}{U}_{n+\theta} = (1-\theta)\underset{\sim}{U}_n + \theta\underset{\sim}{U}_{n+1}$$

$$\underset{\sim}{F}_{n+\theta} = (1-\theta)\underset{\sim}{F}_n + \theta\underset{\sim}{F}_{n+1}$$

$$\underset{\sim}{K}_{n+\theta} \equiv \underset{\sim}{K}(\underset{\sim}{U}_{n+\theta}, \tau_{n+\theta})$$

$$\underset{\sim}{C}_{n+\theta} \equiv \underset{\sim}{C}(\underset{\sim}{U}_{n+\theta}, \tau_{n+\theta}) \quad . \tag{5.11}$$

By substituting eq. 5.11 into eq. 5.10 and after further manipulations, a set of algebraic equations for time step n+1 is produced:

$$[\theta \underset{\sim}{K}_{n+\theta} + \frac{1}{\Delta\tau} \underset{\sim}{C}_{n+\theta}] \underset{\sim}{U}_{n+1} = [(\theta-1)\underset{\sim}{K}_{n+\theta} + \frac{1}{\Delta\tau} \underset{\sim}{C}_{n+\theta}] \underset{\sim}{U}_{n} + \underset{\sim}{F}_{n+\theta} \quad (5.12)$$

These nonlinear equations are solved by a semi-iterative technique based on the Newton-Raphson method. At each iterative stage, the linearized equations were solved directly.

5.2 - Equilibrium equations

The incremental form of the equilibrium equations was expressed in this work as:

$$\int_{\Omega} \underset{\sim}{B}^{T} \underset{\sim}{D}^{n} \underset{\sim}{B} \Delta \underset{\sim}{U}^{n} d\Omega - [\Delta \underset{\sim}{F}^{n} + \int_{\Omega} \underset{\sim}{B}^{T} \underset{\sim}{D}^{n} (\Delta \underset{\sim}{\varepsilon}^{n}_{vp} + \Delta \underset{\sim}{\varepsilon}^{n}_{HT}) d\Omega] = \underset{\sim}{0} \quad (4.34)$$

in which the hygrothermal strain increment tensor is given by:

$$\Delta \underset{\sim}{\varepsilon}^{n}_{HT} = \underset{\sim}{\beta} \Delta C^{n} + \underset{\sim}{\alpha} \Delta T^{n} \quad . \quad (5.13)$$

The incremental viscoplastic strain tensor, $\Delta \underset{\sim}{\varepsilon}^{n}_{vp}$, is a function of the stress itself; hence the form of equation 4.34 is implicit and $\Delta \underset{\sim}{\varepsilon}^{n}_{vp}$ has to be formulated numerically for the solution of this equation. Using an implicit time stepping form [18], $\Delta \underset{\sim}{\varepsilon}^{n}_{vp}$ is expressed as:

$$\Delta \underset{\sim}{\varepsilon}^{n}_{vp} = \Delta\tau_{n} [(1-\theta) \dot{\underset{\sim}{\varepsilon}}^{n}_{vp} + \theta \dot{\underset{\sim}{\varepsilon}}^{n+1}_{vp}] \quad . \quad (5.14)$$

A Taylor series expansion is usefully employed to evaluate $\dot{\underset{\sim}{\varepsilon}}^{n+1}_{vp}$:

$$\dot{\underset{\sim}{\varepsilon}}_{vp}^{n+1} = \dot{\underset{\sim}{\varepsilon}}_{vp}^{n} + \left(\frac{\partial \dot{\underset{\sim}{\varepsilon}}_{vp}}{\partial \underset{\sim}{\sigma}}\right)^{n} \Delta \underset{\sim}{\sigma}^{n} + HOT \tag{5.15}$$

By substituting equation 5.15 into 5.14 one obtains

$$\Delta \underset{\sim}{\varepsilon}_{vp}^{n} = \dot{\underset{\sim}{\varepsilon}}_{vp} \Delta\tau_n + \underset{\sim}{P}^{n} \Delta \underset{\sim}{\sigma}^{n} \tag{5.16}$$

where

$$\underset{\sim}{P}^{n} = \theta \Delta\tau_n \frac{\partial \dot{\underset{\sim}{\varepsilon}}_{vp}^{n}}{\partial \underset{\sim}{\sigma}} \tag{5.17}$$

or

$$\underset{\sim}{P}^{n} \equiv \theta \Delta\tau_n \underset{\sim}{H}^{n} \tag{5.18}$$

where $\underset{\sim}{H}^{n}$ can be termed a pseudo viscoplastic compliance matrix. Inserting eq. 5.16 into eq. 4.33 and solving for $\Delta \underset{\sim}{\sigma}^{n}$ yields:

$$\Delta \underset{\sim}{\sigma}^{n} = \hat{\underset{\sim}{D}}^{n} [\underset{\sim}{B} \Delta \underset{\sim}{U}^{n} - (\Delta \underset{\sim}{\varepsilon}_{HT}^{n} + \dot{\underset{\sim}{\varepsilon}}_{vp}^{n} \Delta\tau_n)] \tag{5.19}$$

where

$$\hat{\underset{\sim}{D}}^{n} \equiv (\underset{\sim}{D}^{-1} + \underset{\sim}{P}^{n})^{-1} \tag{5.20}$$

Substituting eqs. 5.16 and 5.19 into 4.34 produces

$$\int_{\Omega} \underset{\sim}{B}^{T} \hat{\underset{\sim}{D}}^{n} \underset{\sim}{B} \Delta \underset{\sim}{U}^{n} d\Omega = \int_{\Omega} \underset{\sim}{B}^{T} \hat{\underset{\sim}{D}}^{n} (\Delta \underset{\sim}{\varepsilon}_{HT}^{n} + \dot{\underset{\sim}{\varepsilon}}_{vp}^{n} \Delta\tau_n) d\Omega + \Delta \underset{\sim}{F}^{n} \tag{5.21}$$

or, in compact form

$$\underset{\sim}{K}^{n} \Delta \underset{\sim}{U}^{n} = \Delta \underset{\sim}{V}^{n} \tag{5.22}$$

in which the stiffness matrix, $\underset{\sim}{K}^{n}$, and the right-hand vector, $\Delta \underset{\sim}{V}^{n}$, are, respectively:

$$\underset{\sim}{K}^n = \int_\Omega \underset{\sim}{B}^T \hat{\underset{\sim}{D}}^n \underset{\sim}{B} d\Omega$$

$$\Delta \underset{\sim}{V}^n = \int_\Omega \underset{\sim}{B}^T \hat{\underset{\sim}{D}}^n (\Delta \underset{\sim}{\varepsilon}^n_{HT} + \dot{\underset{\sim}{\varepsilon}}^n_{vp} \Delta\tau_n) d\Omega + \Delta \underset{\sim}{F}^n \qquad (5.23)$$

In order to evaluate $\hat{\underset{\sim}{D}}^n$, the pseudo-viscoplastic compliance, $\underset{\sim}{H}^n$, which is defined as:

$$\underset{\sim}{H}^n \equiv \frac{\partial \dot{\underset{\sim}{\varepsilon}}^n_{vp}}{\partial \underset{\sim}{\sigma}} \qquad (5.24)$$

must be determined explicitly.

Let the flow vector, $\underset{\sim}{a}$, be defined as ([181]):

$$\underset{\sim}{a} \equiv \frac{\partial F}{\partial \underset{\sim}{\sigma}} \qquad (5.25)$$

then $\underset{\sim}{H}$ can be expressed in terms of $\underset{\sim}{a}$, using the chain rule of differentiation and the definition of $\dot{\underset{\sim}{\varepsilon}}^n_{vp}$, by:

$$\underset{\sim}{H} = \gamma \{ \phi \frac{\partial \underset{\sim}{a}^T}{\partial \underset{\sim}{\sigma}} + \frac{\partial \Phi}{\partial F} \underset{\sim}{a}\underset{\sim}{a}^T \} \quad . \qquad (5.26)$$

As already mentioned, yield criteria in this work are assumed to have the general form: $F = c J_1 + c_2 (J_2')^{\frac{1}{2}}$. By appropriate differentiation of F with respect to $\underset{\sim}{\sigma}$, and after some simple mathematical manipulations one gets:

$$\underset{\sim}{H} = p_i \underset{\sim}{M}_i \quad (i = 1,2,3,4) \qquad (5.27)$$

in which, for plane stress problems:

$$\underset{\sim}{M}_1 \equiv \begin{bmatrix} \frac{2}{3} & -\frac{1}{3} & 0 \\ & \frac{2}{3} & 0 \\ \text{Sym.} & & 2 \end{bmatrix}, \qquad \underset{\sim}{M}_2 \equiv \begin{bmatrix} s^2_{xx} & s_{xy}s_{yy} & 2s_{xx}s_{xy} \\ & s^2_{yy} & 2s_{yy}s_{xy} \\ \text{Sym.} & & 4s^2_{xy} \end{bmatrix}$$

$$\underset{\sim}{M}_3 \equiv \begin{bmatrix} 1 & 1 & 0 \\ & 1 & 1 \\ \text{Sym.} & & 0 \end{bmatrix}, \underset{\sim}{M}_4 \equiv \begin{bmatrix} S_{xx} & S_{xx}+S_{yy} & S_{xy} \\ & S_{yy} & S_{xy} \\ \text{Sym.} & & 0 \end{bmatrix} \tag{5.28}$$

where S_{xx}, S_{yy} etc. denote the deviatoric stress tensor components, and

$$p_1 = \gamma\{\frac{c_2}{2}(J_2')^2 \phi\}$$

$$p_2 = \gamma\{\frac{4c_2}{2}(J_2')^{-1}[c_2\frac{\partial\phi}{\partial F} - (J_2')^{-\frac{1}{2}}\phi]\}$$

$$p_3 = \gamma\{c_1^2\frac{\partial\phi}{\partial F}\}$$

$$p_4 = \gamma\{c_1c_2(J_2')^{-\frac{1}{2}}\frac{\partial\phi}{\partial F}\} \tag{5.29}$$

A spatial approximation of the equilibrium equation is obtained by finite-strip formulation of the displacements u and v, in the x and y directions respectively, as follows:

$$u \sim \tilde{u} = u_i^m(\tau)N_i(\xi)Y^m(\eta)$$

$$v \sim \tilde{v} = v_i^m(\tau)N_i(\xi)Z^m(\eta) \tag{5.30}$$

where N_i are local trial functions, $Y^m(\eta)$ and $Z^m(\eta)$ are global trial functions, and u_i^m and v_i^m are the approximated values at the i-th nodal point, corresponding to the m-th global trial function. The global trial functions are given by:

$$Y^m(\eta) = \cos(\mu_m\eta)$$

$$Z^m(\eta) = \sin(\mu_m\eta) \tag{5.31}$$

where

$$\mu_m = \frac{m\pi}{2} \qquad (m = 1,2,\ldots,M) \tag{5.32}$$

The above approximations assure that essential boundary conditions are satisfied. Substitution of equations 5.30 into 5.22 yields:

$$\bar{\underset{\sim}{K}}\Delta\underset{\sim}{d} = \Delta\bar{\underset{\sim}{V}} \tag{5.33}$$

where

$$\underset{\sim}{d}^T = [(\underset{\sim}{d}^1)^T, (\underset{\sim}{d}^2)^T, \ldots, (\underset{\sim}{d}^m)^T, \ldots, (\underset{\sim}{d}^M)^T] \tag{5.34}$$

and

$$(\underset{\sim}{d}^m)^T = [u_1, v_1, u_2, v_2, \ldots, u_i, v_i, \ldots, u_I, v_I]^m \tag{5.35}$$

The stiffness matrix, $\bar{\underset{\sim}{K}}$, has the structure represented by the matrix $\underset{\sim}{A}$, eq. 5.9, but in eq. 5.33 the submatrix $\bar{\underset{\sim}{K}}^{ij}$ is calculated by

$$\bar{\underset{\sim}{K}}^{ij} = \int_\Omega (\underset{\sim}{B}^i)^T \hat{\underset{\sim}{D}} \underset{\sim}{B}^j \, d\Omega \tag{5.36}$$

The vector of incremental pseudo loads, for the next time-step, is calculated with the equation:

$$\Delta\underset{\sim}{V}^{n+1} = \int_\Omega \underset{\sim}{B}^T \hat{\underset{\sim}{D}}^{n+1} (\Delta\underset{\sim}{\varepsilon}_{HT}^{n+1} + \dot{\underset{\sim}{\varepsilon}}_{vp}^{n+1} \Delta\tau_n) d\Omega + \Delta\underset{\sim}{F}^{n+1} + \underset{\sim}{R}^{n+1} \tag{5.37}$$

where the residual out-of-balance vector force is defined by:

$$\underset{\sim}{R}^{n+1} \equiv \int_\Omega \underset{\sim}{B}^T \underset{\sim}{\sigma}^{n+1} d\Omega - \underset{\sim}{F}^{n+1} \tag{5.38}$$

6. Results and Discussions

6.1 - Reliability of the mathematical model

Preliminary experiments have shown that the elasto-viscoplastic response of the FM-73 polymer layer can be divided into three main ranges: elastic behavior at stress levels below 5 MPa, primary creep - between 5 and 37 MPa, and secondary creep - above 37 MPa. The values of the visco-plastic parameters - fluidity, γ, and power constant, N - were determined through curve-fitting to the experimental results obtained for the two viscoplastic ranges and, as shown in Figure 26, good correlation was achieved.

The reliability of the numerical solutions was tested by applying the present approach to a wide class of problems which also have other independent numerical or analytical solutions. Here, the authors' main aim was to find the optimal number of strips and global trial functions needed to assure good numerical approximations to the solution of a wide variety of problems. As a first step, the uncoupled diffusion equation was solved for the steady state case with constant coefficients. The solution was compared with well known analytical solutions [19]. In the case referred to the global trial functions in the η direction coincide with the eigenfunctions. Hence, the spatial convergence in the ξ direction can be examined by itself. Eq.(4.13) is of a singular perturbation type, since the highest derivative in the η direction is multiplied by the small parameter, ψ. Thus, as $\psi \to 0$, the interior solution approaches that of the

one-dimensional problem in the ξ direction. For the time-dependent, one-dimensional problem with nonlinear coefficients, analytical solutions are available [26].

Next, the convergence of the present solution with that of the uncoupled linear equilibrium equations, with either a uniform traction loading or a uniform temperature distribution was examined. For the cases of uniform loading either mechanical or thermal as well as for the case of the diffusion equation, in which the diffusivity is function only of ξ, the solution is composed of M uncoupled solutions i.e. the coefficient matrices are of the block diagonal type. Here, the effect of the error introduced by the numerical quadrature can be thoroughly examined. The numerical solution of the uncoupled linear equilibrium equations, for the case of uniform temperature distribution in the NSD model, was compared with the solution based on the classical theory of laminated plates.

Finally, the convergence of the fully coupled nonlinear case was examined. The spatial discretizations are shown in Fig.27. It was found that, in this case (Fig.28) as well as in the previously described cases, a numerical solution based on six strips gives accurate results.

The convergence of the time discretization was tested by comparing results obtained after the same total periods of time but by different time step increments ($\Delta\tau = 2.10^{-3}$ to 10^{-1}). The solutions were found to be unconditionally stable for $\theta > \frac{1}{2}$, and the maximum deviation between them was less

than 0.5 per cent. The character of the processes for longer periods of time is much smoother and thus even more stable and consistent.

A comparison between experimental and theoretical results for the stress dependency of the dimensionless diffusivity is shown in Fig.29. Experimental results were derived from absorption tests under various constant compressive and tensile stresses as described in section 3. FSM results were obtained from successive solutions, compressive or tensile stresses having been imposed on the specimens at constant moisture and temperature. From every solution the RRV was computed, while the value of the constant λ_D, for the relation, $\frac{D(\tau)}{D_o} = 1 + \lambda_D V_R$, was fitted only for the linear relation zone (small stresses). The good correlation shown in Fig.29 implies that the physical basis of the RRV assumption is reasonably solid.

6.2 - Numerical vs. experimental results

6.2.1: thick adhesive NSD model

The temperature distribution along the specimen, at several points of time, is shown in Fig.30. A uniform initial condition has been assumed for the present problem. In order to prevent the physically unrealistic discontinuities at the free edges, initial conditions were smoothed. By using the first four harmonics, the solution behavior can be reconstructed. The temperature distribution across the NSD specimen's thickness at several points of time are shown in Fig.31. Since the thermal diffusivity of aluminum is 3

orders of magnitude greater than that of FM-73, the temperature distribution in the former approaches steady-state more rapidly than in the latter. The pronounced temperature differences created may thereby have a significant effect on the overall stresses and deformations, especially when the viscoplastic behavior of the polymeric layer is considered.

The numerical prediction of the central deflection as a function of time, for different values of moisture diffusion coefficients, is presented in Fig.32. The best correlation with experimental results is obtained for $D_o = 2.5 \cdot 10^{-5}$ mm^2/min. Using this value of D_o, several numerical solutions for the central deflection vs. time, in two different specimens, are shown in Fig.33, and these results are compared with the experimental findings described in Section 3. The FSM solutions, with and without the moisture-stress coupling effect, appear as the dashed and the solid lines, respectively. The coupling effect tends to improve the correlation between numerical and experimental results. This improvement is attributable to the fact that the rate of diffusion is reduced, since the exposed polymeric strip is under compression, so that the rates of swelling and of straightening is also reduced. It should be pointed out that the direction of the coupling effect changes in the T-1 series after about fifteen days. This may be ascribed to the change in the direction of the curvature (Fig.34), which indicates that tensile stresses are prevailing in the outer polymeric strips (Fig.35).

moisture concentration profiles are shown in Fig.35. The average moisture concentration vs. time is shown in Fig.36. For comparison, experimental results are also presented. The improvement in correlation due to the use of coupled effects is clearly demonstrated.

6.2.2: thin adhesive NSD model behavior

Next, a preliminary investigation of 3-layers NSD specimens is presented. The model is composed of a 0° graphite/epoxy layer which glues to 90° graphite/epoxy layer by means of a thin layer of FM 73 epoxy adhesive (Fig.37)*. The numerical solution of this case is based on the same procedure described in section 5.

The main objective is to examine the response of the specimen due to the viscoplastic behavior of the FM 73 adhesive. Therefore, for simplicity, the following assumptions have been added:

1. Each lamina is described by a macroscopically homogeneous orthotropic material. The material is linearly elastic under a generalized Hooke's law.

2. A 2-D stress field is still prevailed in the x-y plane.

3. The problem is uncoupled, namely, the equilibrium equations are solved for given temperature and moisture distributions.

4. The mechanical loading is represented by either a uniform stretching along the y direction or by a pure moment, along z direction, achieved through a couple of forces employed at the "far" edge.

---

* The mechanical and hygro and thermo elastic parameters of the graphite/epoxy and FM 73 adhesive age given in Table 6.

The specimen is loaded according to the following stages:

1. A uniform thermal loading ($\Delta T = -100°C$, $\Delta C = 0$)

2. A given ΔC distribution through the thickness (see Fig.38).

3. A mechanical loading which tends to straighten the deformed specimen.

Numerical results of time dependency of axial stress (σ_y) distribution through the adhesive thickness are shown in Figs. 39-44. The effects of uniform changes of temperature, moisture, axial load and moment on the stress field vs. time functions indicate the following:

- in all cases relaxation process in the adhesive layer is fast and stresses tend to relax to their stable state in a time scale of less than a minute;
- moisture tends to reduce significantly the tensile stresses in the adhesive even in cases of mechanical tensile loading;
- in all cases, variation of axial stresses within the adhesive is small and linear.

The present approach can be directly applied to the analysis of interlaminar failures. In the present problem, the governing equations are of the singular perturbation type. Hence, for small values of the aspect ratio, ψ, it becomes increasingly difficult to solve these equations numerically. Several methods that use singular perturbation theories to improve the accuracy and efficiency of the numerical solution have recently been developed ([20] - [22]). Incorporation of the present approach into those schemes can yield significant improvements for cases of small aspect ratios.

7. Conclusions

Based upon experimental results and numerical solutions of the diffusion and equilibrium equations, the following main conclusions can be drawn:

7.1 - The rate of moisture diffusion depends on the Relative Reduced Volume (RRV) - the rate increases with a rise in the RRV due to tensile stress and decreases due to compressive stress, and hygroscopic swelling.

7.2 - The coupling effect between moisture diffusion and mechanical behavior was determined quantitatively. This effect is pronounced whenever the polymeric phases are the major constituent, as in composites and in thick adhesive layers.

7.3 - The mutual effect between moisture, temperature, and mechanical behavior, was formulated mathematically. The simultaneous solution of the nonlinear coupled diffusion and equilibrium equations provides an insight into the system which may reveal an extreme situation in transition phenomena.

7.4 - The good correlation that was obtained between experimental and numerical results implies that the proposed model and approach are capable of describing these complex phenomena, which are characterized by a pronounced nonlinearity and by time dependency.

7.5 - The finite strip method was found to be an accurate and efficient tool for the solution of such equations.

7.6 - The present study was mainly confined to the nonlinear analysis of two material systems. However, it can be extended to the prediction of the behavior up to failure of any multimaterial anisotropic laminates.

8. Suggestions for future work

8.1 - Analytical study and experimental investigation of the the effects of hygrothermal variables on failure and strength of the bonded system.

8.2 - Investigation of the effect of thermal and humidity fluctuations (environmental cycling) on stresses and strength of the bonded system.

8.3 - Extension of the 2-D analytical solution given in the present report into 3-D analysis which is mainly applicable at the free edges.

8.4 - Application of the present approach and results into the analysis of interlaminar behavior of composite laminates.

9. Publications based on present work

9.1 - G. Yaniv and O. Ishai, Coupling Between Stresses and Moisture Diffusion in Polymeric Adhesives (accepted to be published in: Polymer Engineering and Science Journal, 1986).

9.2 - P. Bar-Yoseph, G. Yaniv and O. Ishai, The Interdependence of Hygrothermal Processes and Elasto-Viscoplastic Behavior in Polymer-Dominated Multi-Material Systems (submitted to International J. of Solids and Structures).

References

1. O. Gilat and S. S. Broutman, Effect of an External Stress on Moisture Diffusion and Degradation in Graphite-Reinforced Epoxy Laminates, Advanced Composite Materials - Environmental Effects, ASTM, STP-658, J. R. Vinson, ed., pp 61-83 (1978).

2. G. Marom and L. J. Broutman, Moisture Penetration into Composites under External Stress, Polymer Composites, 2, 3, pp 132-136 (July 1981).

3. A. A. Fahmy and J. C. Hurt, Stress Dependence of Water Diffusion in Epoxy Resin, Polymer Composites, 1, 2, pp 77-80 (Dec. 1980).

4. G. C. Sih and M. T. Shih, Hygrothermal Stresses in Plastics Subjected to Antisymmetric Time-Dependent Moisture and Temperature Boundary Conditions, J. Thermal Stresses, 3, pp 321-340 (1980).

5. G. C. Sih, M. T. Shih and S. C. Chou, Transient Hygrothermal Stresses in Composites: Coupling of Moisture and Heat with Temperature Varying Diffusivity, Int. J. Eng. Sci., 18, pp 19-42 (1980).

6. O. Ishai, S. Gali and G. Yaniv, Durability of Structural Adhesively Bonded Systems, Technical Report for U.S. Army, Contract No. DAJA 37-80-C-0303, 114 (1981).

7. A. M. Merzer, Modeling of Adiabatic Shear Band Development from Small Imperfections, J. Mechanics and Physics of Solids, 30, 5, pp 323-338 (1982).

8. A. S. Argon and M. I. Bessonov, Plastic Flow in Glassy Polymers, Polymer Engng. and Science, 17, 3, pp 174-182 (March 1977).

9. T. J. Chung and R. J. Bradshaw, Irreversible Hygrothermomechanical Behavior and Numerical Analysis in Anisotropic Materials, J. Composite Materials, 15, pp 502-520 (Nov. 1981).

10. G. S. Springer (ed.), Environmental Effects on Composite Materials, Technomic, 1 (1981).

11. G. S. Springer (ed.), Environmental Effects on Composite Materials, Technomic, 2 (1984).

12. W. Althof, The Diffusion of Water Vapour in Humid Air into the Bondlines of Adhesive Bonded Metal Joints, SAMPE-T.C., 11 (1979).

13. F. W. Crossman, R. E. Mauri and W. J. Warren, Hygrothermal Damage Mechanisms in Graphite-Epoxy Composites, NASA, CR-3189, CNASL-9563, 155 (Dec. 1979).

14. J. M. Whitney and C. E. Browning, Some Anomalies Associated with Moisture Diffusion in Epoxy Matrix Composite Materials, Advanced Composite Materials - Environmental Effects, ASTM, STP-658, J. R. Vinson, ed., pp 43-60 (1978).

15. A. S. Argon and M. I. Bessonov, Plastic Flow in Glassy Polymers, Polymer Engng. and Science, 17, 3, pp 174-182 (March 1977).

16. H. Parkus, Thermoelasticity, Springer-Verlag Pub., Wien (1976).

17. T. J. R. Hughes, Unconditionally Stable Algorithms for Nonlinear Heat-Conduction, Computer Methods in Applied Mechanics and Engng., 10, pp 135-139 (1977).

18. D. R. J. Owen and E. Hinton, Finite Elements in Plasticity - Theory and Practice, Pineridge Press Ltd., Swansea, UK (1980).

19. J. Crank, The Mathematics of Diffusion, Oxford University Press, London (1979).

20. P. Bar-Yoseph, On the Accuracy of Interlaminar Stress Calculation in Laminated Plates, Computer Methods in Applied Mechanics and Engineering, 36, 3, pp 309-329 (1983).

21. P. Bar-Yoseph and G. Siton, The Effect of Material Nonlinearity on the Interlaminar Stress Field in Composite Laminates, Computers and Structures (1984 - in press).

22. P. Bar-Yoseph and M. Israeli, The Asymptotic Finite Element Method for Boundary Value Problems, Invited Chapter in Recent Advances in Numerical Methods in Fluids - Vol. V, Numerical Techniques for Fluid Flows (Taylor, C., Johnson, J. A., and Smith, R. eds.), Pineridge Press, Swansea (1984).

Glossary

A - stiffness matrix components

a - strip length (FSM solution)

$\underset{\sim}{a}$ - flow vector

B - stiffness matrix components

C - moisture concentration

c - strength theory coefficients

D - moisture diffusion coefficient

d - displacement vector

E - elastic modulus

F - effective, equivalent stress

f - external tractions vector

G - shear modulus

h - width, thickness

J_i - stress invariants

K - thermal conductivity

ℓ - length

M - relative moisture content (weight)

m - moisture weight

N_i - local trial functions

p - compliance matrix components

R - residual diffusion equations

S_{ij} - deviatoric stress tensor components

S_R - relative reduced surface

T - temperature

t - time

U - physical variable

u - displacement vector (x-direction)

V_R - relative reduced volume

v - displacement vector (y-direction)

W - dissipative work

W_d - weight of dry material

w - displacement vector (z-direction)

X - basis function (x-direction)

Y^m - global trial function

Z^m - global trial function

α - thermoelastic expansion coefficient

β - hygroelastic expansion coefficient

γ - fluidity coefficient

Γ - region bound

δ - central displacement

ε - strain tensor

η - non-dimensional coordinate (x-direction)

θ - numerical summation parameter

κ - strain hardening coefficient

λ - compressive-tensile strength ratio

λ_i - temperature, moisture, viscoplastic work coupling coefficients

λ_D - stress-moisture coupling coefficient

μ_m - m-term argument

ξ - non-dimensional coordinate (in x-direction)

ρ - density

σ - stress tensor

τ - normalized time

ϕ - flow function

ψ - strip length to width ratio

Ω - problem range

Abbreviations

CFRP - carbon fiber reinforced plastics

FEM - finite element method

FSM - finite strip method

HT - hygrothermal

HOT - higher order term

NSD - non symmetrical doubler

RMC - relative moisture content

RRS - relative reduced surface

RRV - relative reduced volume

RT - room temperature

VE - viscoelastic

VP - viscoplastic

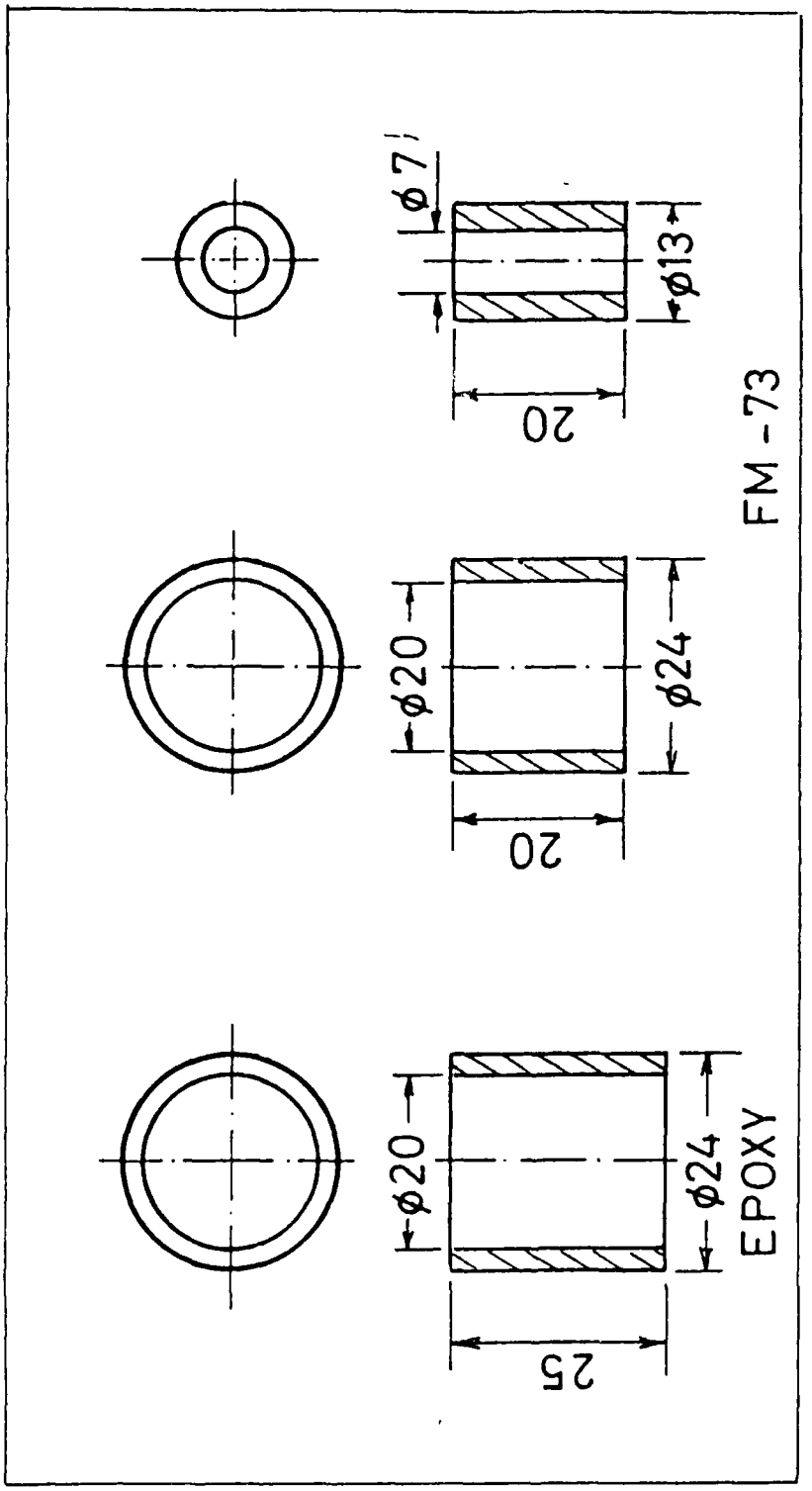

Fig. 1 Specimen configurations for moisture absorption experiment under compressive load. (Dimensions in mm)

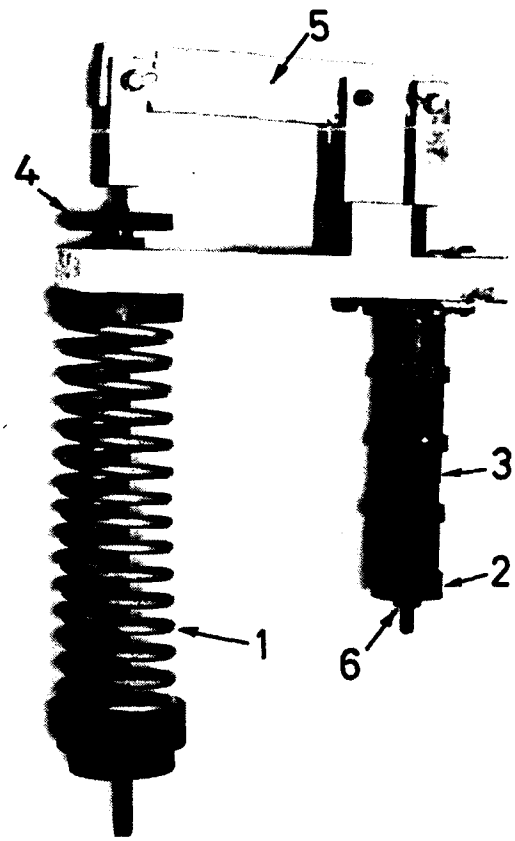

Fig. 2 Mechanical loading device for moisture absorption in compressive loading test

1 - loading spring
2 - loading disc
3 - specimen
4 - load lock nut
5 - loading arm
6 - specimen removal nut

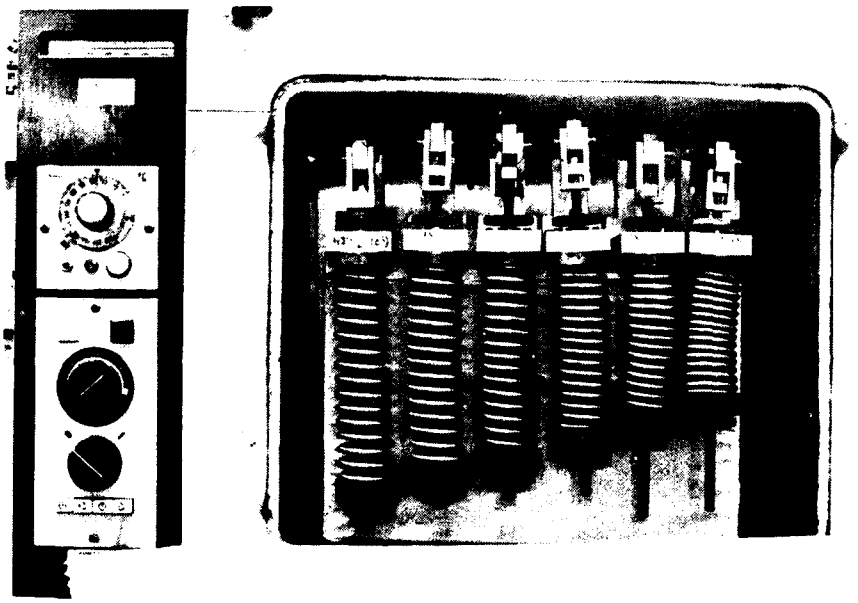

Fig. 3 Compressive test assembly

(for details see Fig. 2).

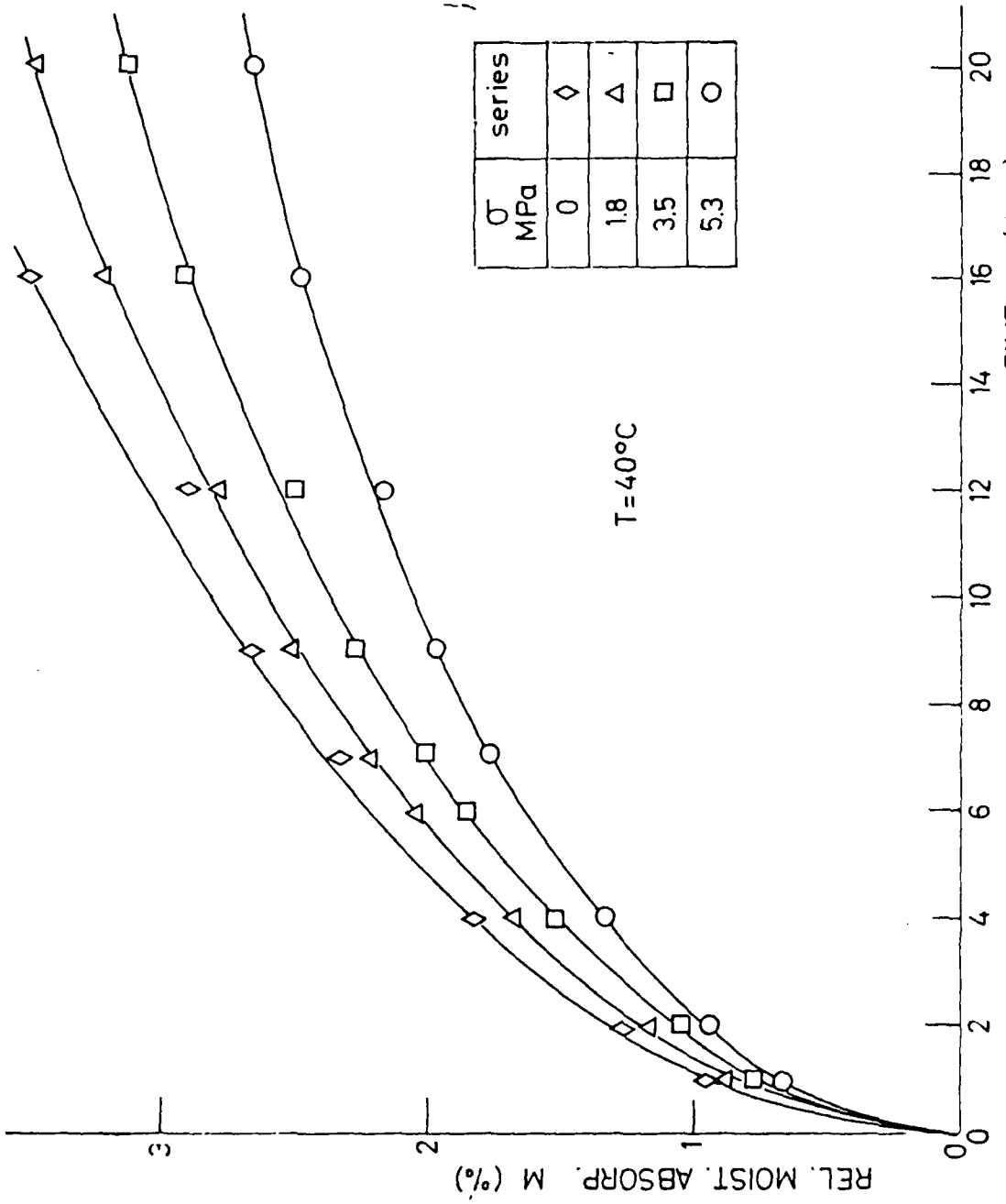

Fig. 4 Relative moisture concentration vs. time for epoxy specimens under different compressive loadings

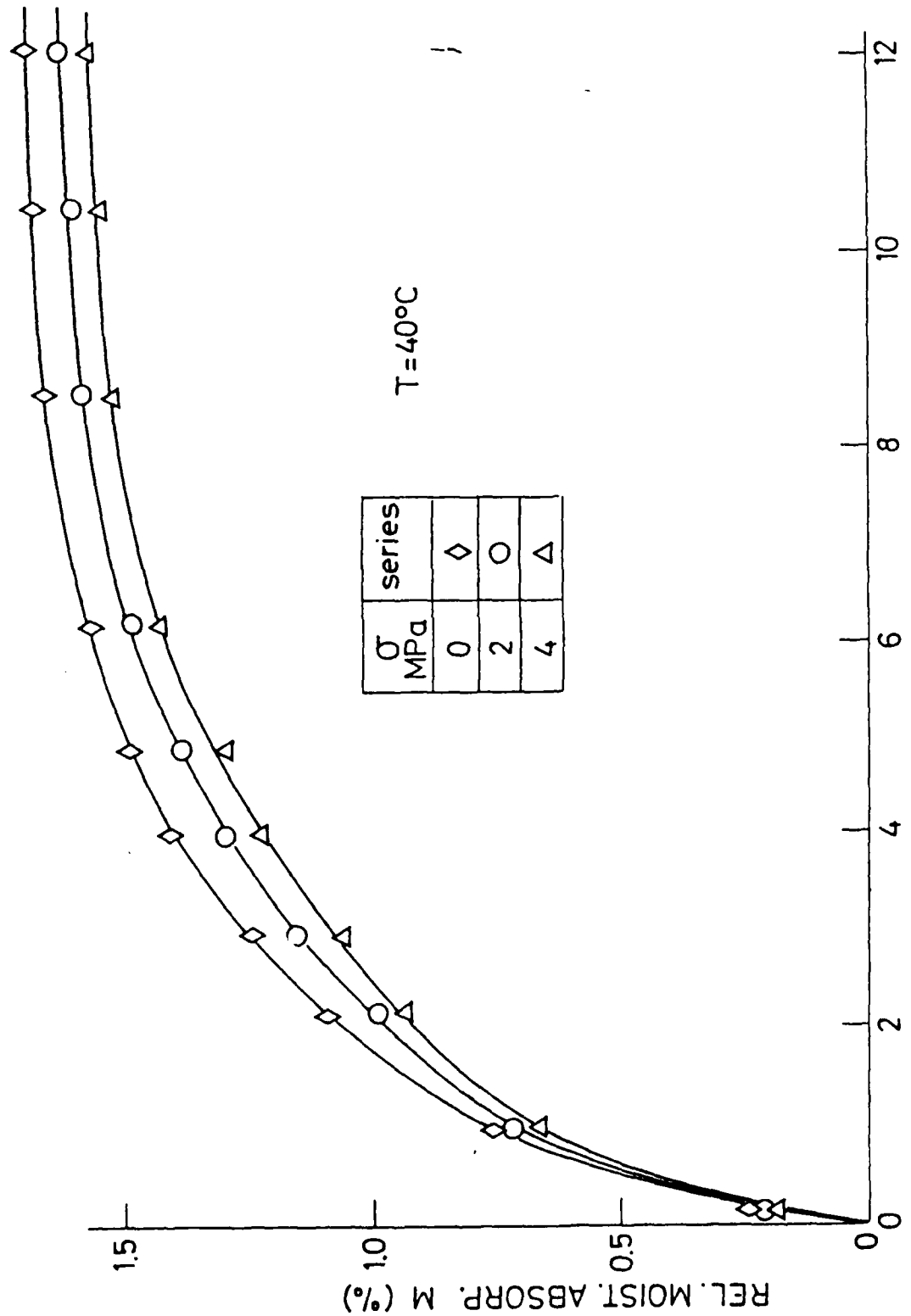

Fig. 5 Relative moisture concentration vs. time for FM-73 specimens under low compressive loadings

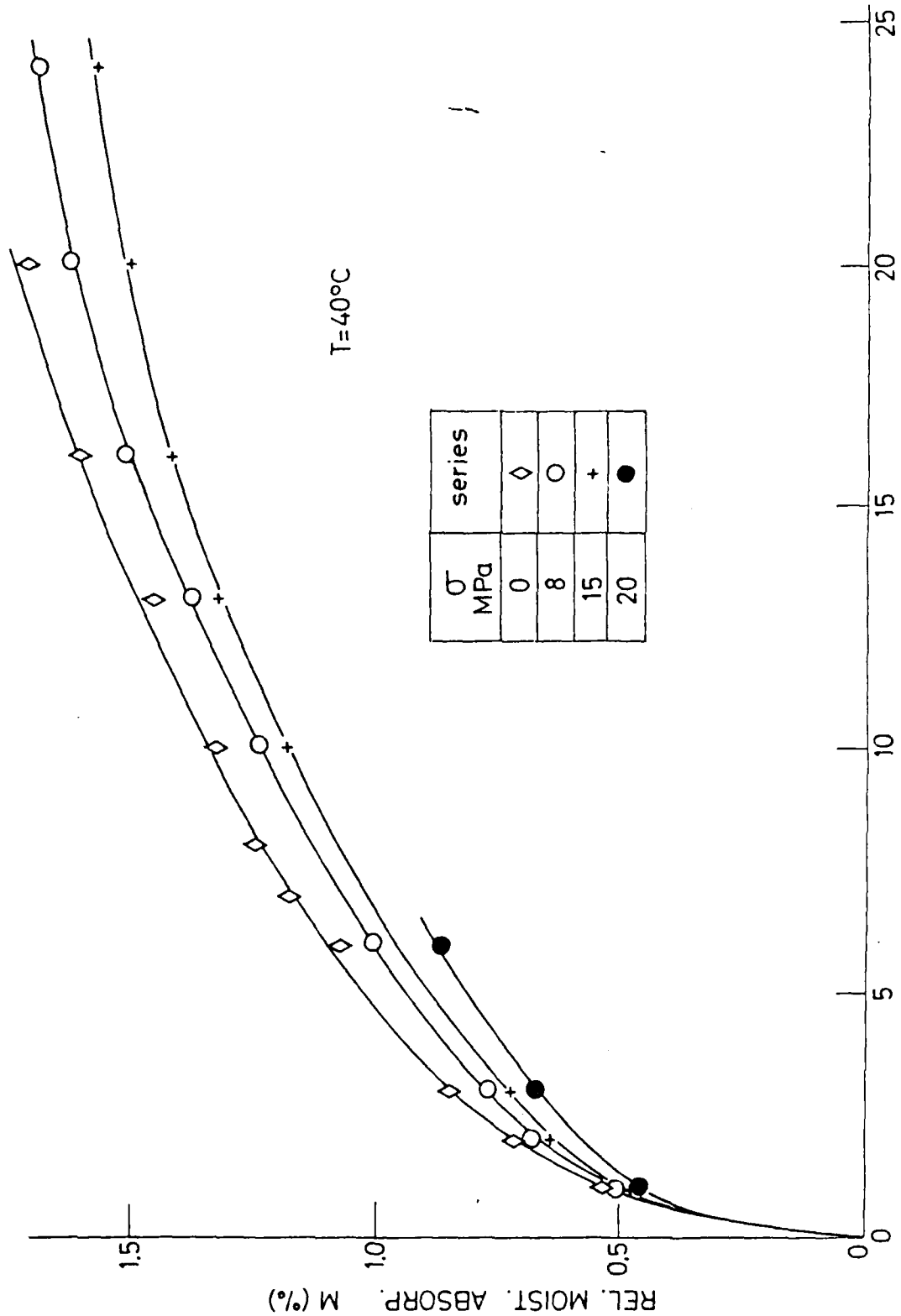

Fig. 6 Relative moisture concentration vs. time for FM-73 specimens under high compressive loadings

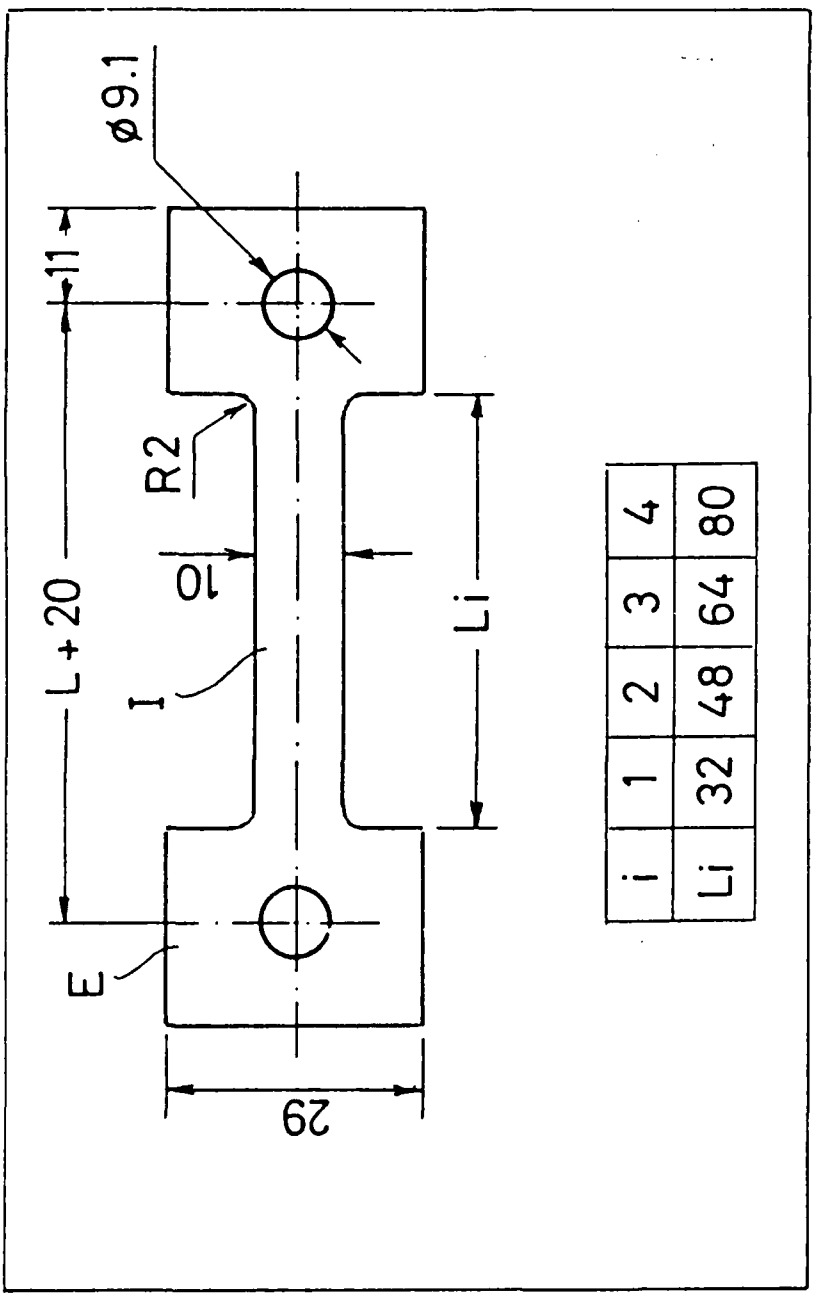

Fig. 7 Specimen configurations for moisture absorption experiment under tensile load. (Dimensions in mm)

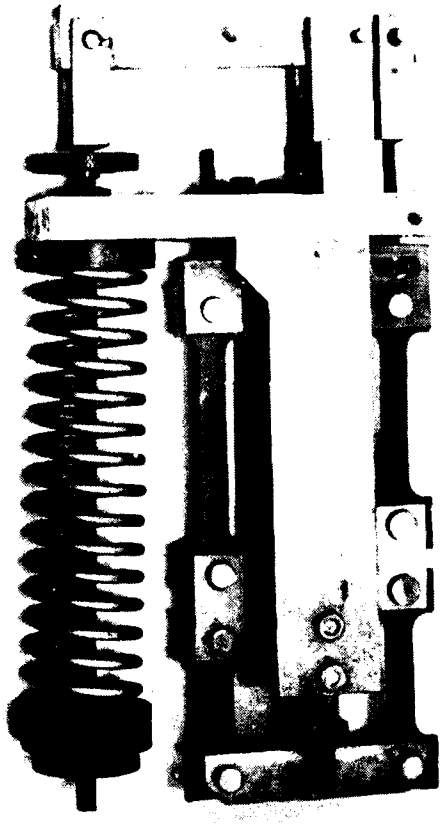

Fig. 8 Mechanical loading device for moisture absorption in tensile loading test (see Fig. 2).

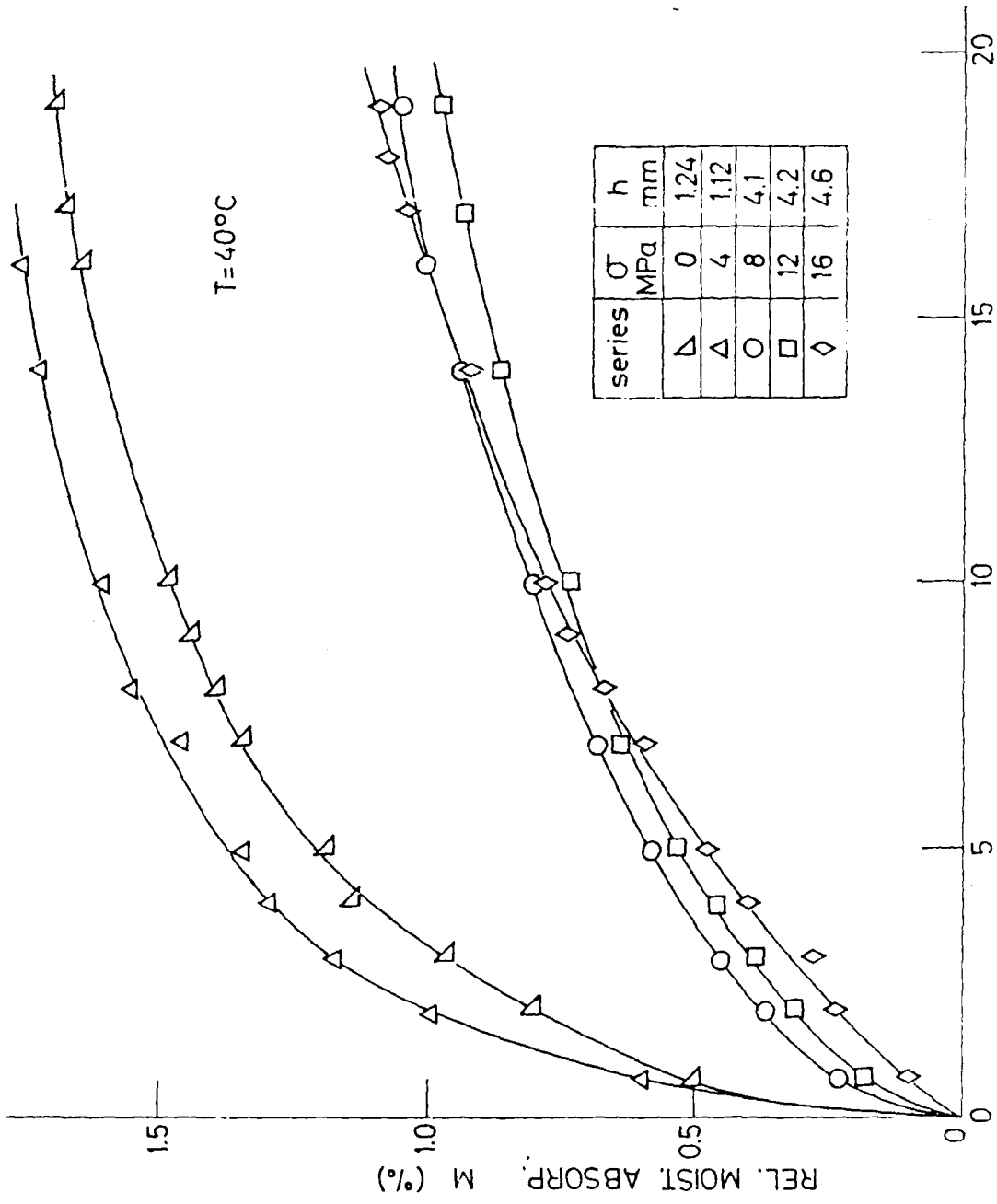

Fig. 9 Relative moisture concentration vs. time for FM-73 specimens under different tensile loadings

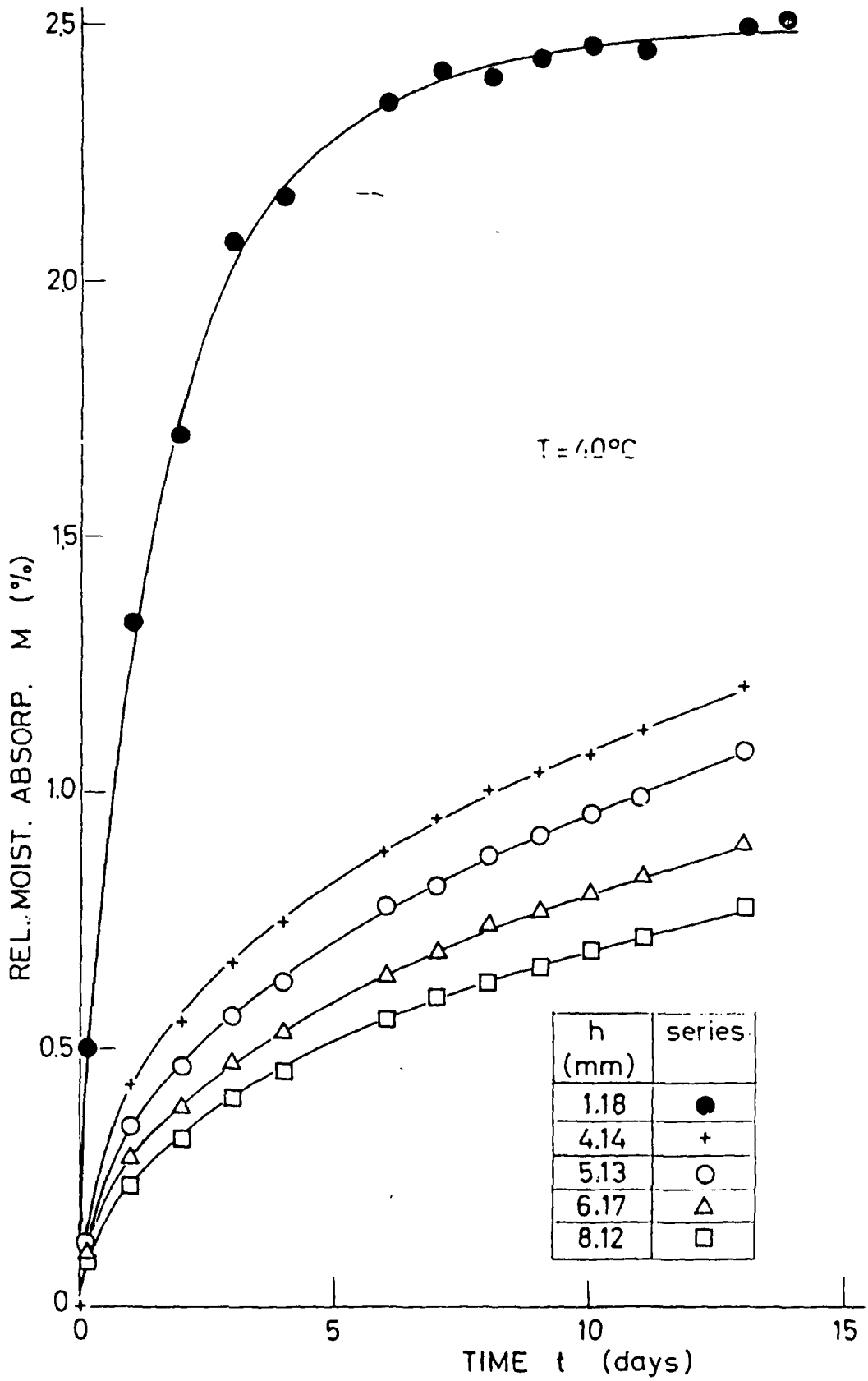

Fig. 10 Relative moisture concentration vs. time for stress-free FM-73 specimens with different thicknesses

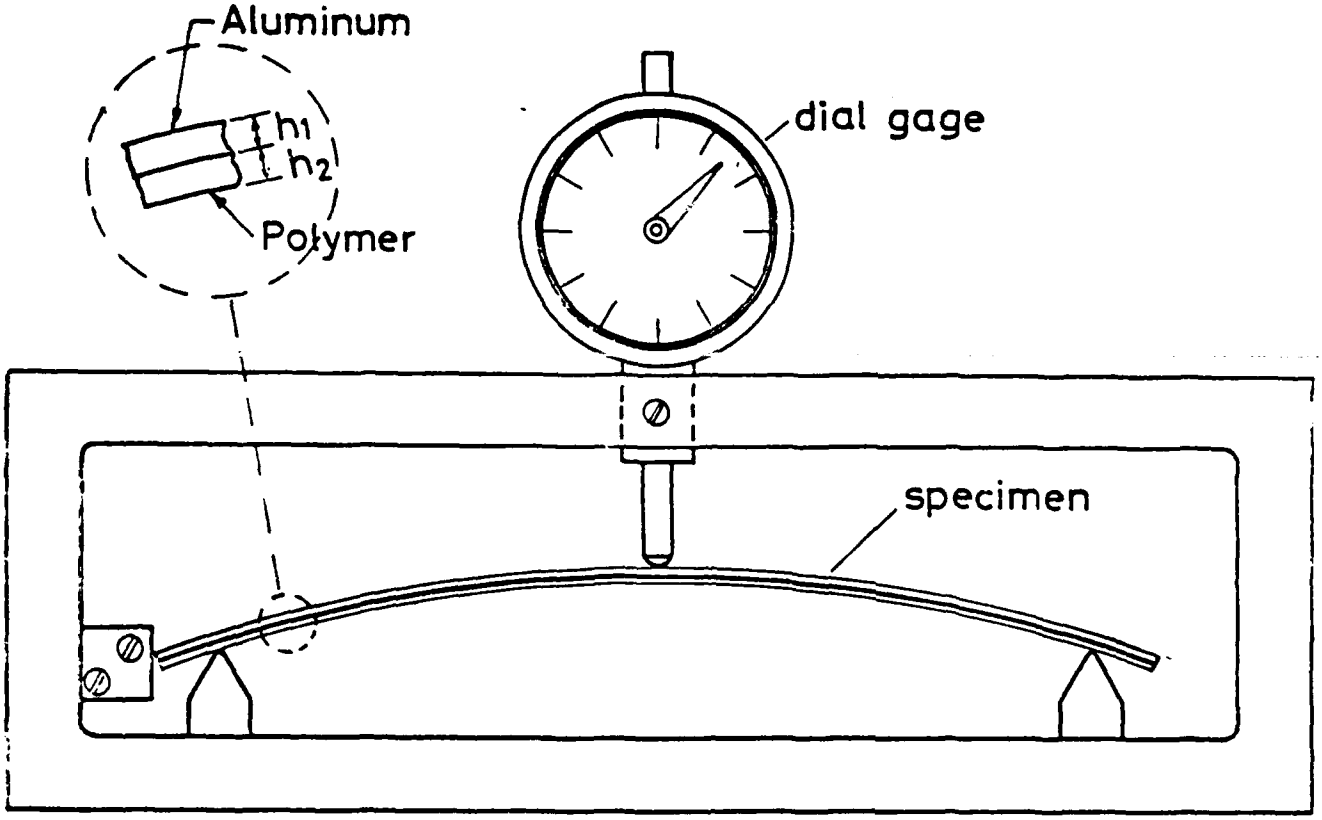

Fig. 11 Device for measuring variations in central flexural displacement of bonded specimens during H.T.exposures

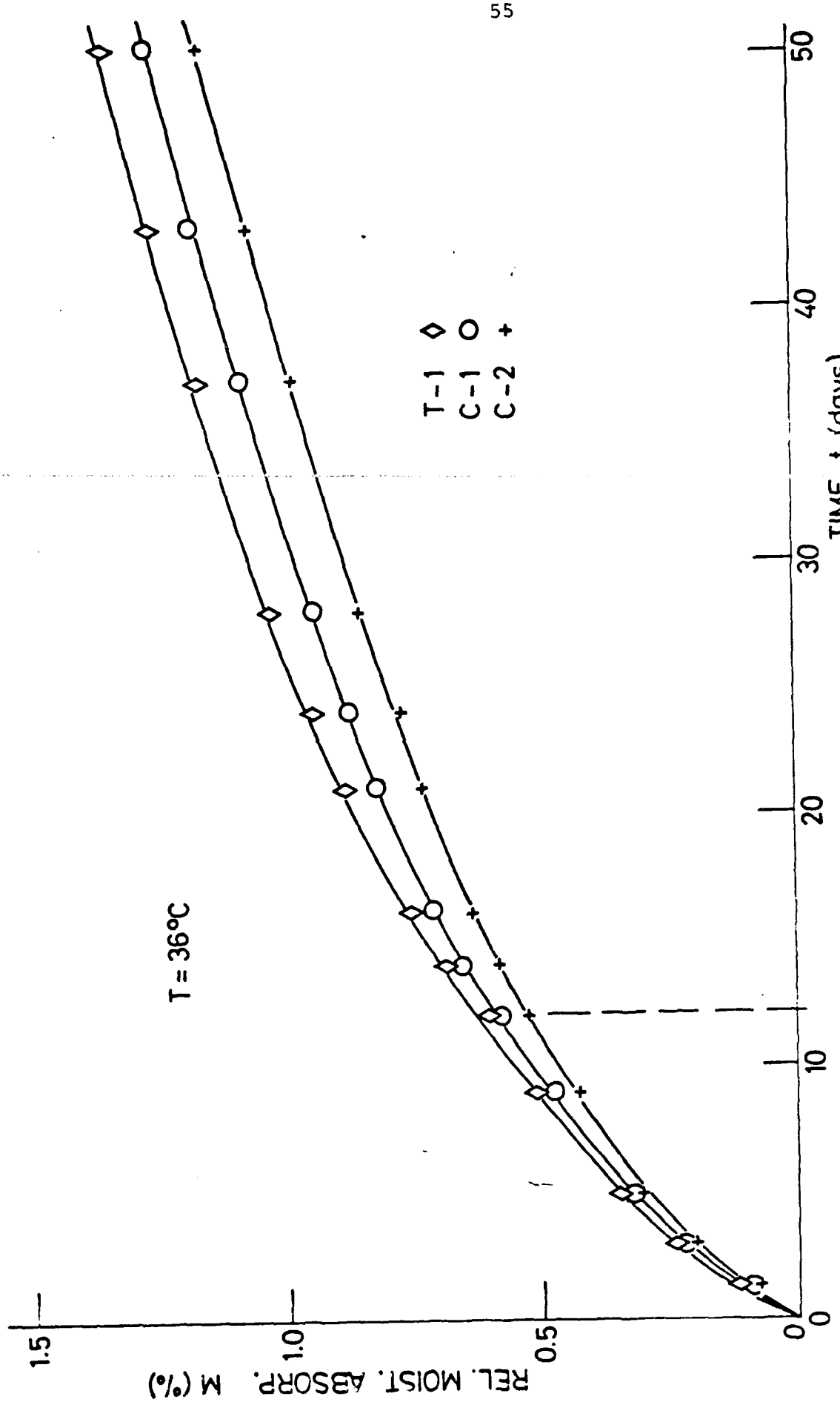

Fig. 12 Relative moisture concentration vs. time for NSD specimens (Aluminum & FM-73)

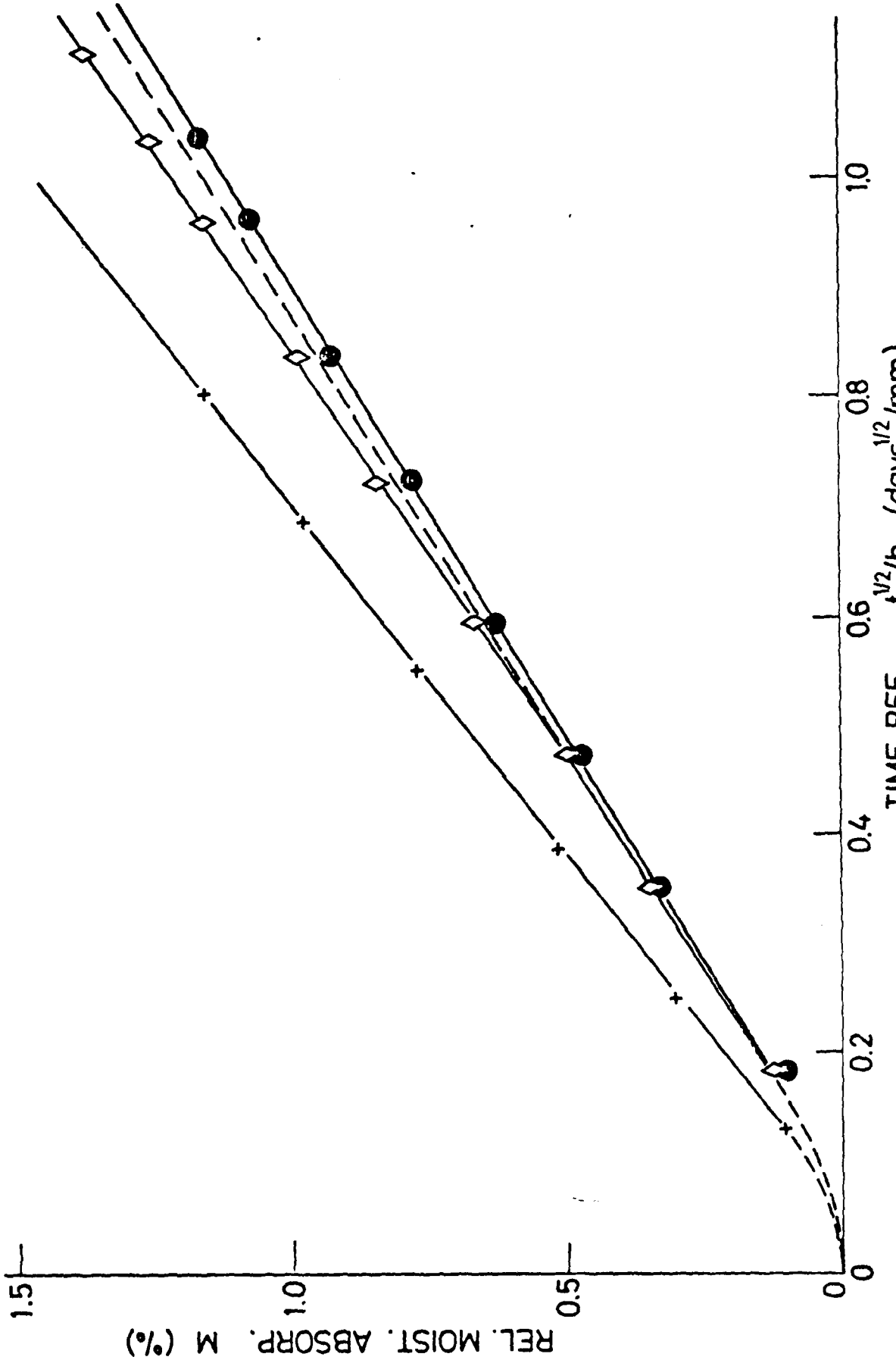

Fig. 13 The effect of material-heterogenity restraint on moisture absorption of NSD specimens (Diffusivity variations)

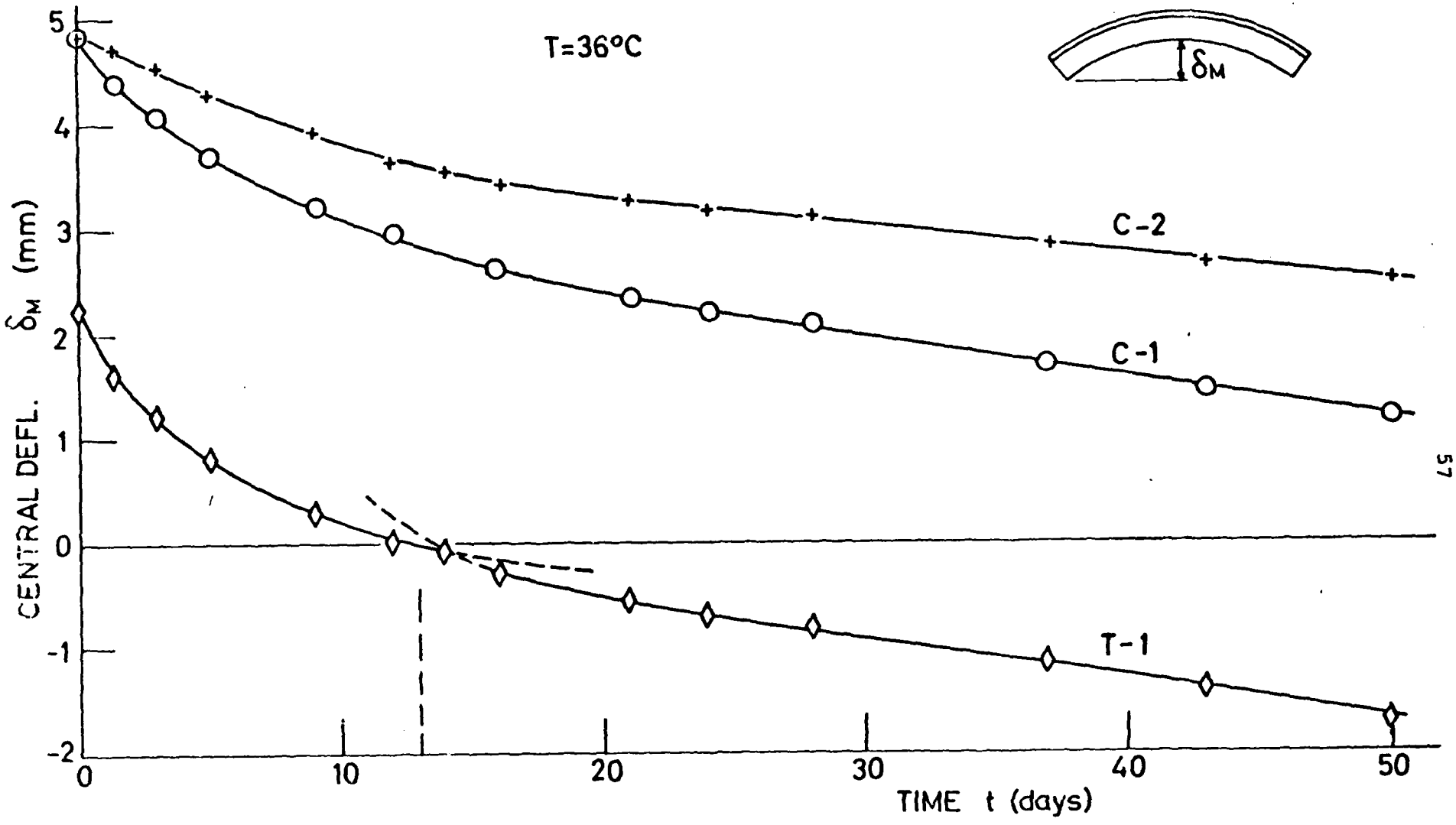

Fig. 14 Central deflection vs. time of NSD specimens (Aluminum & FM-73)

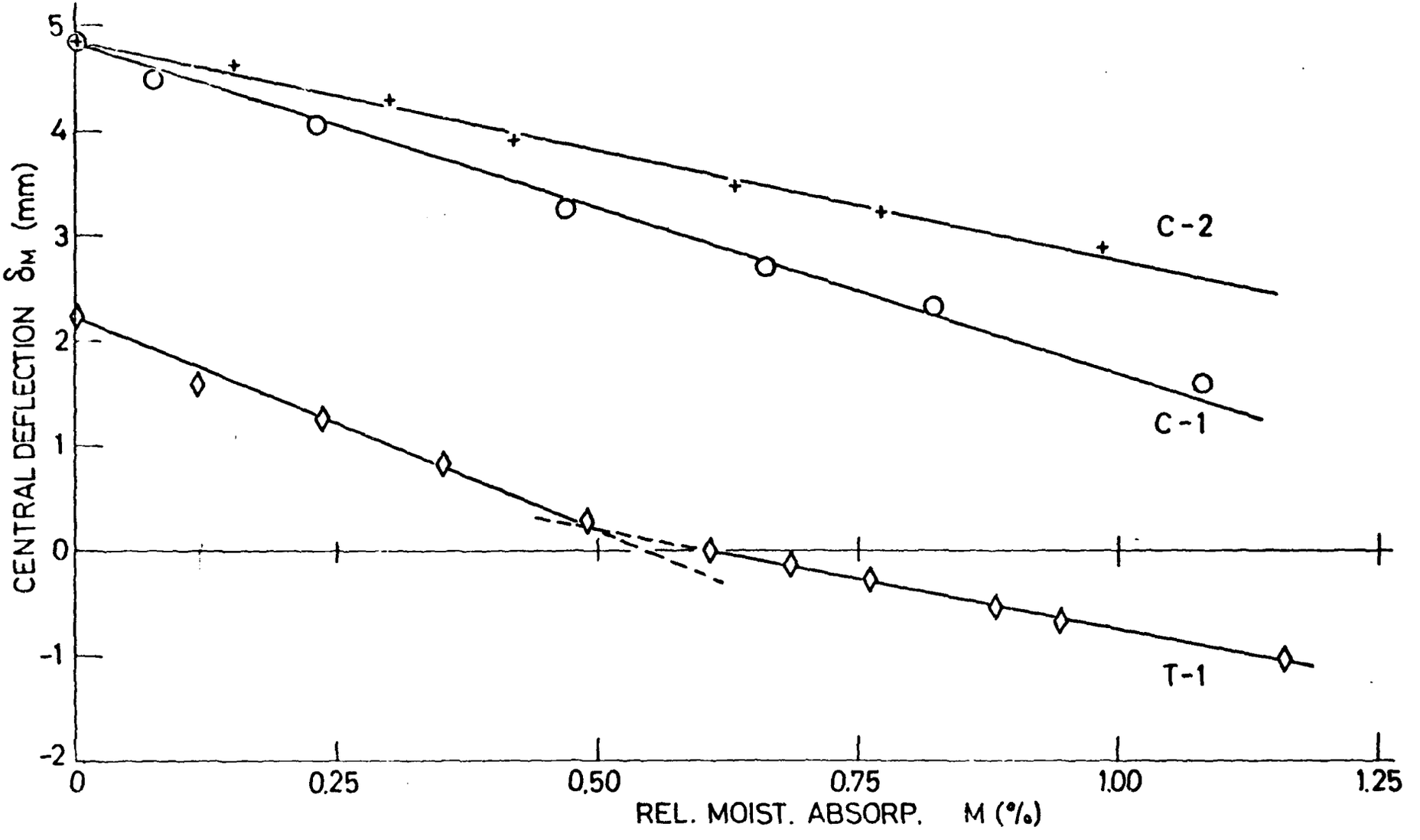

Fig. 15 Central deflection vs. relative moisture content of NSD specimens (Aluminum & FM-73)

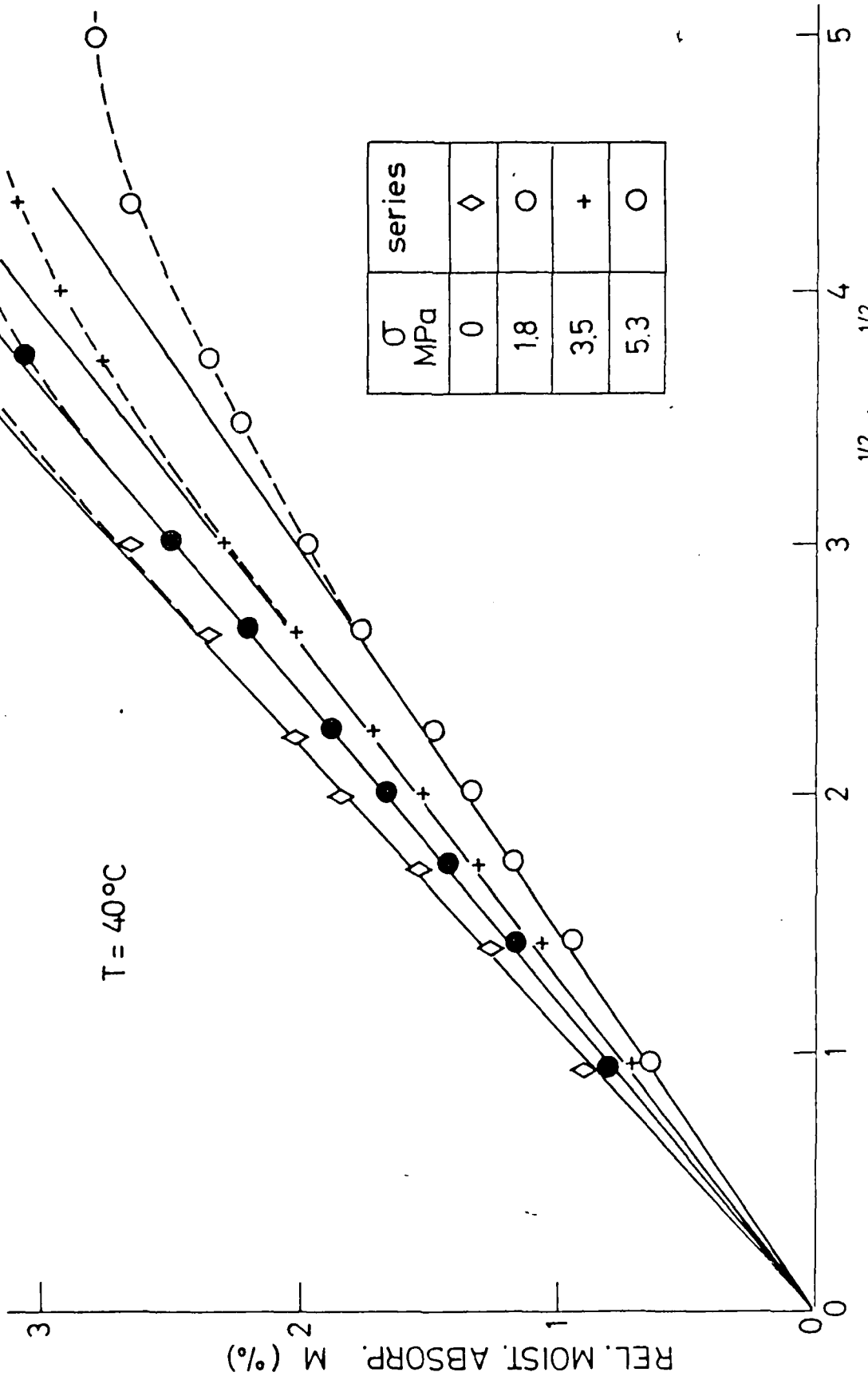

Fig. 16 Compressive load effect on relative moisture absorption (Diffusion coefficient variation), epoxy specimens

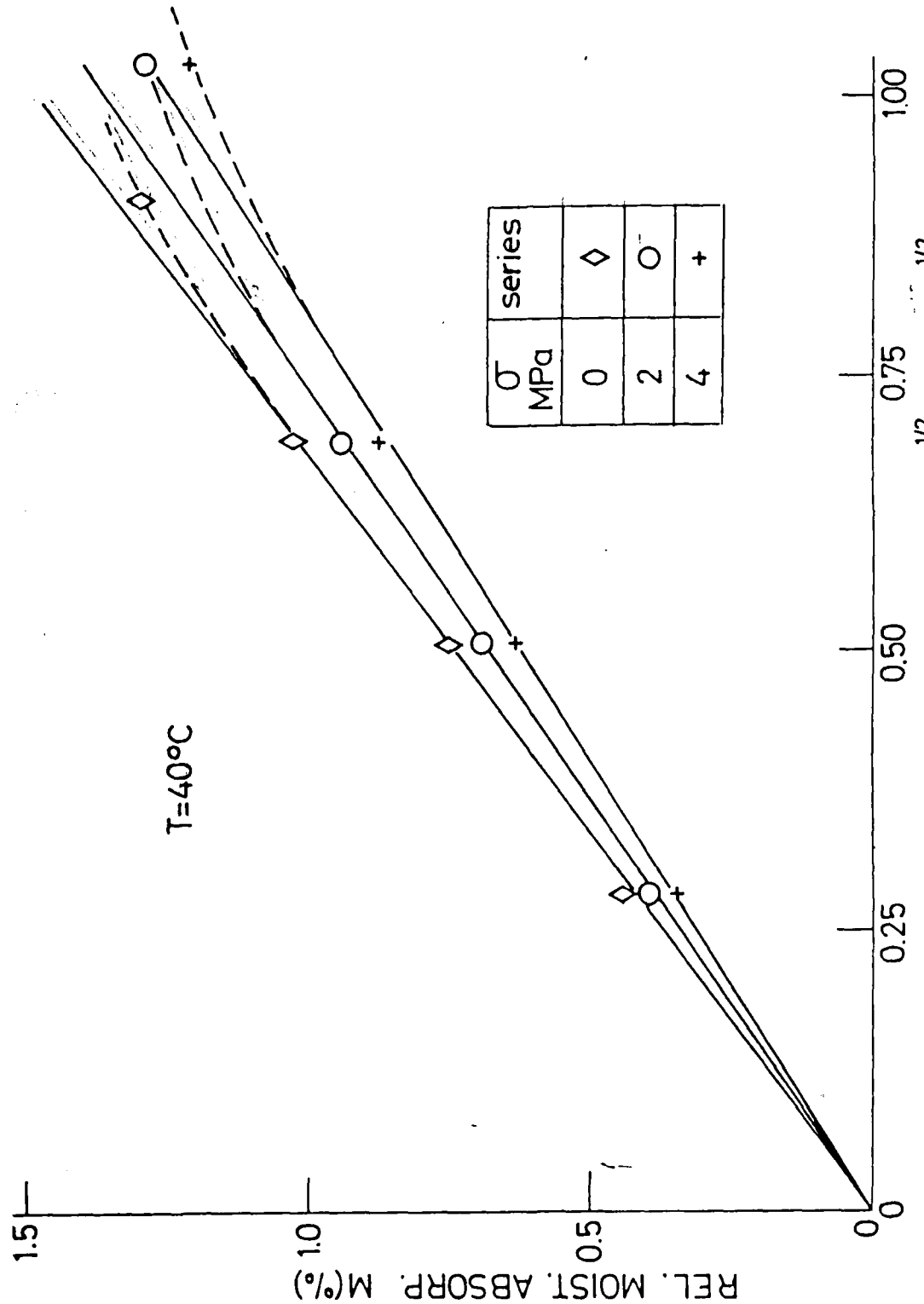

Fig. 17 Compressive load effect on relative moisture absorption (Diffusion coefficient variation), FM-73 specimens (low loading)

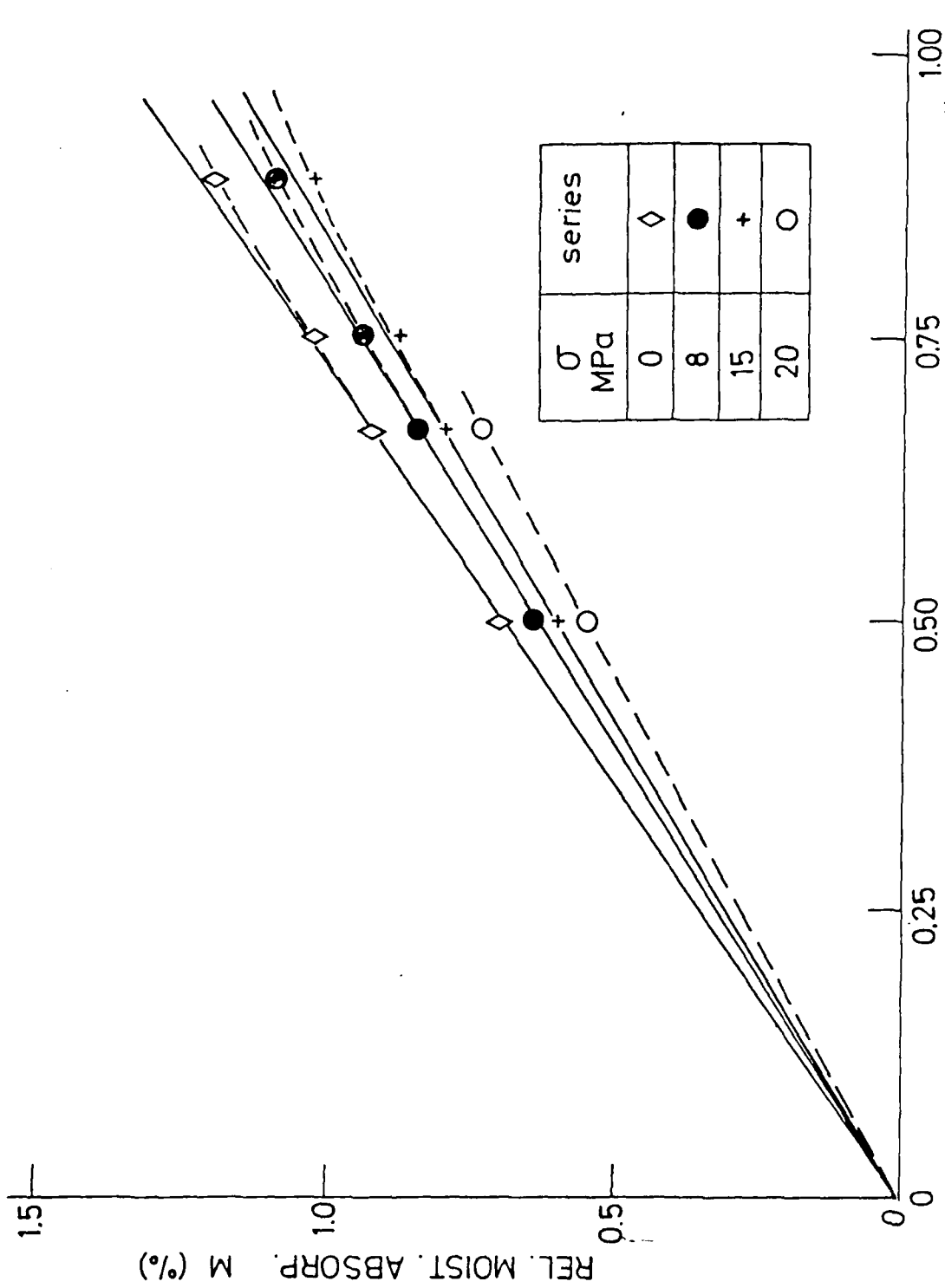

Fig. 18 Compressive load effect on relative moisture absorption (Diffusion coefficient variation), FM-73 specimens (high loading)

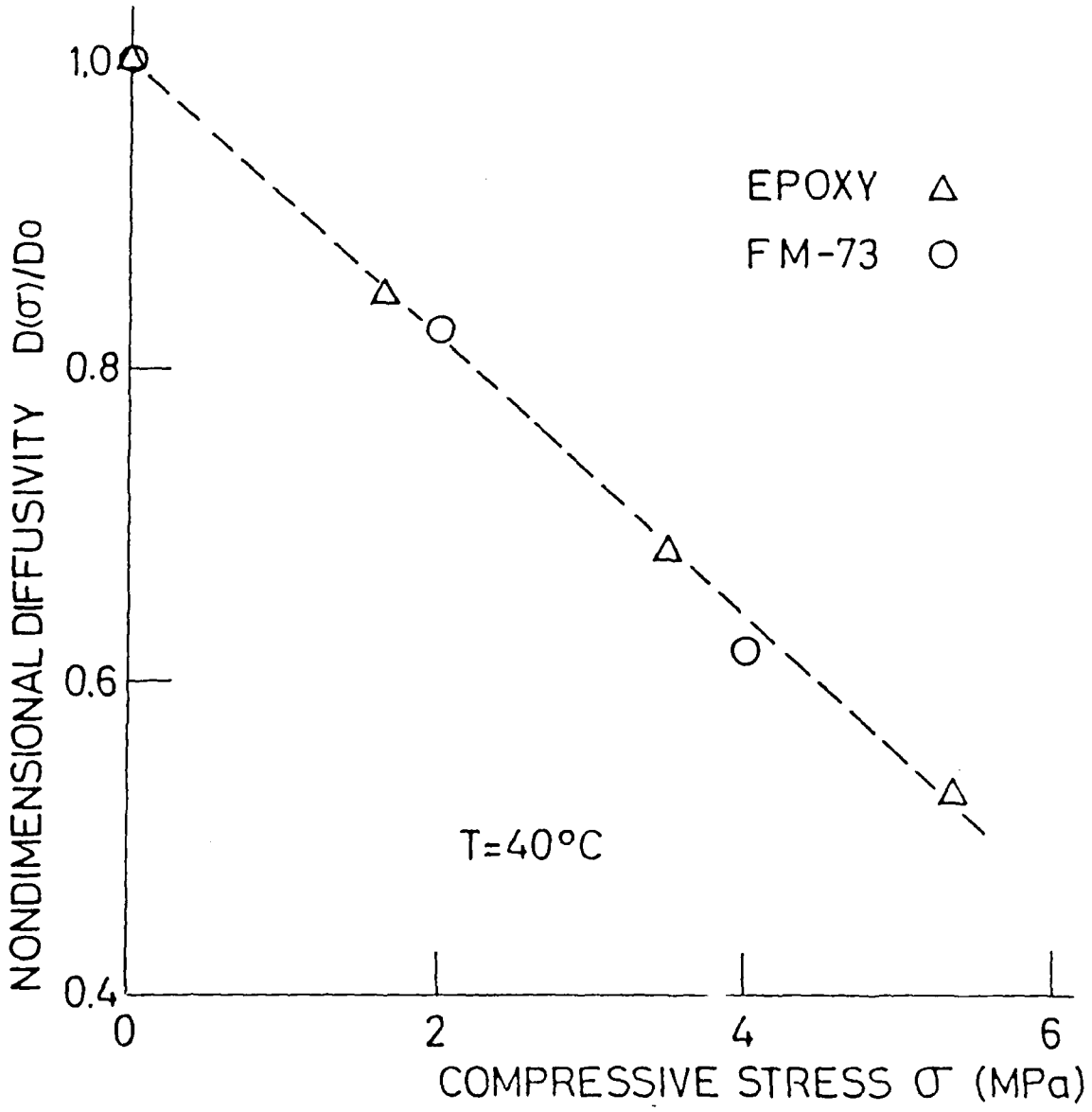

Fig. 19 Compressive stress effects on relative diffusivity of FM-73 specimens

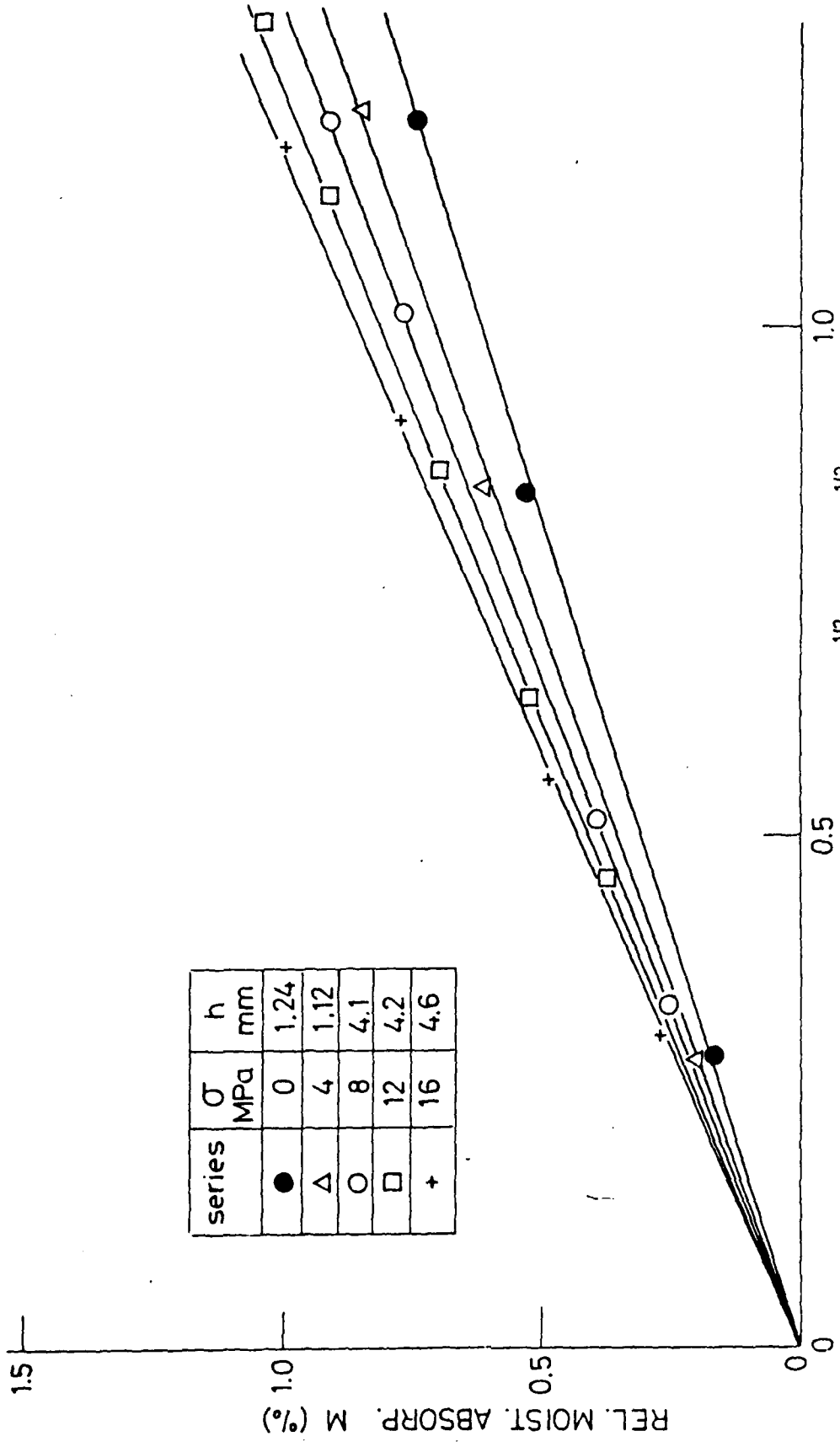

Fig. 20 Tensile load effect on relative moisture absorption (Diffusion coefficient variation), FM-73 specimens

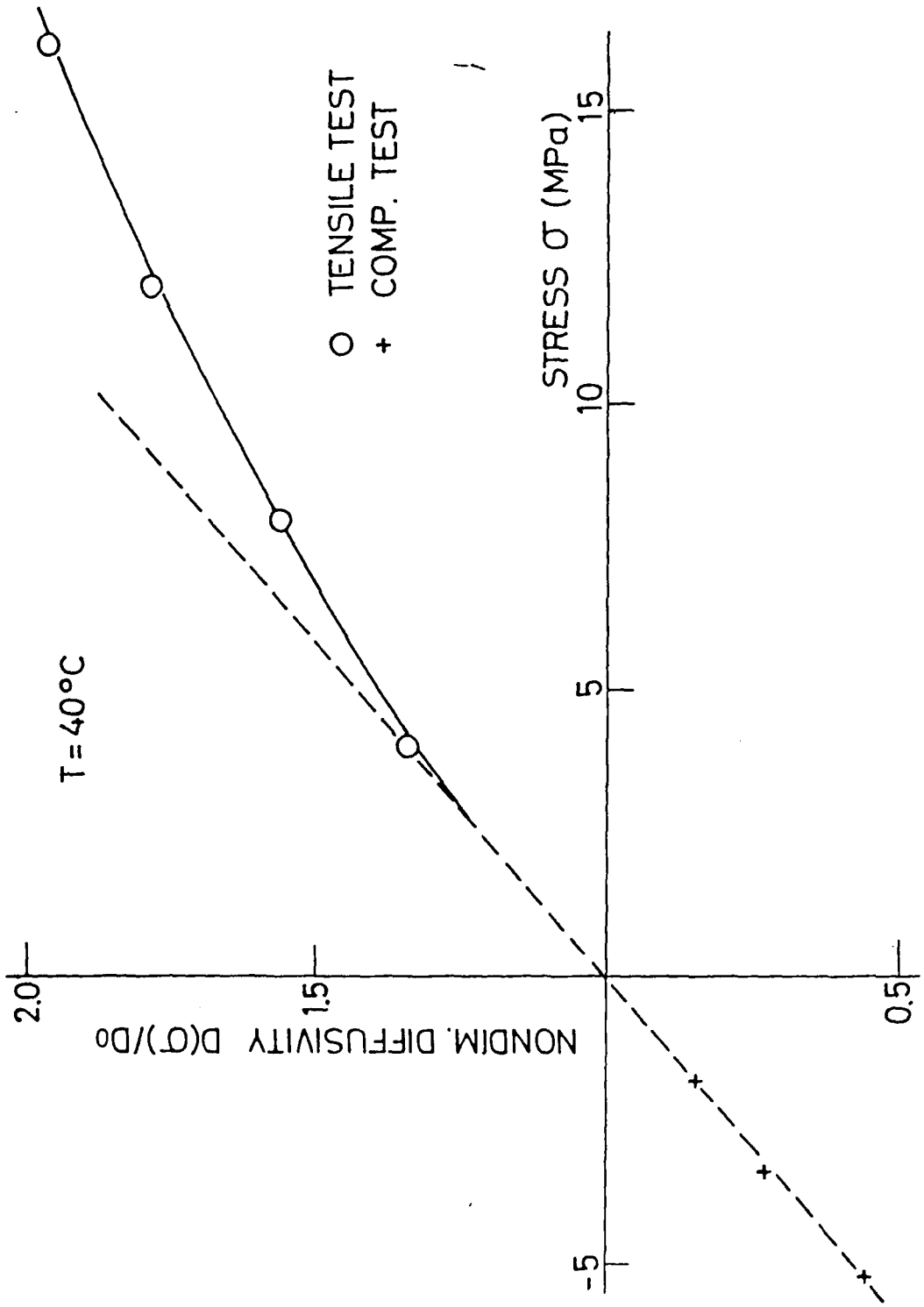

Fig. 21 Tensile stress effect on relative diffusivity of FM-73 specimens

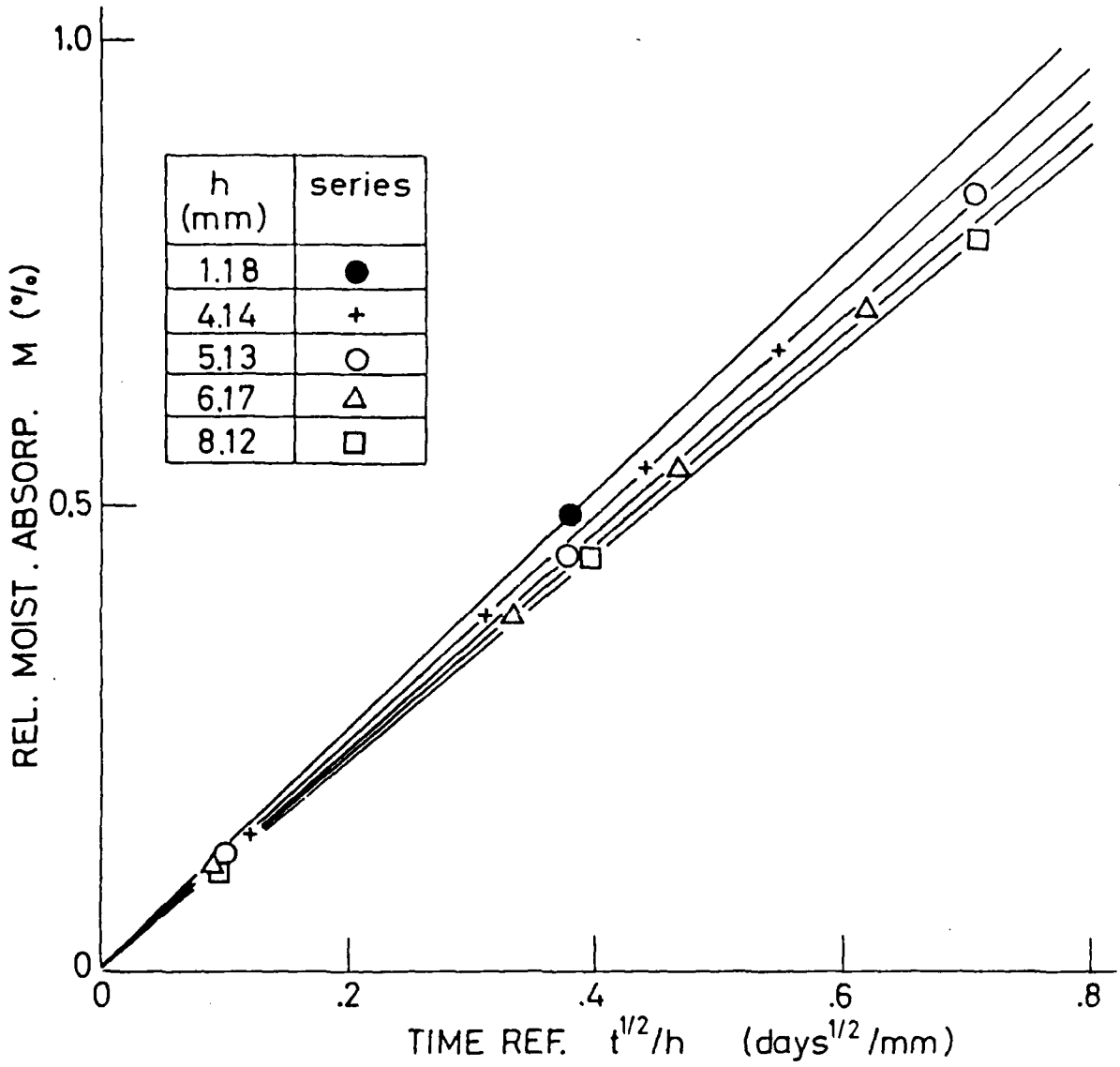

Fig. 22 Internal constraint/effect of homogeneous material (FM-73) or its moisture absorption (diffusion coefficient variation)

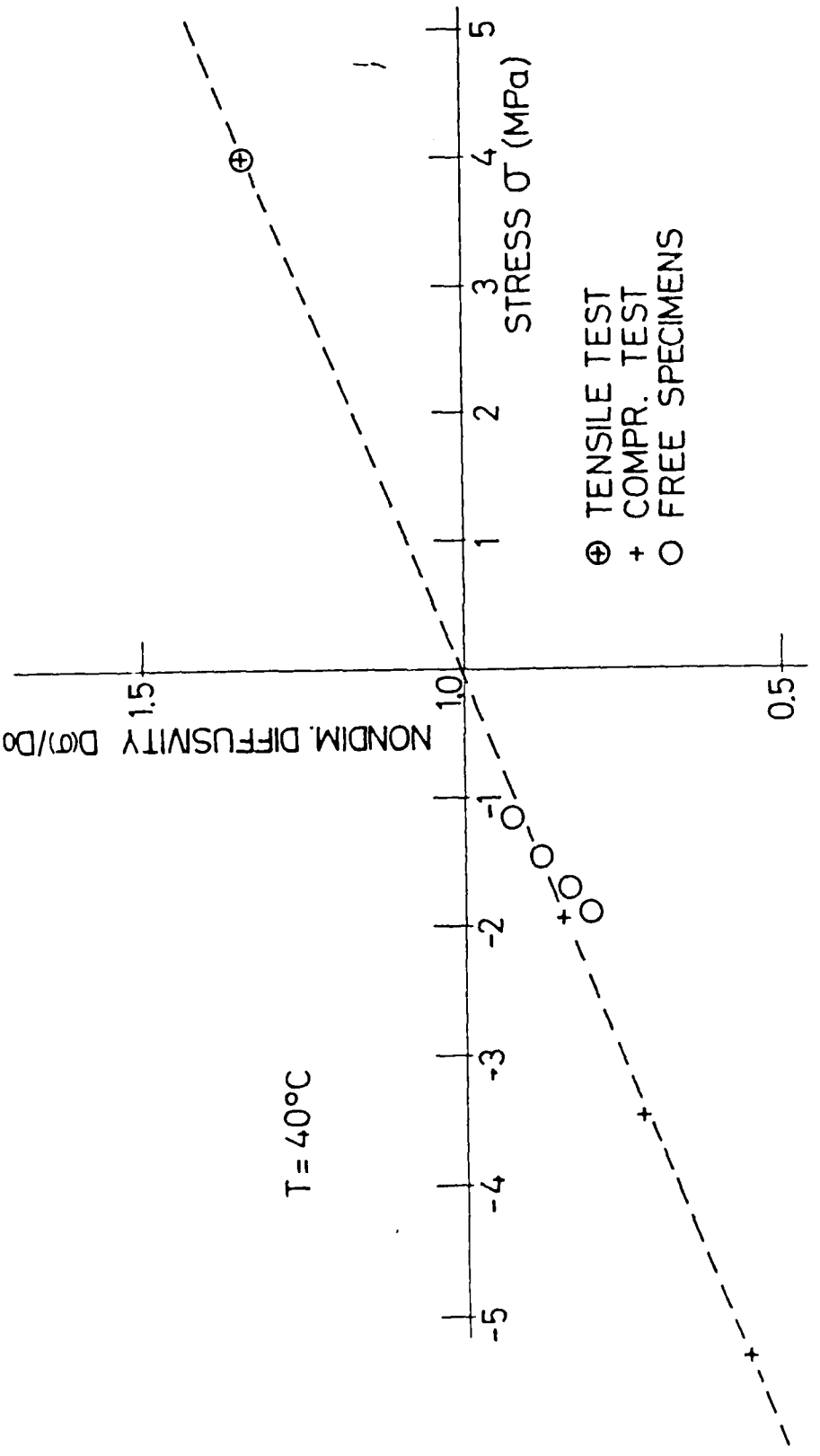

Fig. 23 Equivalent hygroelastic compressive stress effect on relative diffusivity in comparison to external compressive loads

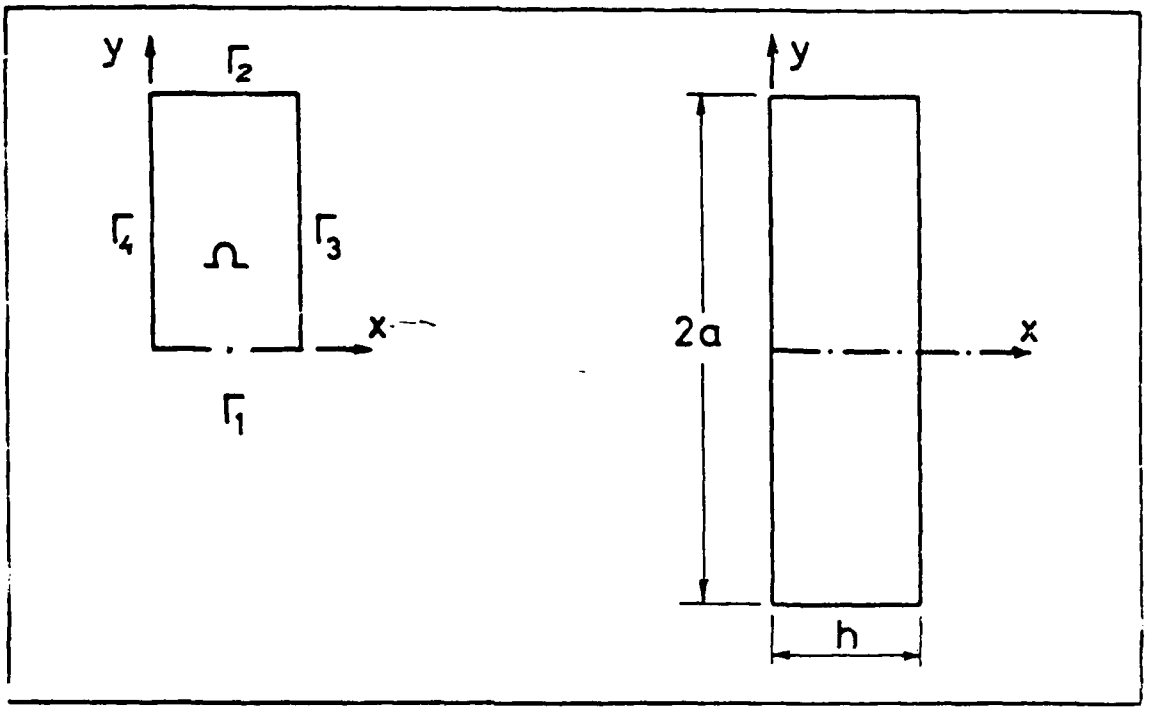

Fig. 24 Configuration and boundary conditions of the domain for the diffusion problem

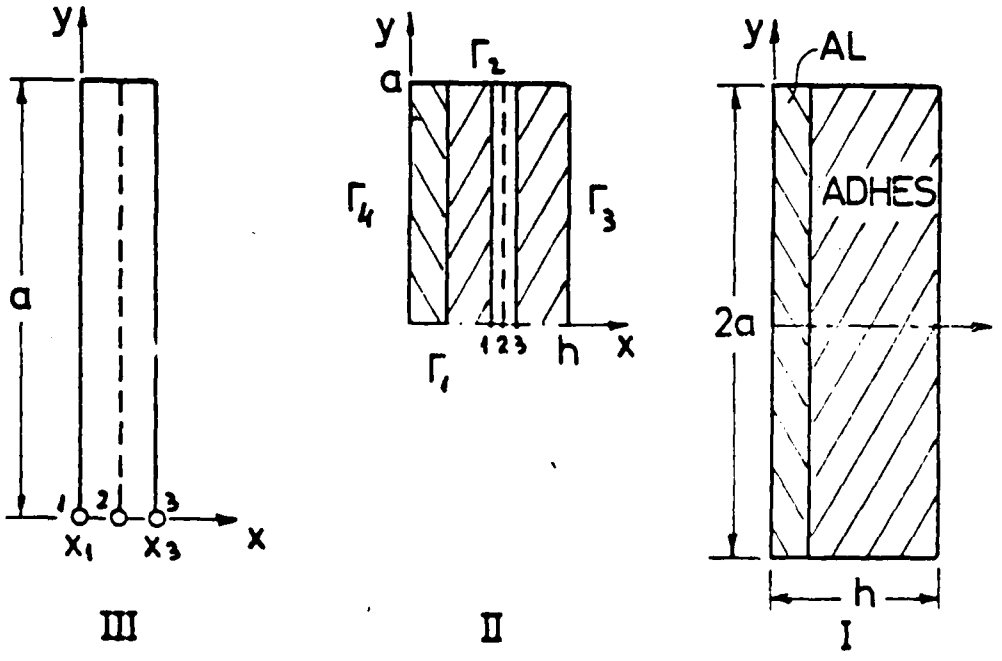

Fig. 25 Asymmetrical doubler - finite strip discretization

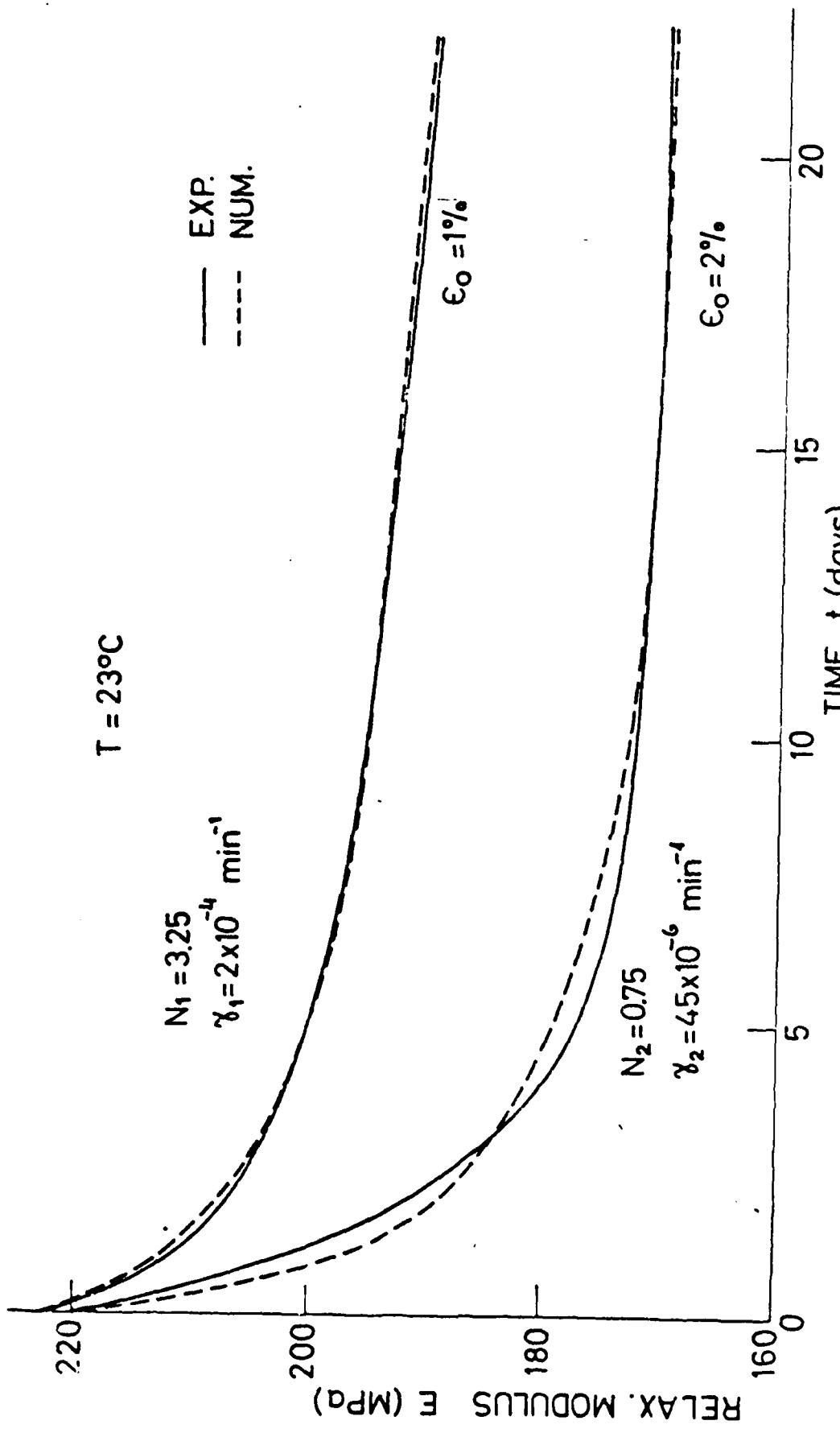

Fig. 26 Calibration of elasto-viscoplastic model parameters trough relaxation experiment with FM-73 (4 strips, 4 harmonics)

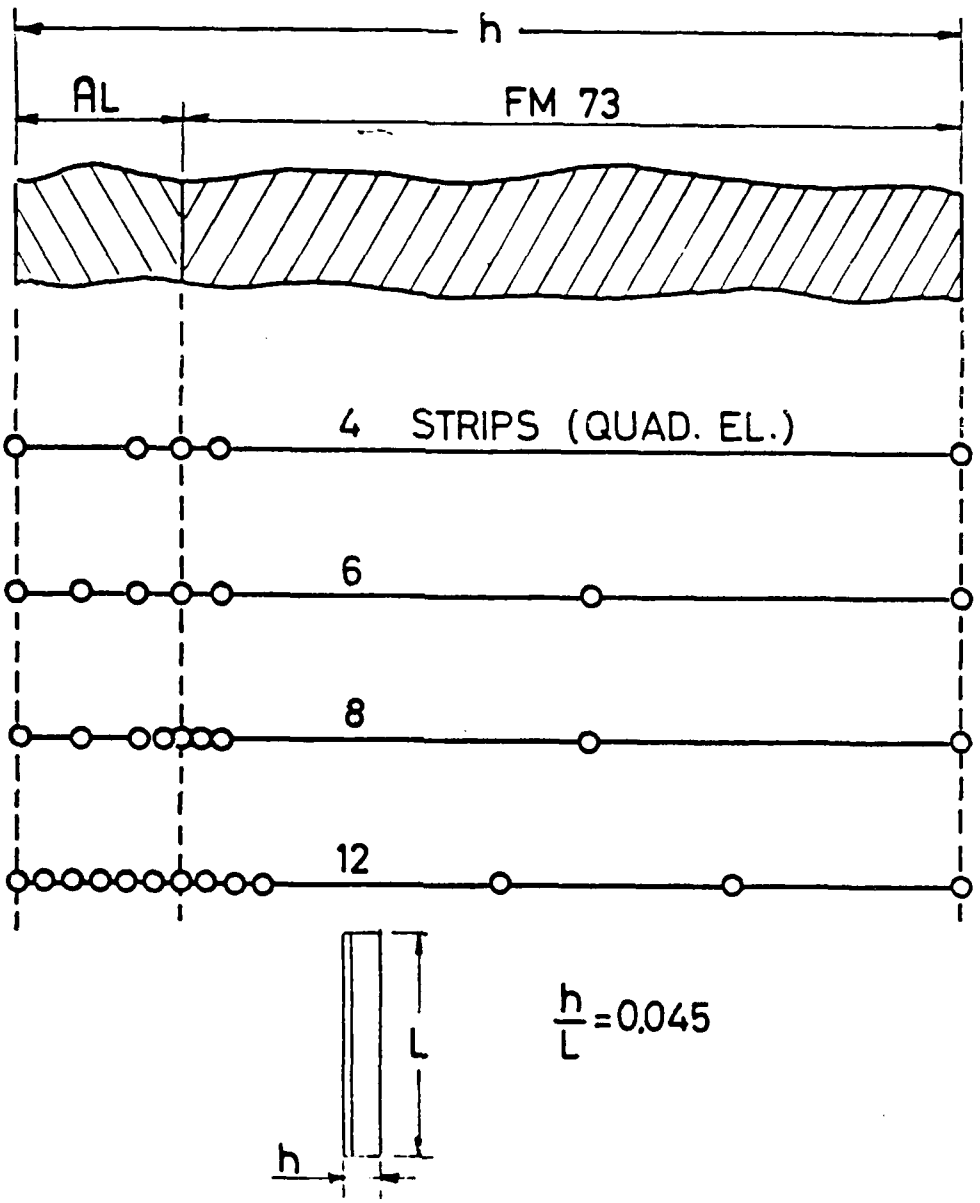

Fig. 27 Width discretization into longitudinal strips

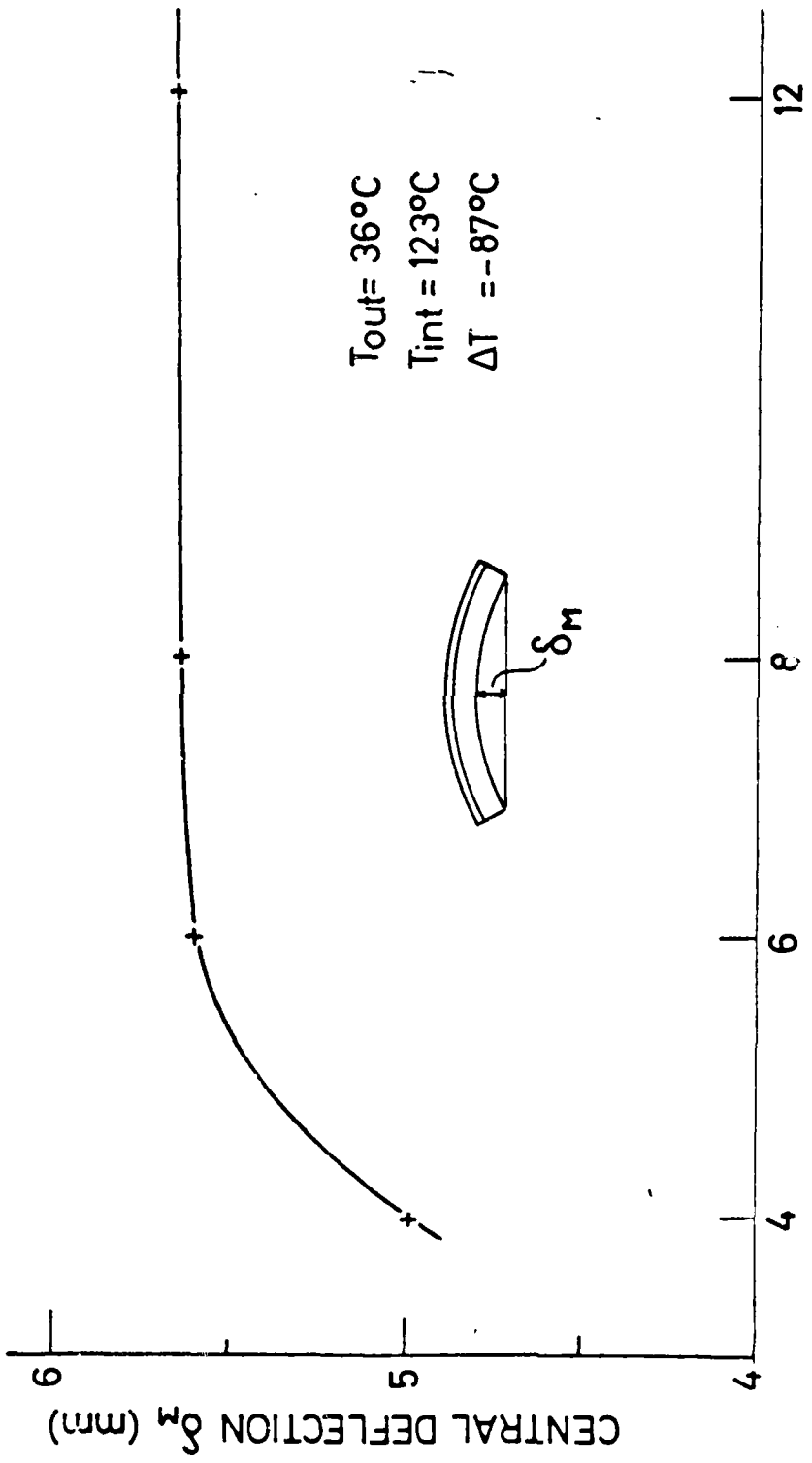

Fig. 28 Influence of total number of strips on the reliability of numerical solutions

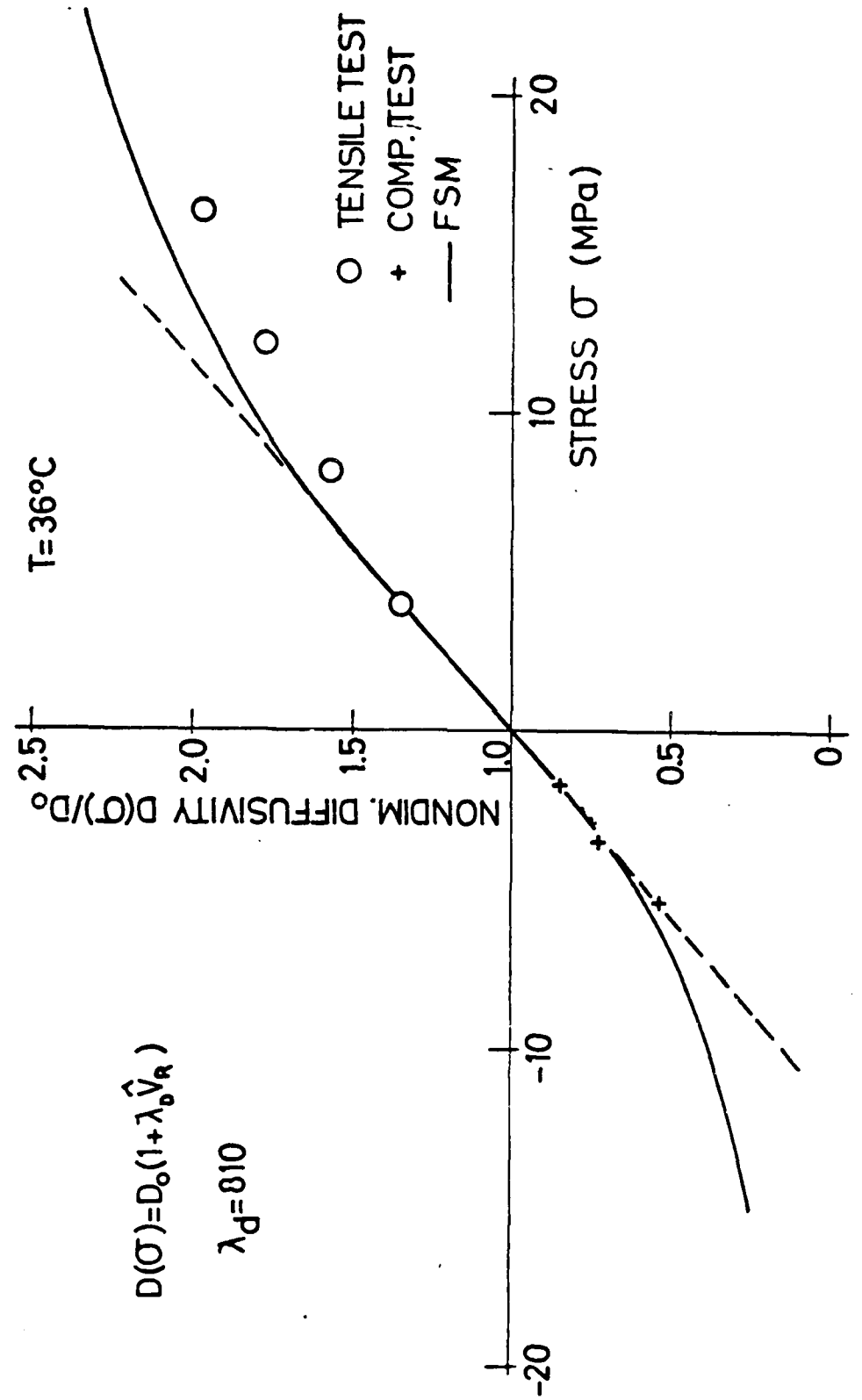

Fig. 29 Dependence of relative diffusivity on stress (1st invariant J1) comparison between expr. results and numerical evaluations of the influence of RRV variations

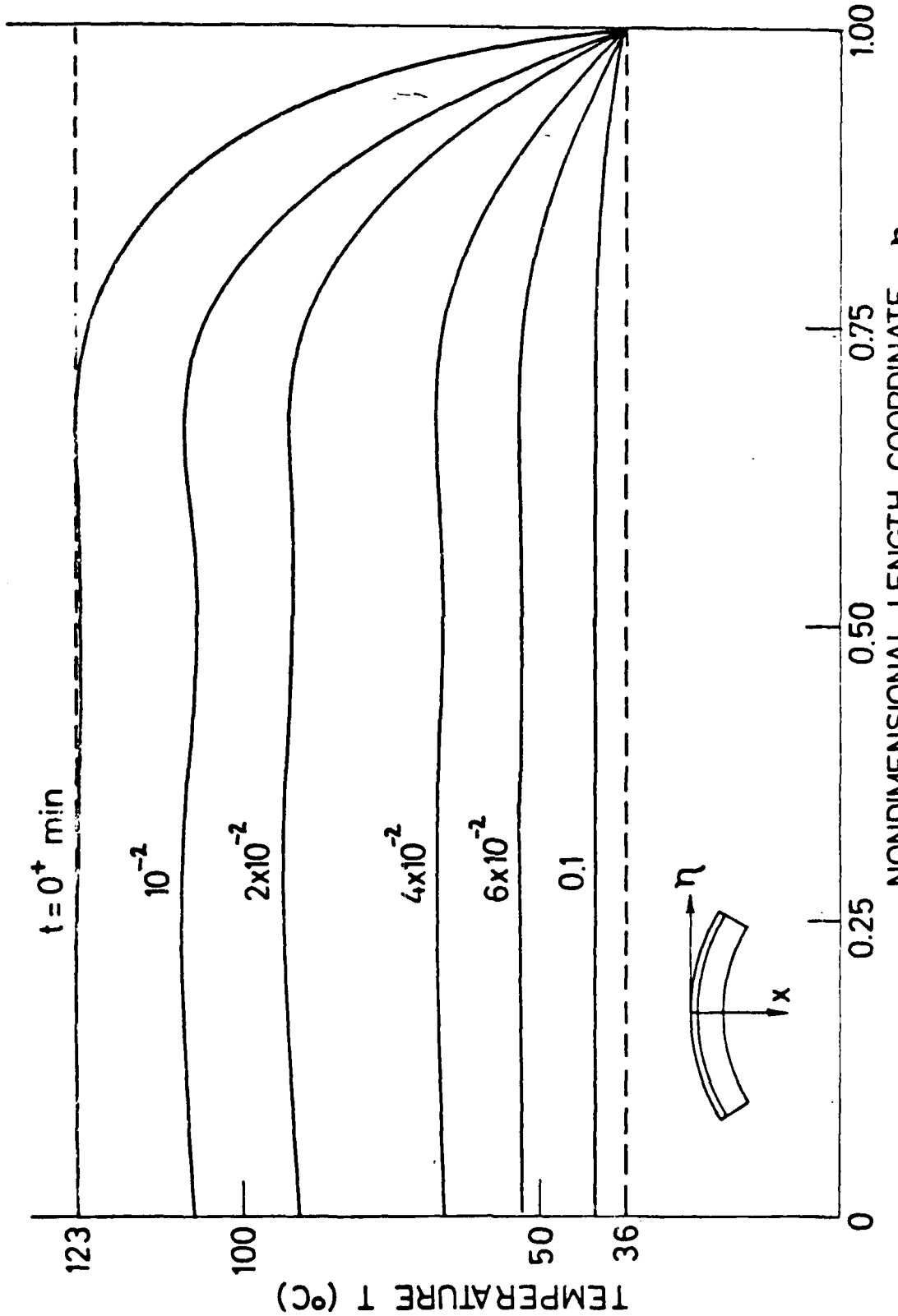

Fig. 30 Longitudinal temperature distributions at various time levels (12 strips, 4 harmonics, x=2.75 mm)

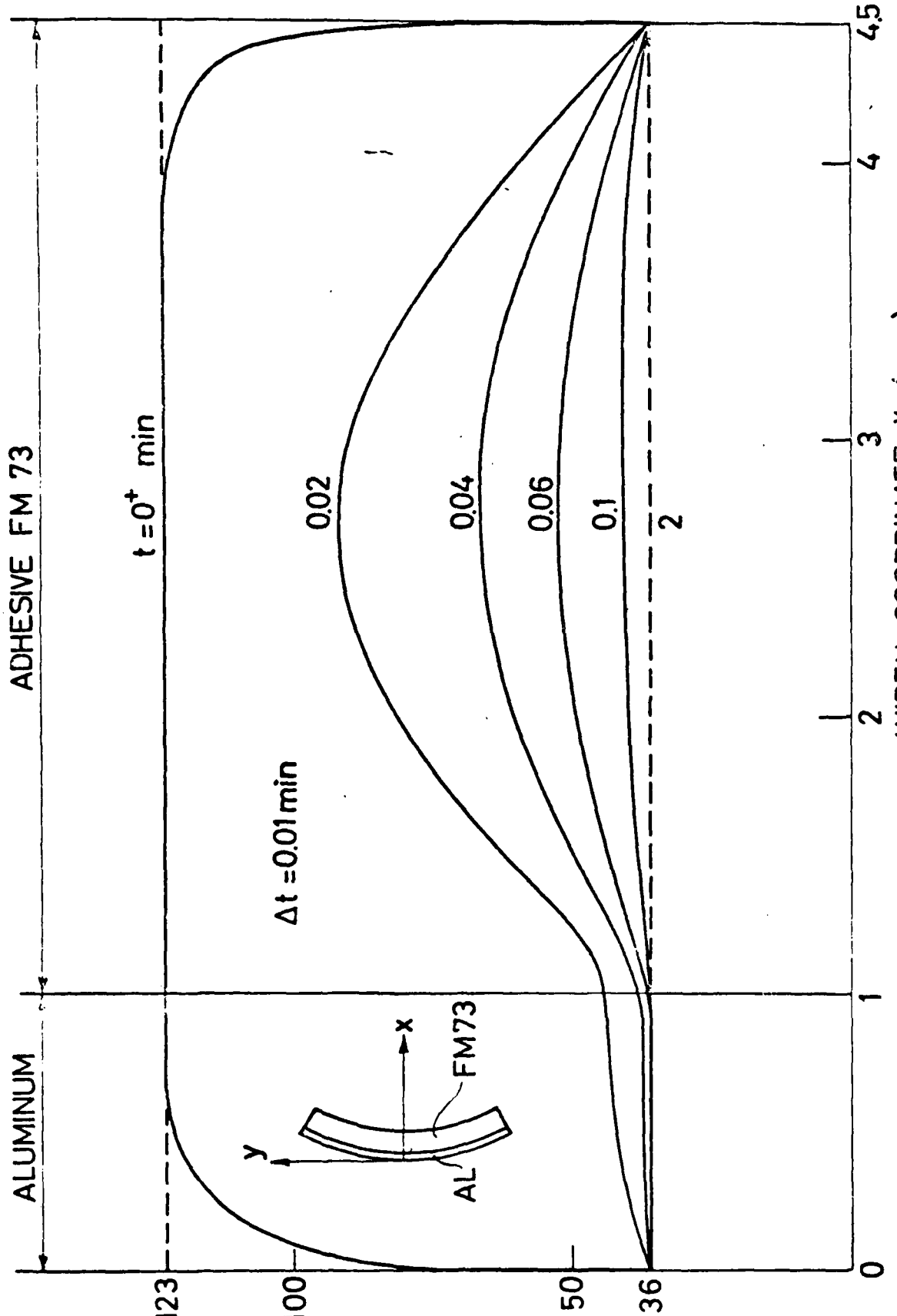

Fig. 31 Transverse temperature distributions at various time levels (12 strips, 4 harmonics, y=0)

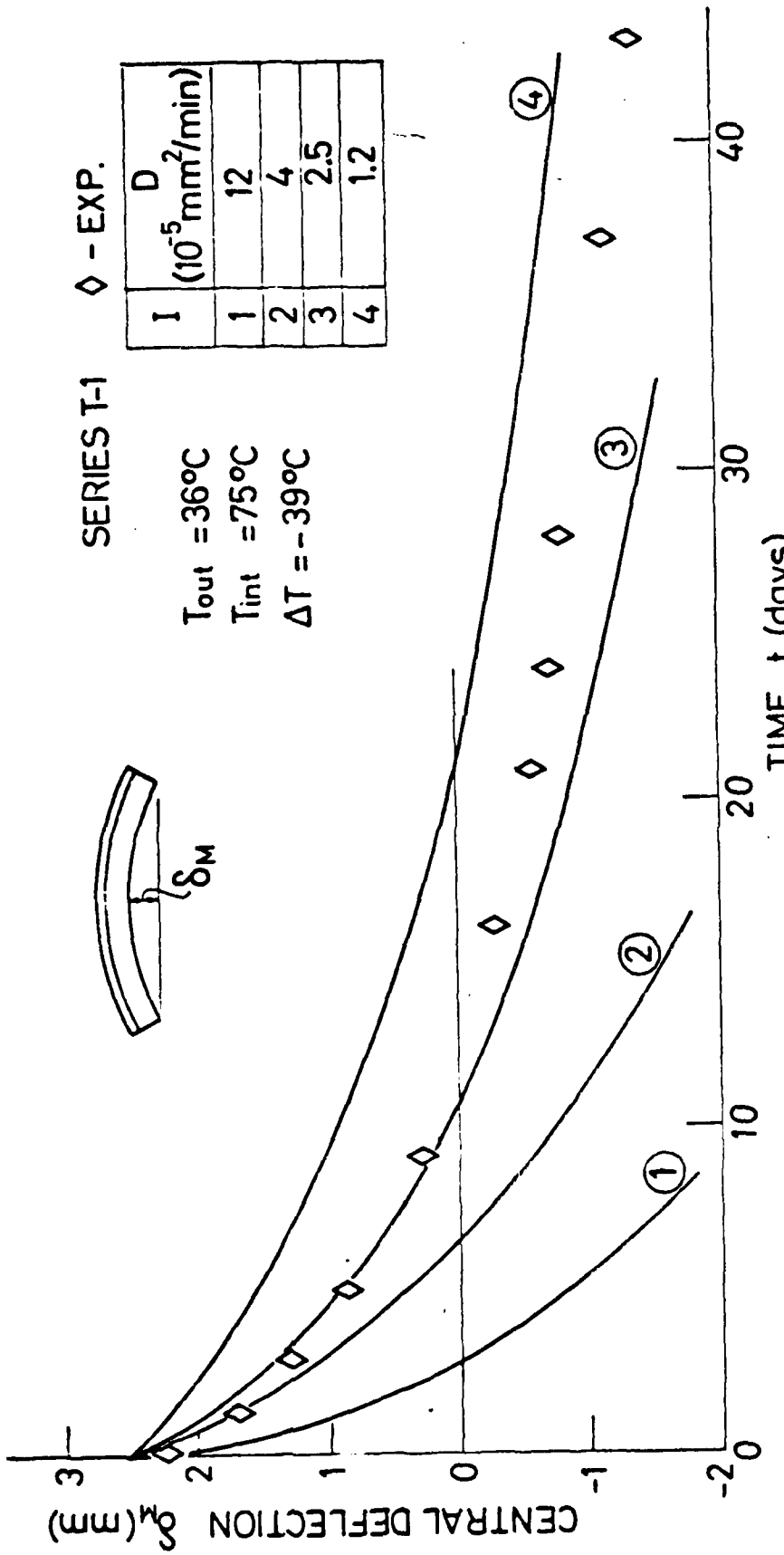

Fig. 32 Influence of various diffusion coefficients on the time-dependent central deflection (12 strips, 4 harmonics)

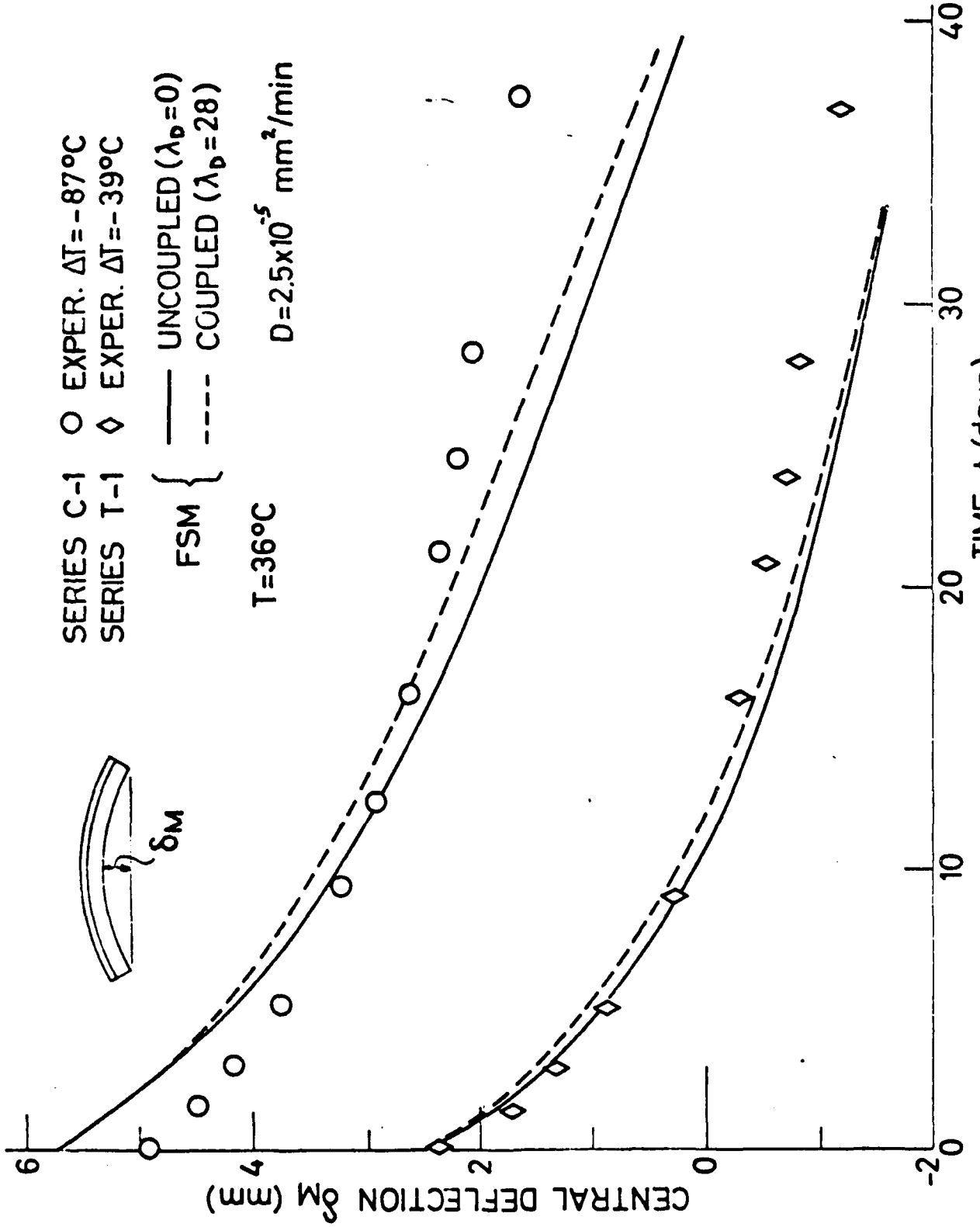

Fig. 33 The combined effect of stress and moisture diffusion on the central deflection (12 strips, 4 harmonics)

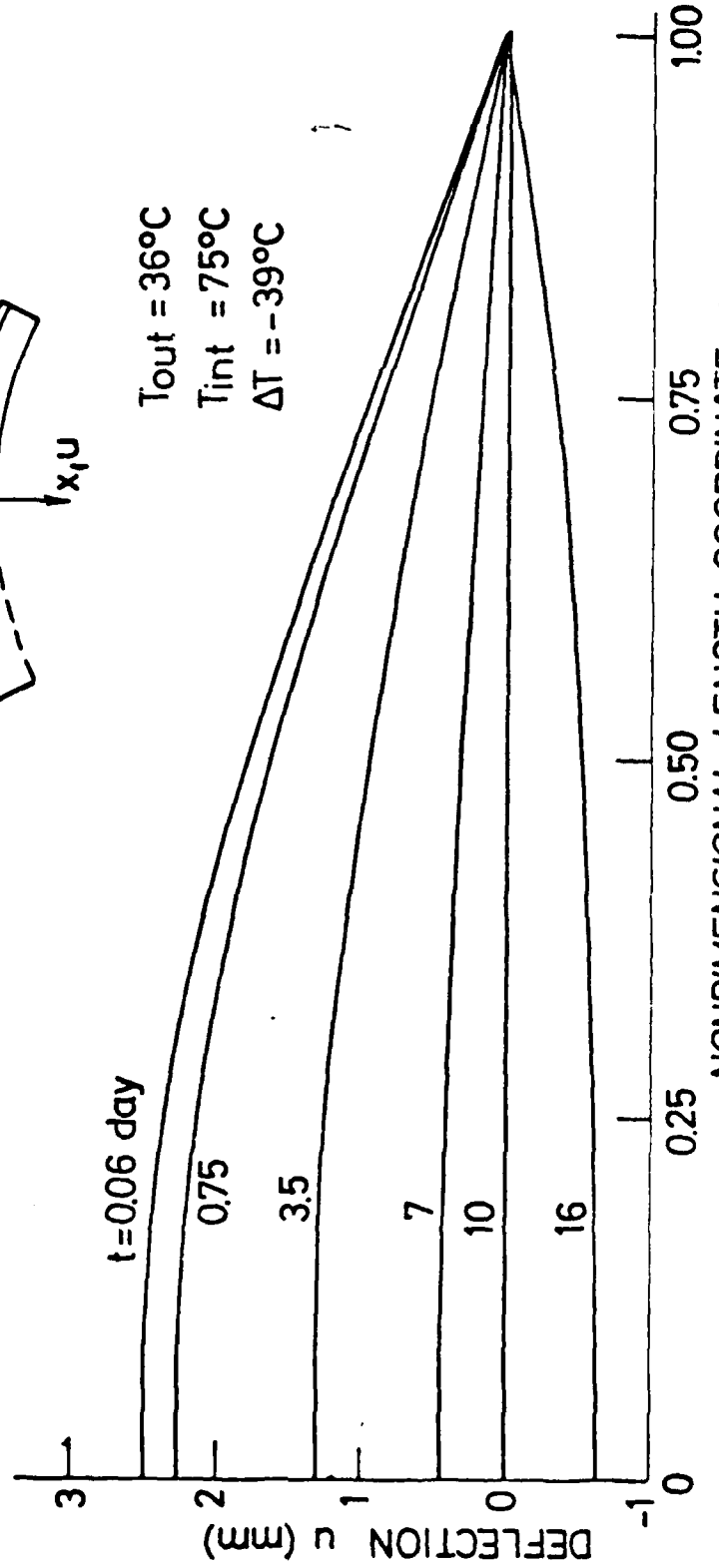

Fig. 34 Distribution of the deflections of specimens of several time levels

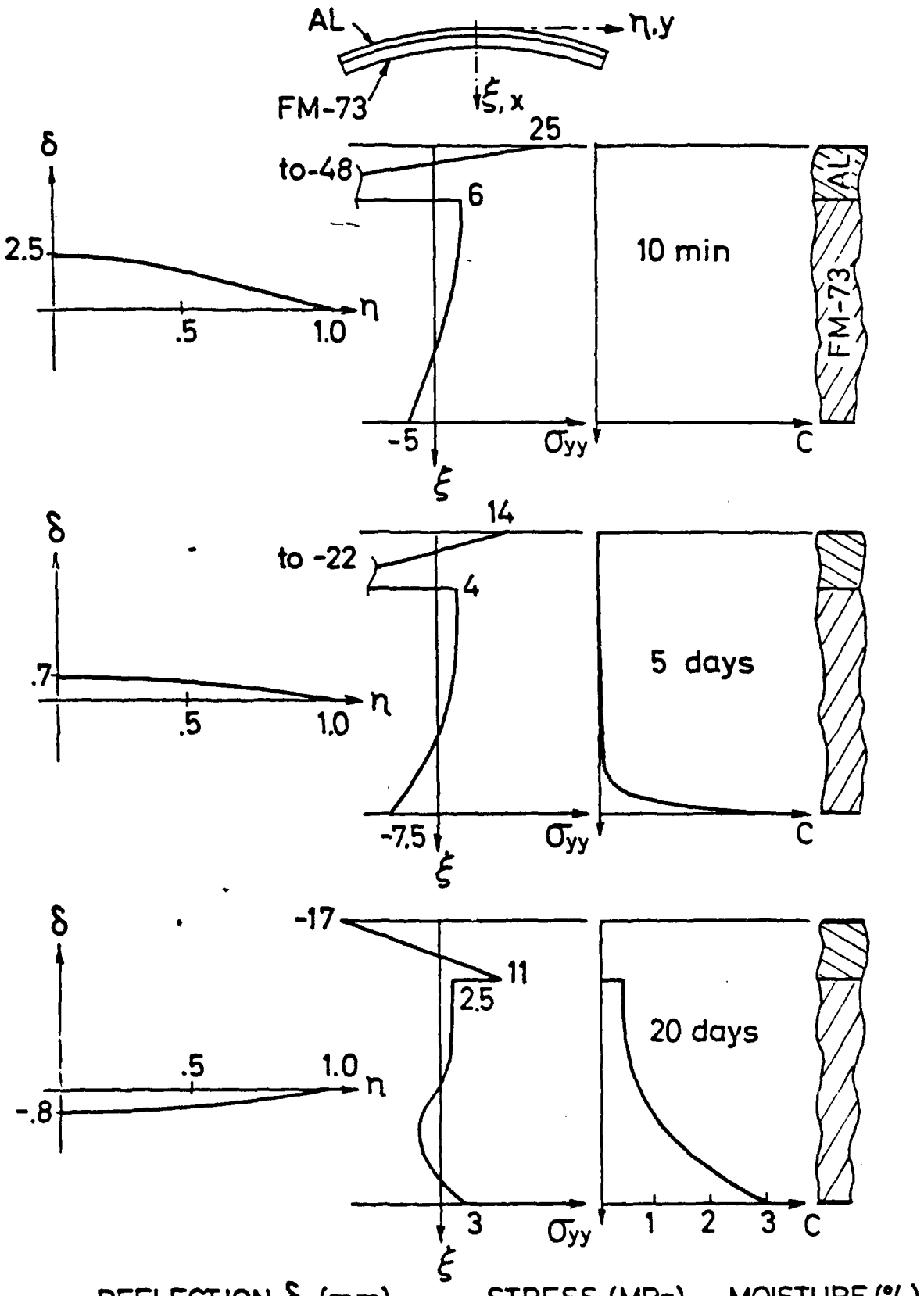

Fig. 35 Schematic description of moisture and stress thickness distributions and deflections along the specimen at different time levels (T=-39°C)

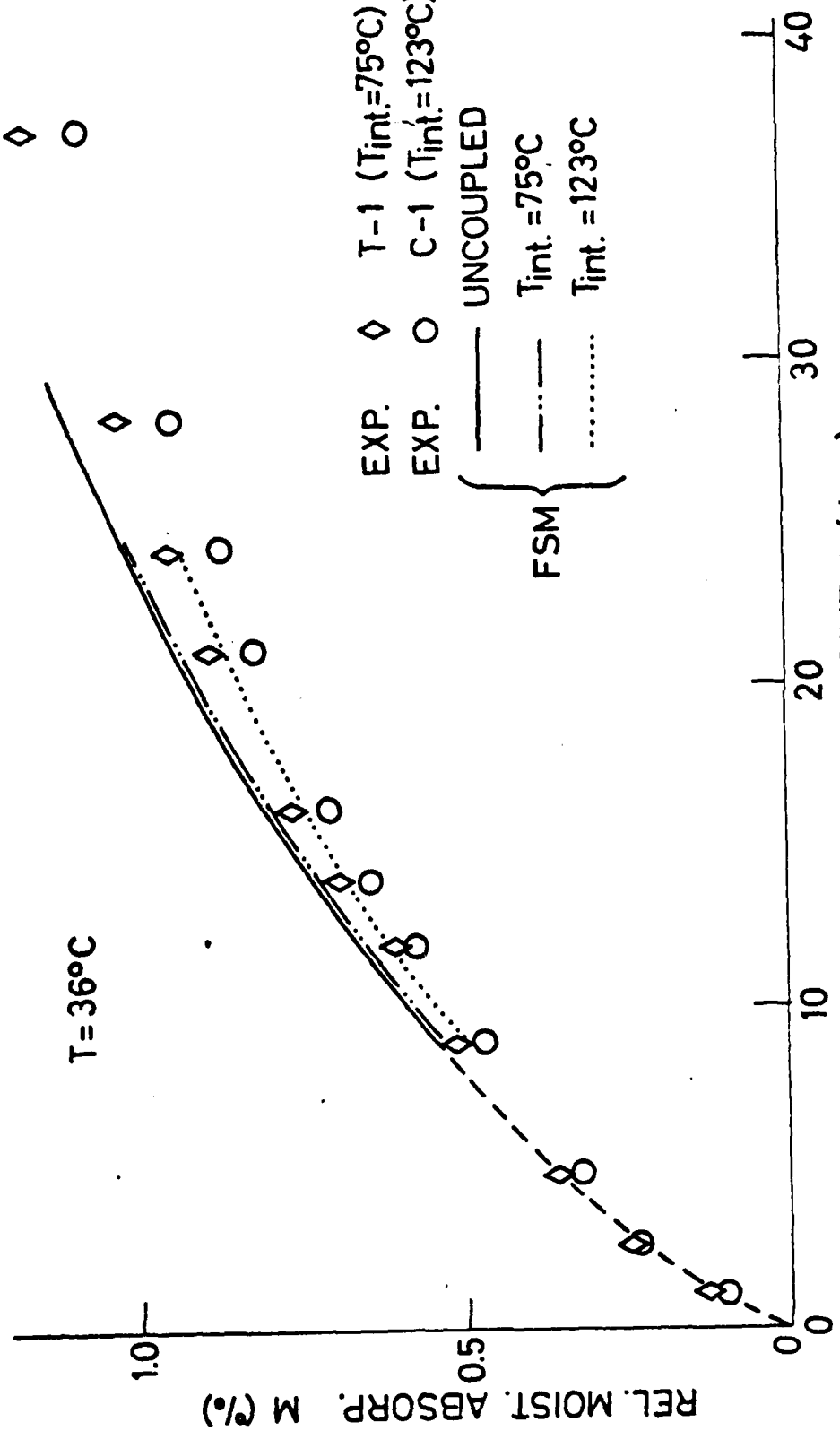

Fig. 36 The combined effect of stress and moisture diffusion on the relative moisture absorption (12 strips, 4 harmonics)

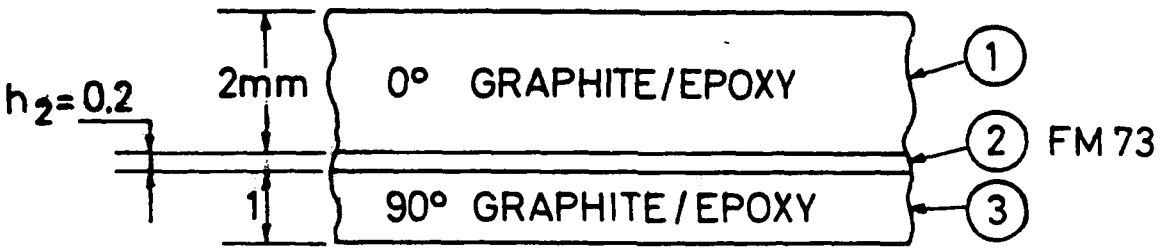

Fig. 37 A 3 layers thin adhesive NSD specimen geometry and properties

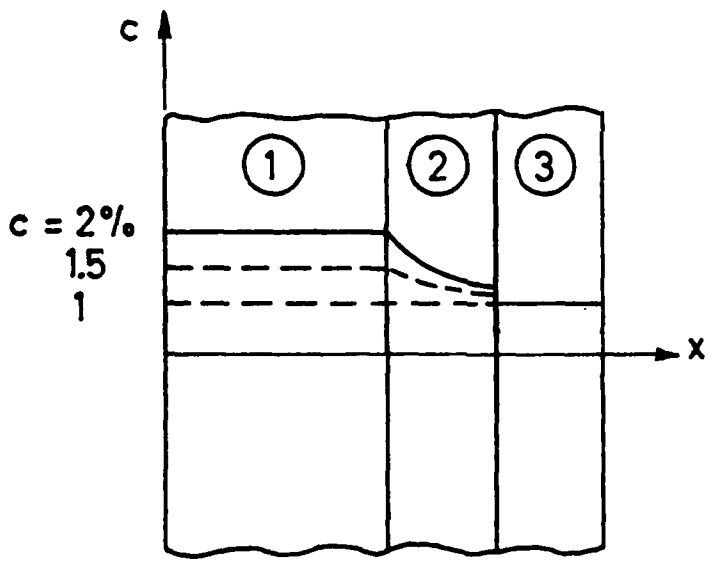

Fig. 38 Typical moisture profiles

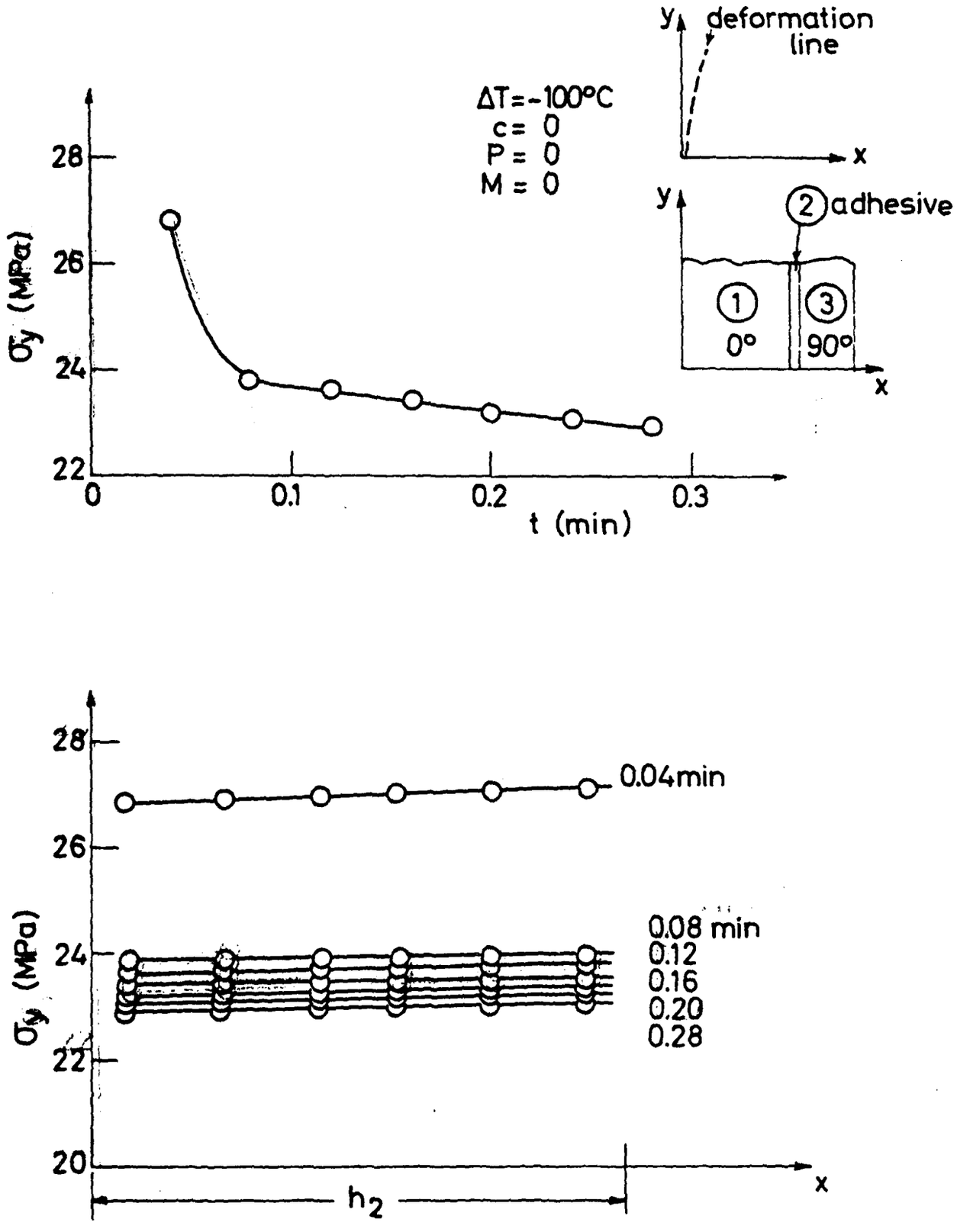

Fig. 39 Axial stress distribution vs. time within the adhesive layer in a non-symmetrical thin adhesive model (T=-100°C, c=0, P=0, M=0)

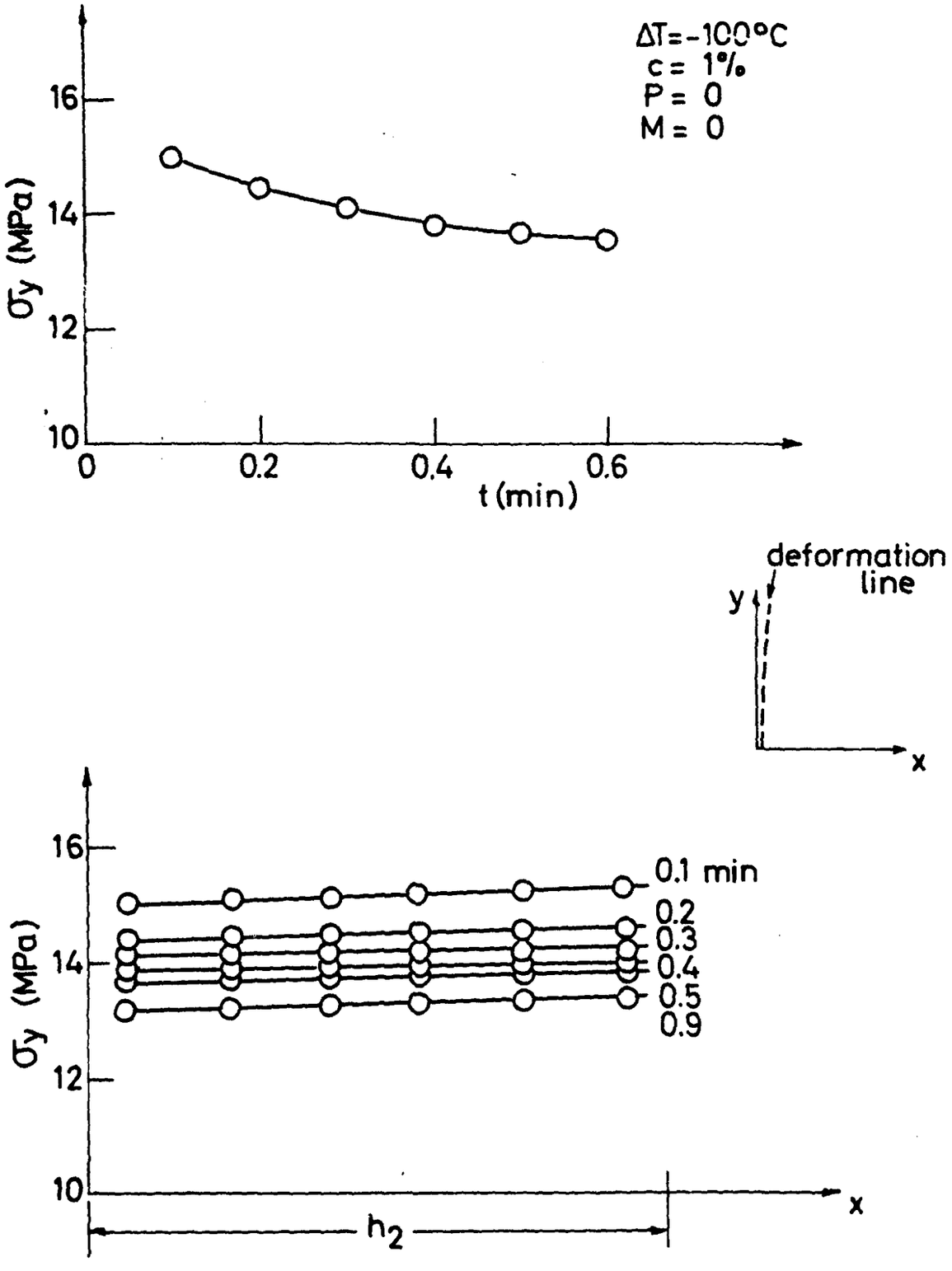

Fig. 40 Axial stress distribution vs. time within the adhesive layer in a non-symmetrical thin adhesive model
(T=-100°C, c=1%, P=0, M=0)

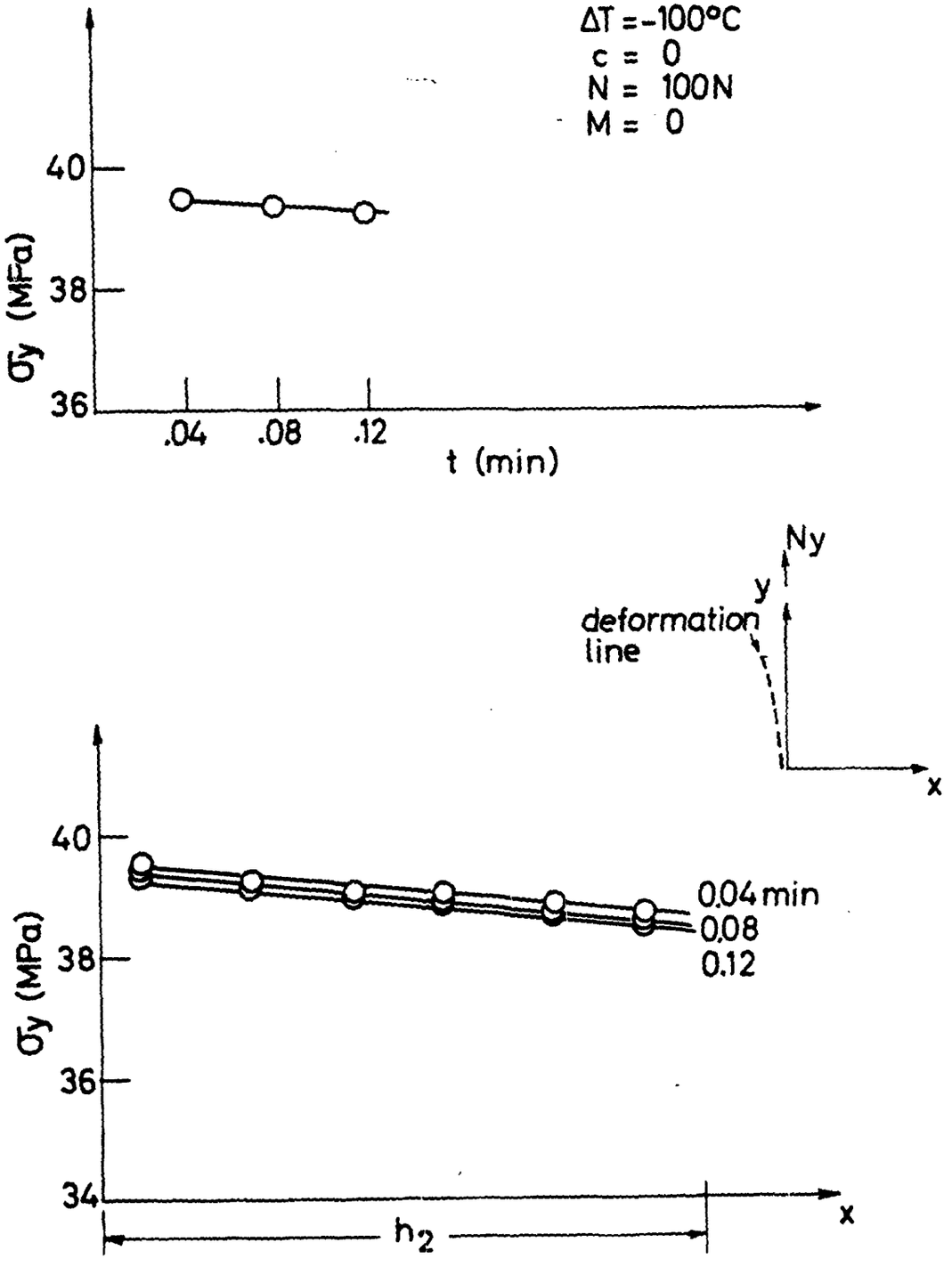

Fig. 41 Axial stress distribution vs. time within the adhesive layer in a non-symmetrical thin adhesive model (T=-100°C, c=0, N=100N, M=0)

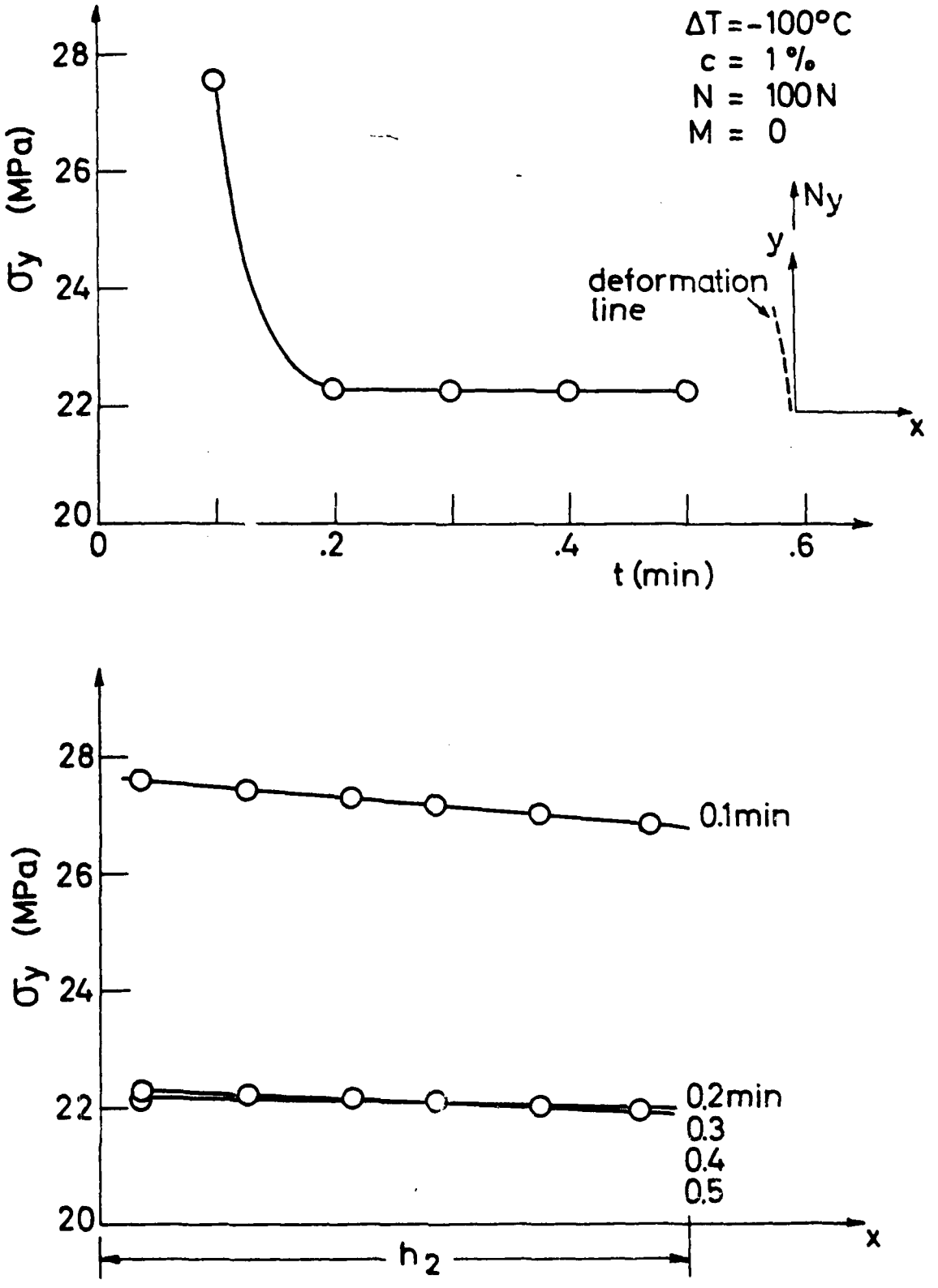

Fig. 42 Axial stress distribution vs. time within the adhesive layer in a non-symmetrical thin adhesive model
(T=-100°C, c=1%, N=100N, M=0)

AD-A170 708 DURABILITY OF STRUCTURAL ADHESIVELY BONDED SYSTEMS(U) 2/2
TECHNION RESEARCH AND DEVELOPMENT FOUNDATION LTD HAIFA
(ISRAEL) O ISHAI ET AL. JAN 86 DAJA45-84-C-0050

UNCLASSIFIED F/G 20/11 NL

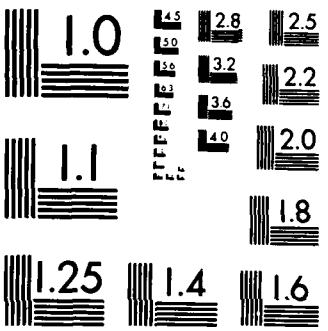

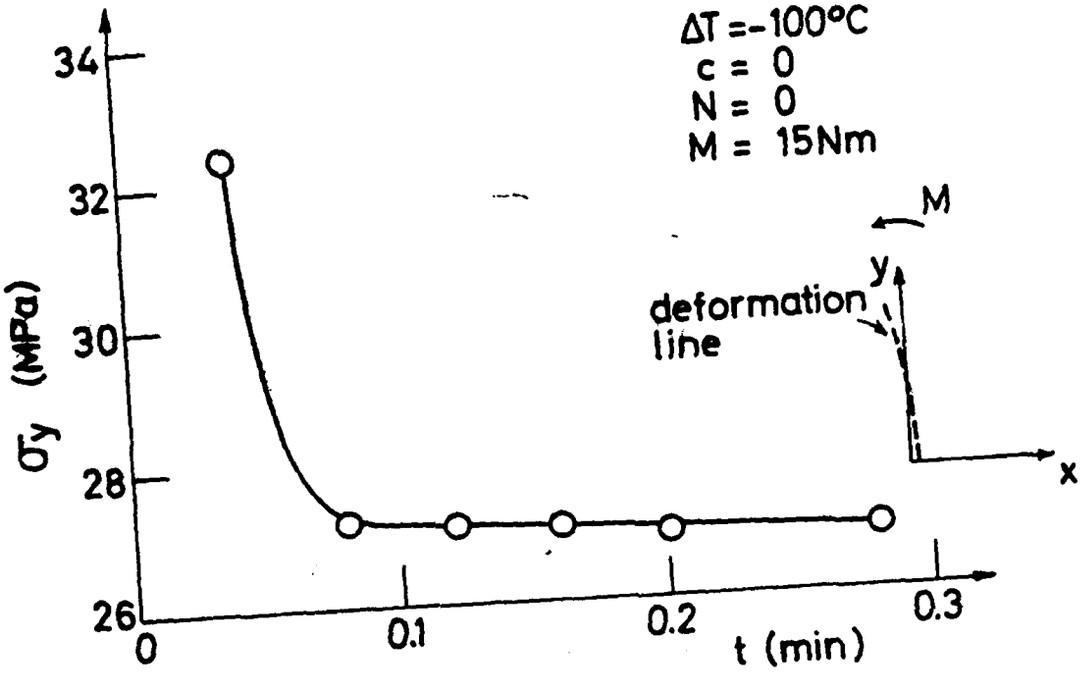

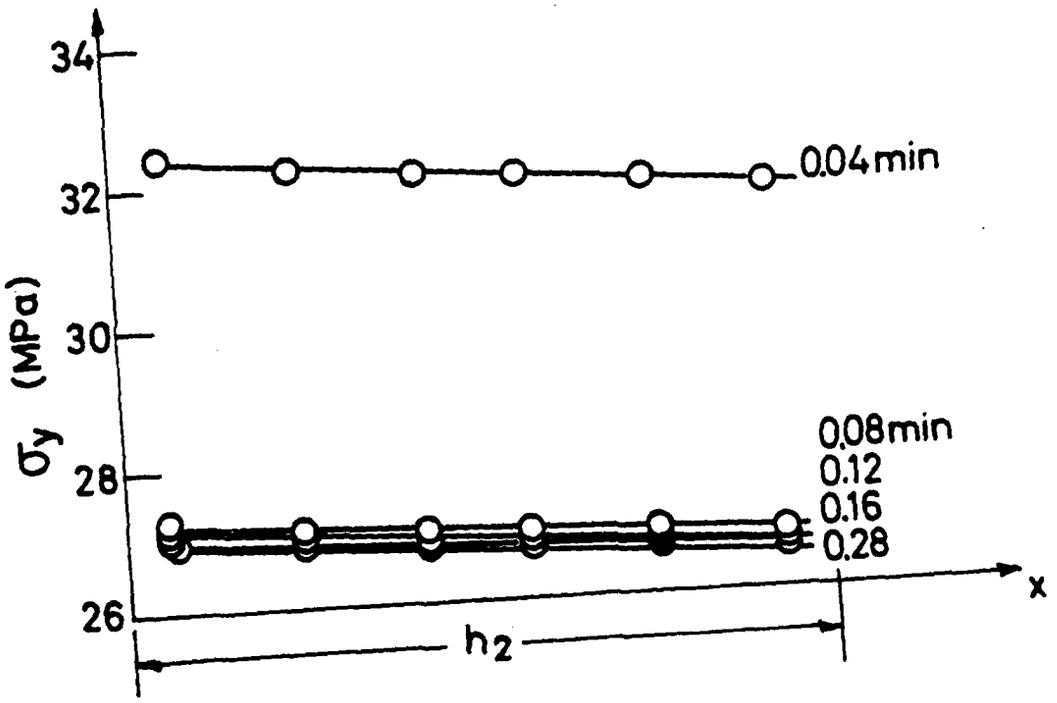

Fig. 43 Axial stress distribution vs. time within the adhesive layer in a non-symmetrical thin adhesive model (T=-100°C, c=0, N=0, M=15Nm)

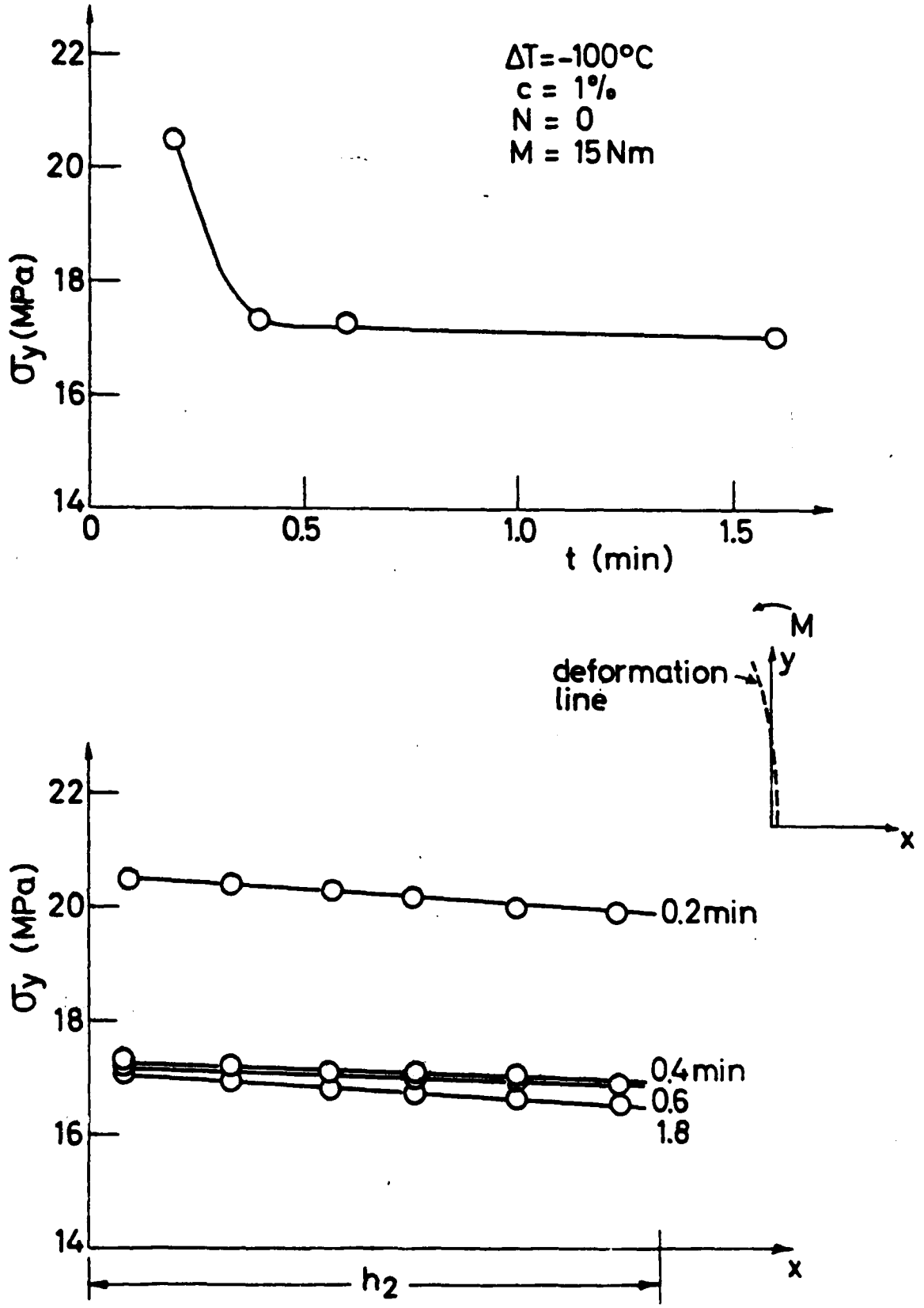

Fig. 44 Axial stress distribution vs. time within the adhesive layer in a non-symmetrical thin adhesive model
(T=-100°C, c=1%, N=0, M=15Nm)

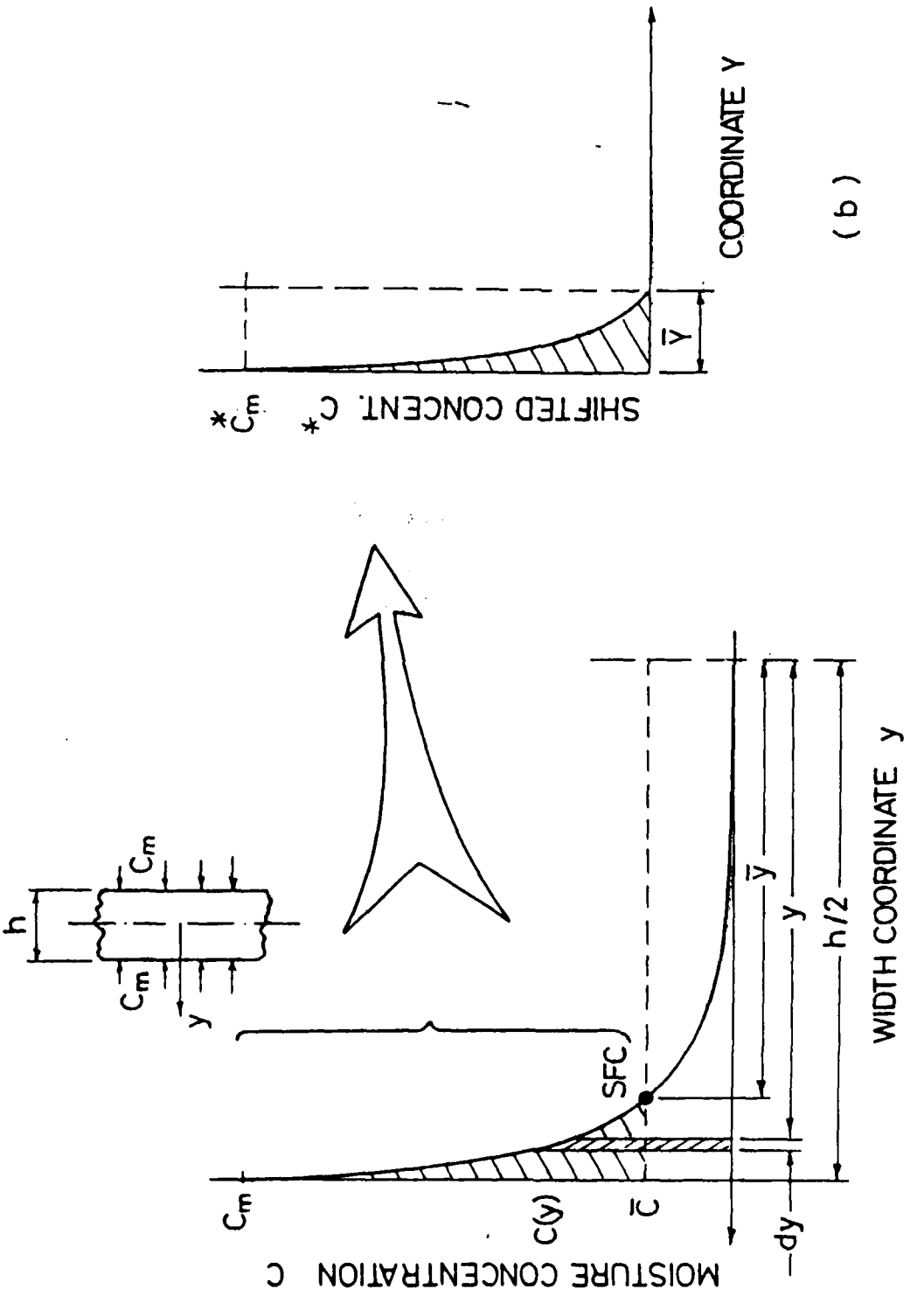

Fig. 45 a. Moisture distribution over specimen width at free absorption
b. Hygroelastic compression zone

Table 1: Hygrothermomechanical Conditions for Epoxy Specimens (Compression)

Comments	Test Duration (no. days)	Compressive Load (MPa)	Test Temperature (°C)	Series
3 specimens	30	0	40	E-1
3 specimens	30	1.8	40	E-2
2 specimens	30	3.5	40	E-3
3 specimens	30	5.2	40	E-4
Failure	14	7.6	40	E-5

Table 2: Hygrothermomechanical Conditions for FM-73 Specimens Compression (Low Loading).

Comments	Test Duration (no. days)	Compressive Load (MPa)	Test Temperature (°C)	Series
4 specimens	14	0	40	FM-1
4 specimens	14	2	40	FM-2
4 specimens	14	4	40	FM-3
Failure	4	6	40	FM-4

Table 3: Hygrothermomechanical Conditions for FM-73 Specimens Compression (High Loading).

Comments	Test Duration (no. days)	Compressive Load (MPa)	Test Temperature (°C)	Series
2 specimens	60	0	40	H-1
2 specimens	60	8	40	H-2
2 specimens	60	155	40	H-3
2 specimens	8	20	40	H-4
Failure	2	25	40	H-5

Table 4: Hygrothermomechanical Conditions for FM-73 Specimens (Tension)

Comments	Test Duration (no. days)	Tensile Load (MPa)	Test Temperature (°C)	Series
4 specimens	21	0	40	TM-1
4 specimens	21	4	40	TM-2
4 specimens	21	8	40	TM-3
4 specimens	21	12	40	TM-4
4 specimens	21	16	40	TM-5
Failure	6	20	40	T-6

Order	Adherend 1		Adherend 2		T_{SF} [°C]
	Material	h_1 [mm]	Material	h_2 [mm]	
T-1	Aℓ-2024 T3	1	FM-73	3.5	70
C-1	Aℓ-2024 T3	1	FM-73	3.5	123
C-2	Aℓ-2024 T3	1	FM-73	5.2	123

Table 5 Material composition and dimensions of bonded specimens

Properties	Elastic Parameters				Strength Properties					H.T. Coefficient		
Material Systems	E_{11}	E_{22}	G_{12}	ν_{12}	F_{1t}	F_{1c}	F_{2t}	F_{2c}	F_6	α_1	α_2	β_2
	MPa	MPa	MPa		MPa	MPa	MPa	MPa	MPa	10^{-6}	$C^{\circ -1}$	
AS4-3502 Graphite/Epoxy	140000	10000	6000	0.34	1750	1750	51	250	85	-0.2	30	0.55
FM 73 Film Adhesive	2200	2200	800	0.38	47	65	47	65	31	85	85	0.30

Table 6 Mechanical and hygro-thermo-elastic properties of the constituents layers in the non-symmetrical thin adhesive bonded model. (fig.37)

Appendix A - Method for Determination of Relative Moisture (RMC) Absorbed by Specimens Under Tension

The RMC was calculated as follows:

The weight of a dry specimen is given by:

$$W_d = {}_E W_d + {}_I W_d \qquad \text{(A-1)}$$

where ${}_E W_d$ and ${}_I W_d$ are the dry weights of the end and inner zones, respectively.

The total weight of a wet specimen is

$$W = {}_E W + {}_I W \qquad \text{(A-2)}$$

and the absorbed moisture is:

$$m = {}_E m + {}_I m \quad . \qquad \text{(A-3)}$$

The RMC, calculated for the uniformly-stressed inner zone, is given as:

$$M = \frac{{}_I m}{{}_I W_d} \qquad \text{(A-4)}$$

or, for the k-th specimen (k = 1,2,3,4)

$$M^k = \frac{m^k - {}_E m^k}{{}_I W_d^k} \quad . \qquad \text{(A-5)}$$

Since the end zones are not included, the RMC of the k-th and the k+1 specimens (in the same test) should be the same:

$$M^k = M^{k+1} \quad . \qquad \text{(A-6)}$$

Substituting eq. (A-5) in (A-6), and solving for ${}_E m$ we obtain:

$$E^m = ({}_I W_d^{k+1}\, m^k - {}_I W_d^k m^{k+1}) / ({}_I W_d^{k+1} - {}_I W_d^k) \qquad \text{(A-7)}$$

where ${}_E m^k = {}_E m^{k+1} = {}_E m$.

Substitution of $_{E}m$ from eq. (A-7) in eq. (A-5) yield:

$$M^k = \frac{(W^{k+1} - W^k) - (W_d^{k+1} - W_d^k)}{(W_d^{k+1} - W_d^k)} \qquad \text{(A-8)}$$

or:

$$M = \frac{\Delta W}{\Delta W_d} - 1 \qquad \text{(A-9)}$$

where ΔW is the weight difference between two wet specimens in the same test, and ΔW_d the dry weight difference between them. It should be noted that the result for each test is an average of six values, although there are four specimens.

Appendix B - Evaluation of Equivalent Hygroelastic Stress in Unstressed Thick Specimens

Let the distribution of moisture concentration at a certain time, $C(y,t)$, be described by Fig.45a. The dashed line designates the average concentration, $\bar{C}$. The point SFC (stress-free concentration) divides the thickness of the specimen into a hygroelastically compressed region - $\bar{y} \leq y \leq h/2$ with moisture concentration above $\bar{C}$, and a tensile region $0 \leq y \leq \bar{y}$ with concentration below $\bar{C}$.

The total axial strain of a layer dy at distance y from the centerline of the specimen is given by:

$$\varepsilon_x(y) = \varepsilon_e + \varepsilon_H \qquad \text{(B-1)}$$

or

$$\varepsilon_x(y) = \frac{1}{E}\sigma_x(y) + \beta C(y) \qquad \text{(B-2)}$$

where σ_x is the axial normal stress, β the coefficient of hygroelastic expansion (CHE), and C is moisture concentration.

The compressive stress required to reduce the strain, within the range $\bar{y} \leq y \leq h/2$ to its average level, $\bar{\varepsilon}$ is:

$$\sigma_x(y) = E[\beta C(y) - \bar{\varepsilon}] \quad , \qquad \text{(B-3)}$$

or, with the average strain expressed in terms of the average concentration $\bar{C}$:

$$\sigma_x(y) = \beta E[C(y) - \bar{C}] \quad . \qquad \text{(B-4)}$$

Let us concentrate on the compressed zone, Fig.45b, and define a new coordinate system as follows:

$$Y = \frac{h}{2} - y \tag{B-5}$$

$$C^*(Y) = C(y) - \bar{C} \quad .$$

According to equations B-5, the equivalent compressive stress can be defined as:

$$\bar{\sigma}_x = \frac{1}{\bar{Y}} \int_0^{\bar{Y}} \beta E C^*(Y)\, dY \quad . \tag{B-6}$$

Assuming β and E to be independent of Y, we may approximate:

$$\bar{\sigma}_x = \frac{1}{3}\beta E C^*_m \quad . \tag{B-7}$$

Transformation to the original coordinate system yields the expression for the equivalent stress:

$$\bar{\sigma}_x(t) = \frac{1}{3}\beta E [C_m - \bar{C}(t)] \quad . \tag{B-8}$$

Appendix C - The Procedure of the Computer Program

The program relates to a structure with rectangular bounds composed of general layers of different materials, which is exposed to a given hygrothermomechanical external conditions. The program is able to compute the tempterature, moisture and mechanical fields which are developed within the layered structure and the interaction - coupling between all these process variables. The computer program is composed of two main parts - the first solves the diffusion equations whereas the second computes the mechanical response cf the structure based on assumption of visco-elasto-plastic behavioral model. The first part is solved iteratively up to the level of desired convergence, (Modified Newton-Raphson, Newton-Raphson-Picard). In the second part, the residual load (or the out-of-balance load) is added to the load vector of the next time step.

The numerical solution is conducted by the finite strip method (FSM). The division of the structure into longitudinal strips is done automatically, whereas there is a possibility of obtaining three different division regions through the width of the structure. The proportions between the different division regions and the number of elements in each region are free to be determined according to the given requirements. In case of bi-material structure, one region at each side of the interface is selected. To improve the precision of the solution, the strips were divided into two sub-regions at which an additional division to sub-strips of a different number and density is possible.

In the present work, the integrals were calculated numerically according to the Gauss-Legendre scheme. This was done for three integration points in each direction through the strip width and along the sub-strip, to obtain optimal adjustment for computation for square interpolation functions.

The computer program starts with the determination of dynamic dimensions for most of the main systems to save memory resources (use of memory volume is required without useless surplus). An additional means of saving memory resources is by determination of joint working spaces. Detailed illustration of the computer program scheme and steps is given in the following flow charts (Fig.46).

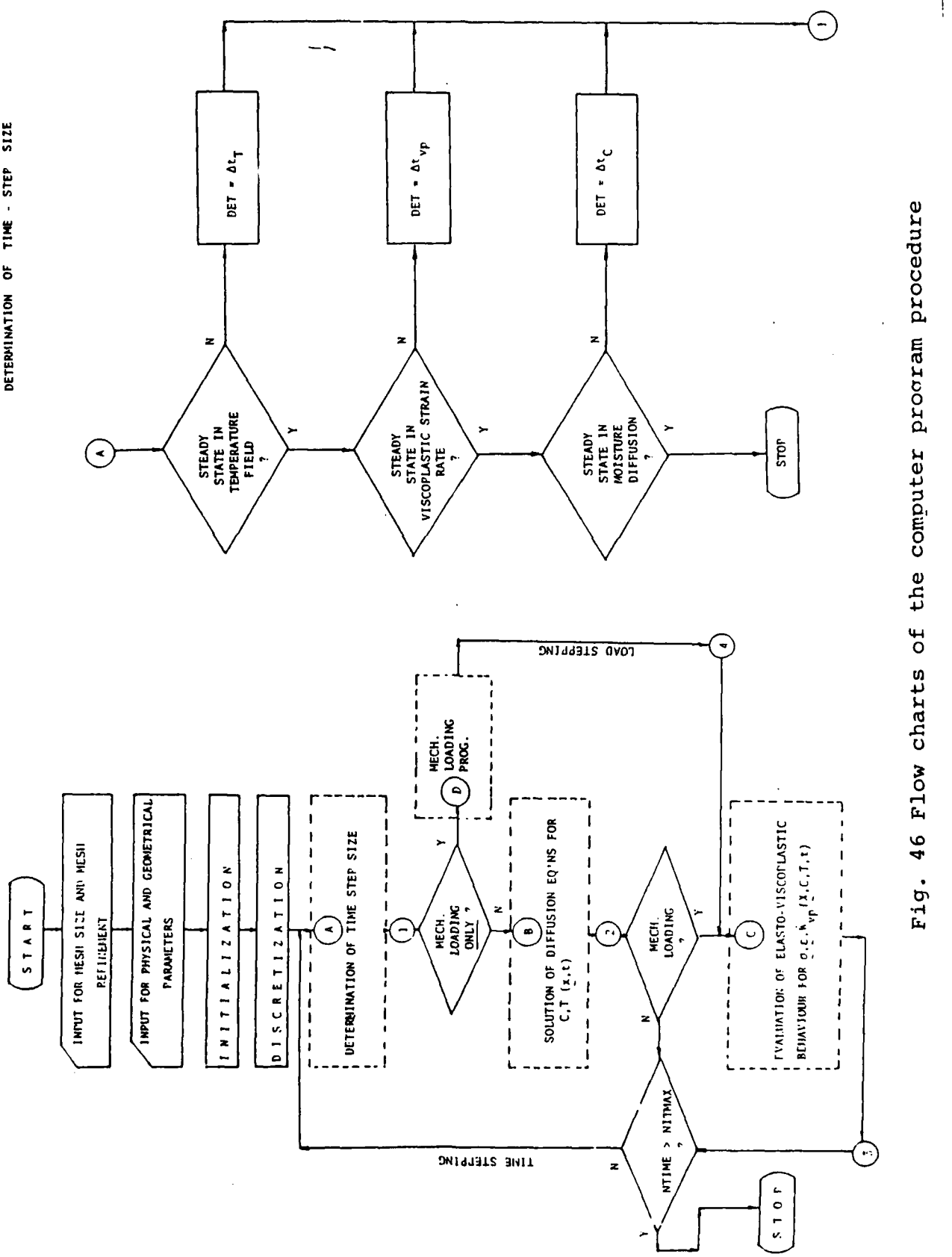

Fig. 46 Flow charts of the computer program procedure

MECHANICAL LOADING PROGRAM

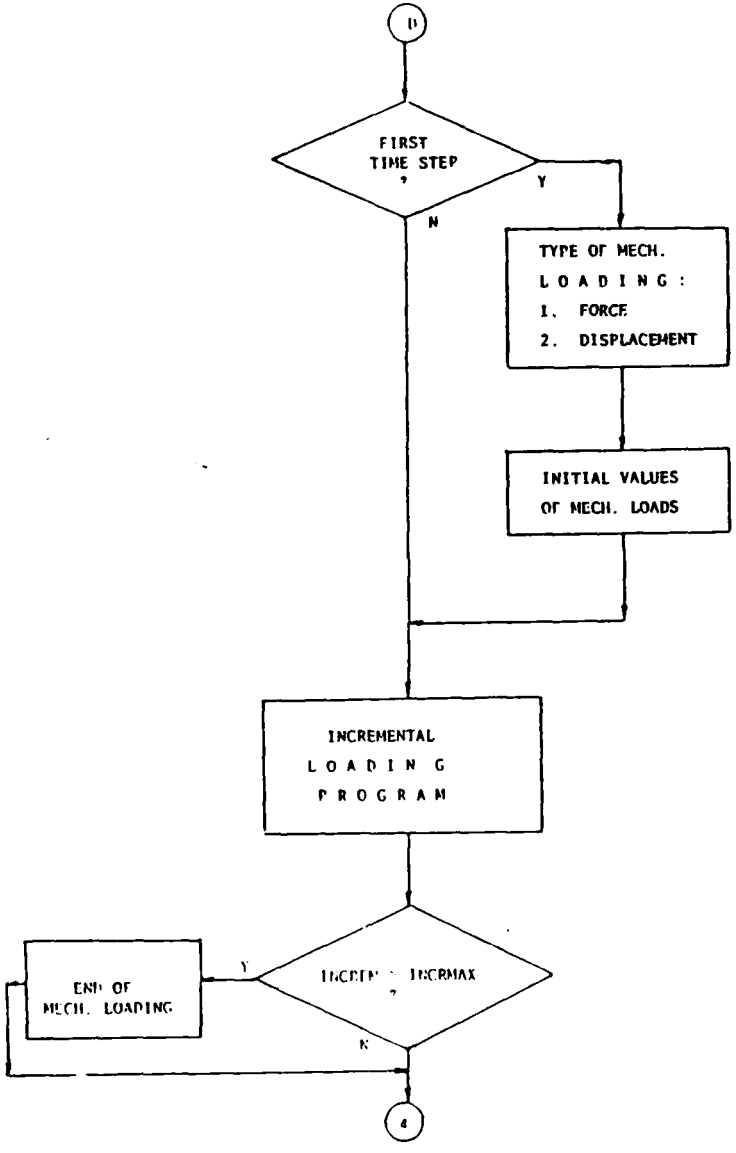

SOLUTION OF DIFFUSION EQUATIONS

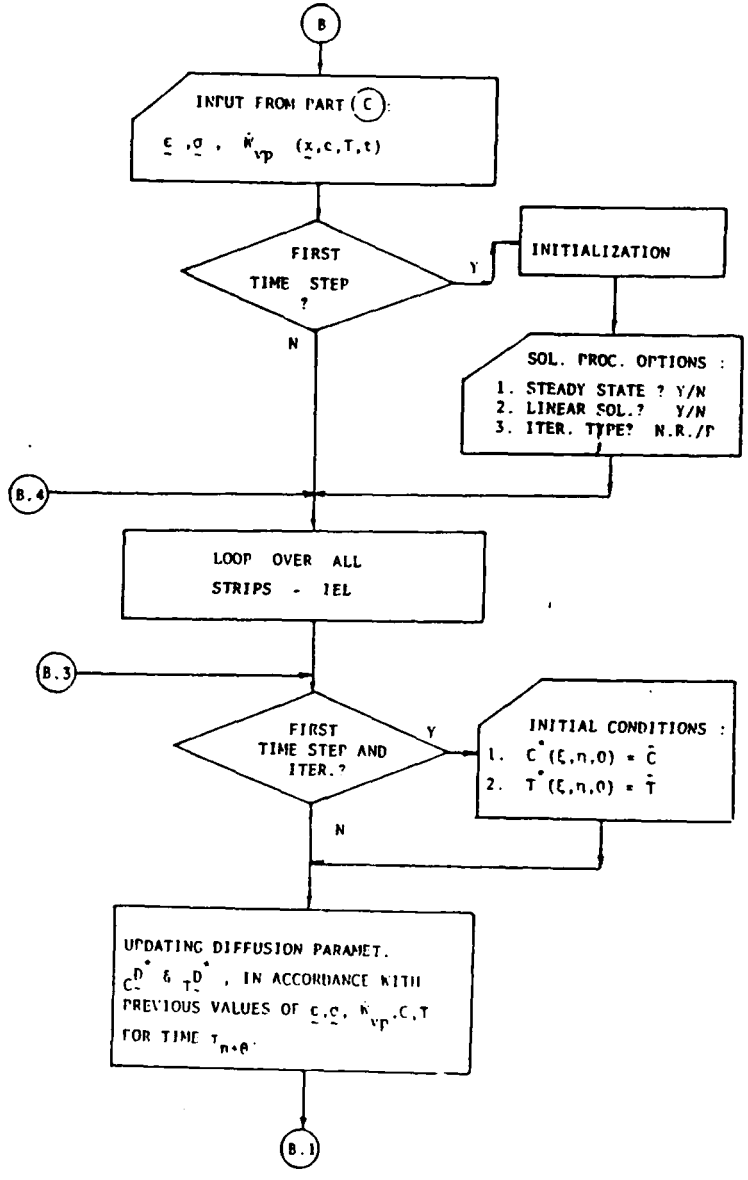

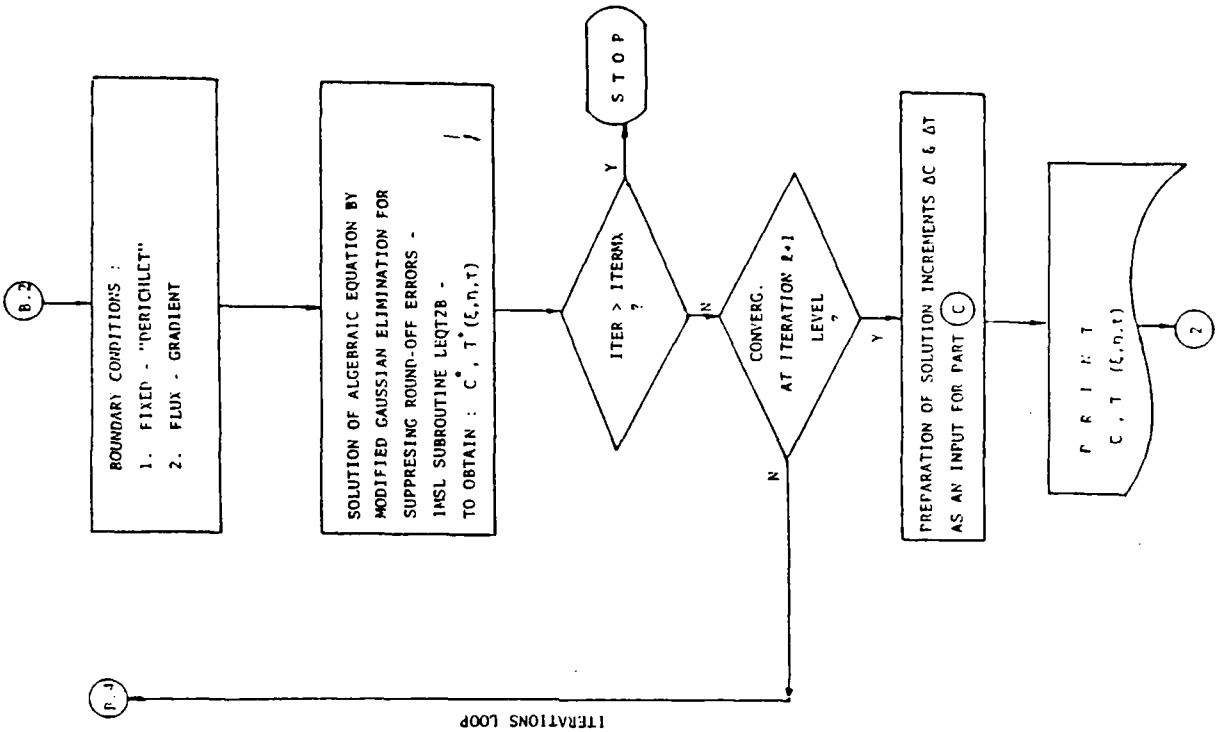
B.2
BOUNDARY CONDITIONS :
1. FIXED - "DERICHLET"
2. FLUX - GRADIENT
SOLUTION OF ALGEBRAIC EQUATION BY MODIFIED GAUSSIAN ELIMINATION FOR SUPPRESING ROUND-OFF ERRORS - IMSL SUBROUTINE LEQT2B - TO OBTAIN : C*, T*(ξ,η,τ)
ITER > ITERMX ?
Y
STOP
N
CONVERG. AT ITERATION k+1 LEVEL ?
N
Y
PREPARATION OF SOLUTION INCREMENTS ΔC & ΔT AS AN INPUT FOR PART C
C
PRINT C, T (ξ,η,τ)
2
ITERATIONS LOOP
B.1

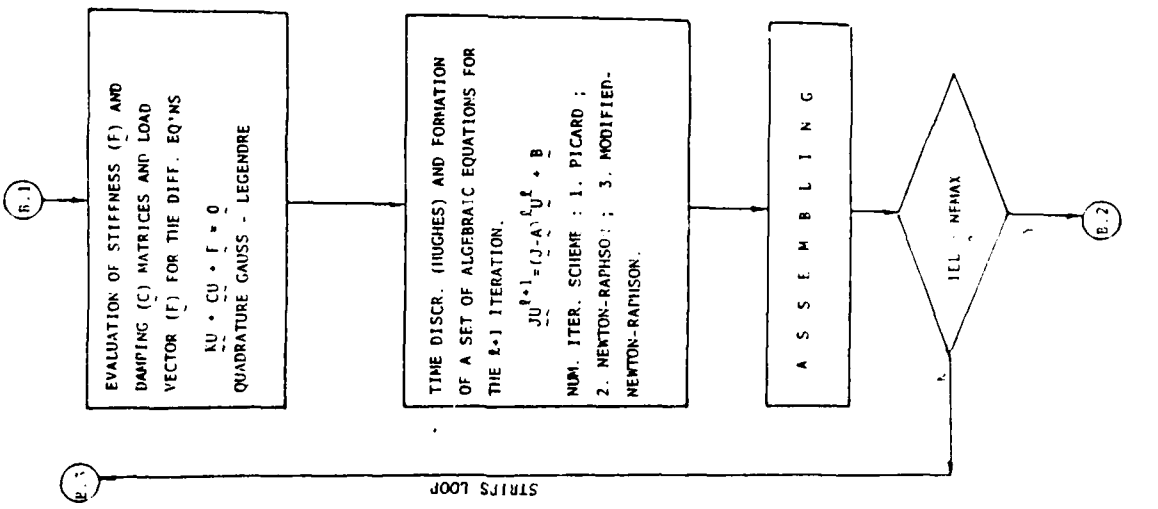
B.1
EVALUATION OF STIFFNESS (K) AND DAMPING (C) MATRICES AND LOAD VECTOR (F) FOR THE DIFF. EQ'NS
KU + CU̇ + F = 0
QUADRATURE GAUSS - LEGENDRE
TIME DISCR. (HUGHES) AND FORMATION OF A SET OF ALGEBRAIC EQUATIONS FOR THE k+1 ITERATION.
JU^(k+1) = (J-A)U^k + B
NUM. ITER. SCHEME : 1. PICARD ; 2. NEWTON-RAPHSON ; 3. MODIFIED-NEWTON-RAPHSON.
A S S E M B L I N G
ITER > NEMAX
B.2
STRIPS LOOP
B.1

EVALUATION OF ELASTO - VISCOPLASTIC BEHAVIOR

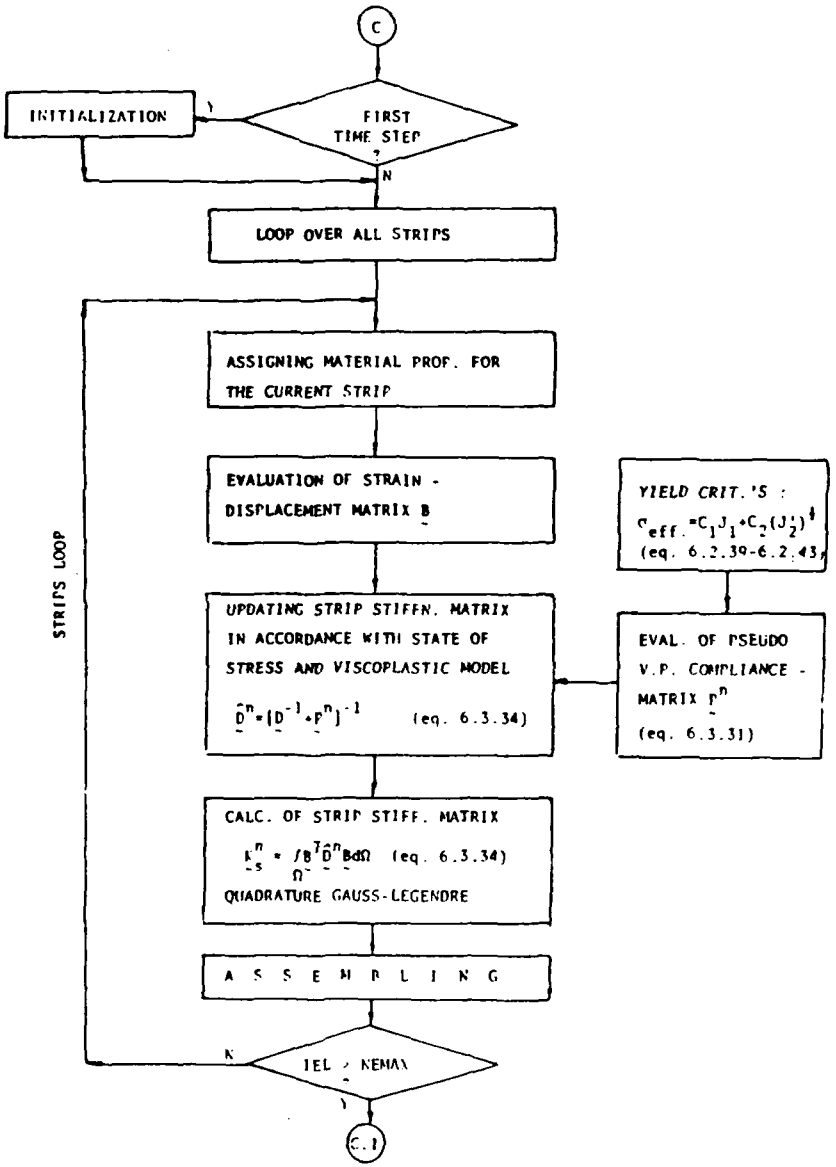

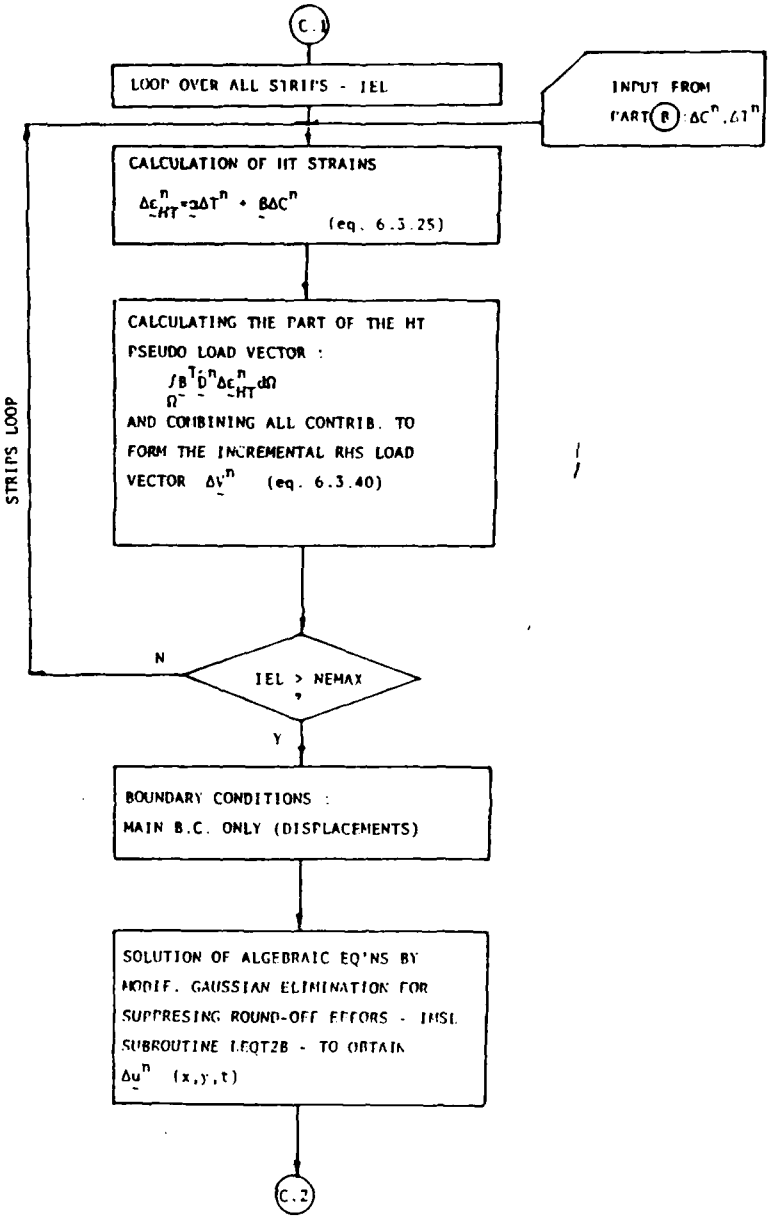

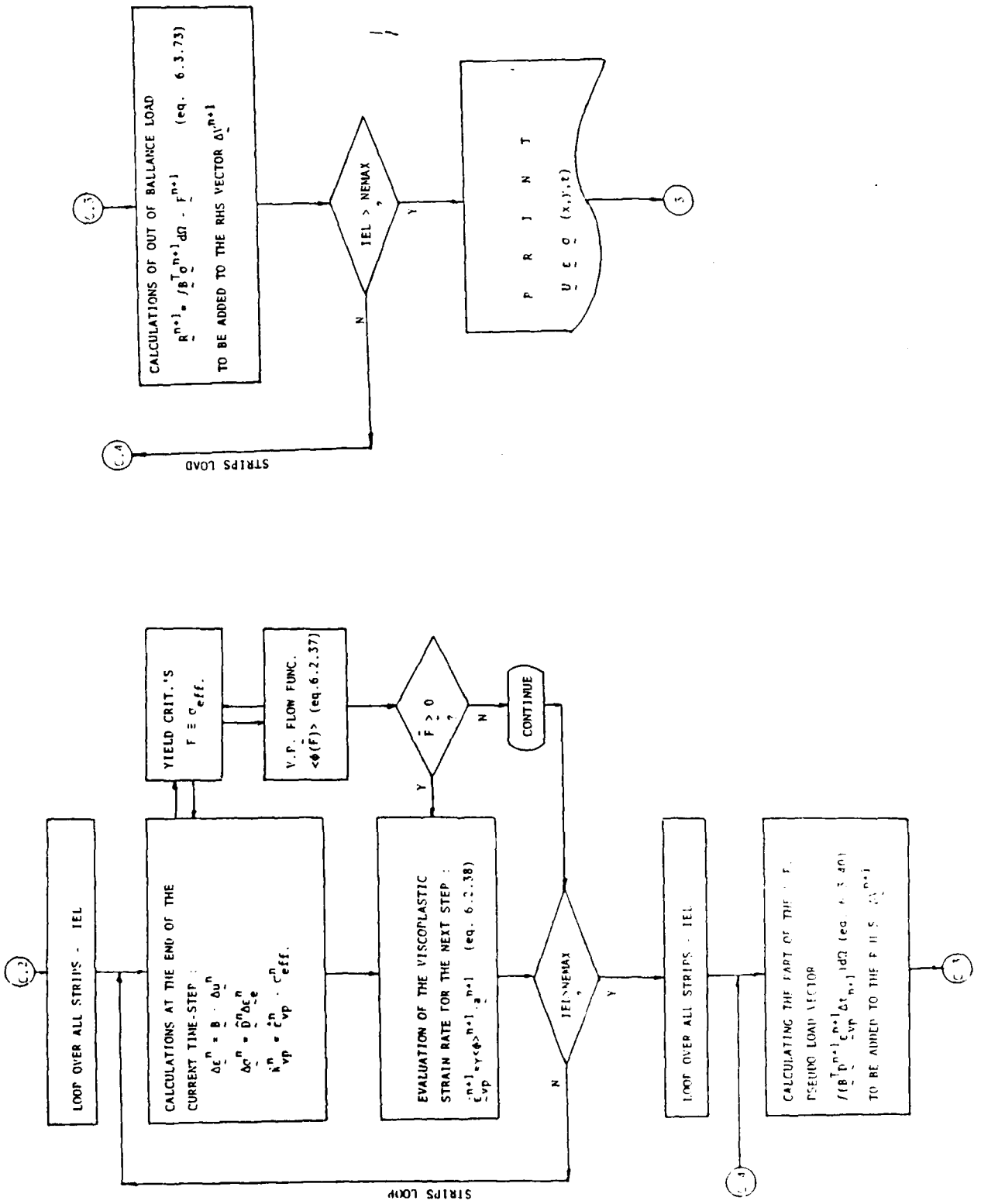
LOOP OVER ALL STRIPS - IEL
CALCULATIONS AT THE END OF THE CURRENT TIME-STEP :
YIELD CRIT.'S F ≡ σ_eff.
V.P. FLOW FUNC. <Φ(F)> (eq.6.2.37)
F ≥ 0 ?
N
CONTINUE
Y
EVALUATION OF THE VISCOPLASTIC STRAIN RATE FOR THE NEXT STEP : (eq. 6.2.38)
IEL=NEMAX ?
N
Y
LOOP OVER ALL STRIPS - IEL
CALCULATING THE PART OF THE F.
PSEUDO LOAD VECTOR
TO BE ADDED TO THE F
STRIPS LOOP
CALCULATIONS OF OUT OF BALLANCE LOAD
(eq. 6.3.73)
TO BE ADDED TO THE RHS VECTOR
IEL > NEMAX ?
Y
N
P R I N T
STRIPS LOAD

END

DTIC

9-86